

# POLITECNICO DI TORINO

Master's Degree in Mechanical Engineering



Master's Degree Thesis

## Assesment of a innovative high-tech flowmeter

Supervisors

Prof. Alessandro FERRARI

Dr. Oscar VENTO

Candidate

Alessandro CORALLO

December 2021

## Abstract

Goal of the thesis is to develop a meter for the measurement of the instantaneous flow rate at high pressures (the experimental tests oscillate between a minimum pressure of 600 bar and a maximum of 1800 bar).

The research and studies took place with the collaboration of the Rabotti company and all experimental tests were conducted in the laboratory of the Energy Department of the Polytechnic.

The meter is based on the detection of pressure, carried out by means of two high-performance piezoresistive transducers, in two points placed at an appropriate distance along a sufficiently rigid duct with a constant diameter where diesel, petrol or mineral oil flows inside.

The instrument to be designed has a high technological content and brings a significant innovation in terms of the market since there are no reliable instruments on the market capable of evaluating the instantaneous flow rate in liquid flows characterized by large levels of pressures.

The experimental readings of the pressure and temperature sensors are sent to an acquisition card for high and low frequency signals and are then processed by a cRIO platform.

The platform initially performs a filtering and then determines the instantaneous flow rate associated with the liquid flow that passes along the duct.

The cRIO platform is also able to carry out post-processing concerning the flow signal.

The primary goal is to implement an advanced filtering technique to correct the results that the platform returns.

The methodology must take into account many parameters: processing times, general efficiency, reliability and complete generality (having to do with numerous experimental tests, each test will have its own behavior and introducing a general methodology is not easy).

Furthermore, since it is not possible to perform a validation with a master type meter, in addition to the realization of the prototype, a number-experimental methodology will be defined for its validation.

The experimental tests on the prototype will be carried out on fuel supply systems for internal combustion engines as they allow to reach high pressures.

After the implementation of the filtering techniques we will pass from the modeling (using CAD-3D Solidworks) of the meter to the actual physical design.

All production processes for the engineering of the final product will be analyzed and studied.

The thesis can therefore be divided into two large sections: in the first a methodology

was introduced to identify a technique for the correct filtering of the meter results and in the second everything was integrated with the modeling and mechanical design of the meter itself.



# Acknowledgements

Questi anni a Torino sono stati davvero intensi, ci sono stati periodi di grandi soddisfazioni, ma non lo nego, periodi dove ho anche pensato di lasciare tutto in quanto non riuscivo a ottenere i risultati che desideravo.

Fortunatamente la passione per le discipline scientifiche e le persone accanto a me hanno fatto in modo di farmi andare avanti e di arrivare alla fine di questo percorso.

Ci tengo, inizialmente, a ringraziare il Professore Alessandro Ferrari per avermi permesso di entrare in questo progetto e l'Ingegnere Oscar Vento, che mi ha seguito costantemente e mi ha permesso di ampliare le mie conoscenze.

Ringrazio mia madre Lucia e mio padre Angelo, mi avete permesso, mediante il vostro amore e il vostro sostegno, di essere ciò che sono oggi, mi avete fatto capire che, con sacrifici e tanta volontà, si può arrivare ovunque.

Ringrazio te Daniela, sei presente sin dall'inizio, mi dai forza ogni giorno e, grazie all'amore che mi trasmetti, mi fai capire quanto sia importante avere affianco una persona di cui fidarsi, ma soprattutto da amare.

Ringrazio mio fratello Andrea per avermi sempre supportato e per avermi strappato una risata anche quando le situazioni erano difficili.

Ringrazio l'altro fratello mio Gaetano, sei sempre presente e mi supporti sempre, ripenso sempre ai periodi spensierati passati insieme e questi mi hanno sempre dato forza per continuare il mio percorso.

Ringrazio la mia carissima nonna Silvana, mi hai trasferito tutta la maturità che ti contraddistingue, ti sarò sempre grato per questo.

Ringrazio tutti gli altri miei parenti che sono sempre stati presenti, Cinzia, Susanna, zia Ninni, zia Rita, zio Tonio, zio Massimo, zio Peppe, grazie anche ai vostri consigli sono la persona che sono adesso.

Non posso non esprimere la mia gratitudine ai miei coinquilini Nicola, Pietro e Simone, con voi ho passato la maggior parte del tempo qui a Torino, vi voglio ringraziare di tutti i bei momenti passati, di tutte le esperienze condivise, belle e brutte, dal primo piatto preparato insieme al lockdown condiviso.

Non posso non ringraziare tutti i miei amici che mi hanno accompagnato in questo percorso, ognuno di voi mi ha insegnato qualcosa, tutti questi insegnamenti li

terrò sempre dentro di me, grazie Tarik, Amerigo, Antonino, Pino, Gabriele, Jack, Simone, Gabriele, Lorenzo, Marco, Riccardo, Angelo e Martina  
Grazie anche a chi ha sempre creduto in me e a chi non sono riuscito a menzionare, ma solo con un piccolo consiglio o un singolo sorriso è riuscito a farmi andare avanti, giorno dopo giorno.

*“Ai miei genitori  
Angelo e Lucia”*



# Table of Contents

<b>List of Tables</b>	VII
<b>List of Figures</b>	VIII
<b>Acronyms</b>	XIV
<b>1 Fourier Analysis</b>	1
1.1 From the series to the Fourier transform . . . . .	1
1.2 From the transform to the Discrete Fourier transform (DFT) . . . . .	5
<b>2 Test bench</b>	8
2.1 Hydraulic circuit . . . . .	8
2.2 Oil tank . . . . .	10
2.3 Feed pumps and cooling circuits . . . . .	11
2.4 KMM flow-meter . . . . .	12
2.5 EMI2 meter . . . . .	13
2.6 EVI meter . . . . .	16
<b>3 Before algorithms</b>	19
3.1 Presentation of the problem . . . . .	19
3.2 Multiplicative factor MF and linearization of the spectrum . . . . .	25
3.3 Extension to all situations . . . . .	31
3.4 Different speeds of rotation . . . . .	37
3.4.1 Experimental tests with rotation speed $n = 600$ rpm . . . . .	37
3.4.2 Experimental tests with rotation speed $n = 1500$ rpm . . . . .	41
<b>4 Implementation of the algorithms</b>	45
4.1 Introduction to the first check . . . . .	45
4.2 Second check . . . . .	50
4.3 Third check . . . . .	57
4.4 Introduction to the simplified algorithm . . . . .	60

<b>5</b>	<b>Comparison of algorithms</b>	66
5.1	A brief summary . . . . .	66
5.2	Processing time . . . . .	67
5.3	Identification of the intersection line with the initial spectrum . . .	69
5.4	Final point . . . . .	71
5.5	Accuracy and efficiency . . . . .	76
5.6	Absence of the solution . . . . .	78
<b>6</b>	<b>Conclusions and Future Prospects</b>	84
<b>A</b>	<b>Mechanical design of the flowmeter</b>	86
A.1	Piezoresistive high pressure sensor . . . . .	87
<b>B</b>	<b>Fundamentals of Fluid Dynamics Model of the Flowmeter</b>	92
B.1	Introduction to Navier-Stokes equations . . . . .	92
B.2	Stress tensor in dynamics . . . . .	93
B.3	Classic 1D Euler's equations . . . . .	94
B.4	Generalized Euler equations . . . . .	96
B.5	Numerical algorithm for the flor-rate evaluation . . . . .	97
	<b>Bibliography</b>	100

# List of Tables

1.1	Differences between the Fourier series and the Fourier transform . .	4
3.1	PCV regulation, data to derive analytical equation between peak frequency, pump rotation speed and number of pumping elements .	44
5.1	Comparison of times for all the tests listed, PCV regulation, n=1000 rpm . . . . .	68
A.1	Technical Data of the transducer . . . . .	88

# List of Figures

1.1	Example of Fourier Series of a generic periodic function $F$ . . . . .	2
2.1	Hydraulic circuit of the test bench . . . . .	9
2.2	Oil refrigeration system . . . . .	10
2.3	Feed and cooling pumps . . . . .	11
2.4	KMM meter's scheme . . . . .	12
2.5	Structure of EMI2 meter . . . . .	14
2.6	Operating diagram of EMI2 meter . . . . .	15
2.7	Structure of EVI meter . . . . .	16
2.8	Operating diagram of EVI meter . . . . .	17
3.1	Low pressure: 800 bar, regulation with FMV, 700 $\mu s$ ET, respectively pressure measured by the upstream sensor and instantaneous flow rate	20
3.2	Intermediate pressure: 1400 bar, regulation with PVC, 1000 $\mu s$ ET, respectively pressure measured by the upstream sensor and instantaneous flow rate . . . . .	21
3.3	High pressure: 1800 bar, regulation with PVC, 1000 $\mu s$ ET, respectively pressure measured by the upstream sensor and instantaneous flow rate . . . . .	22
3.4	Fourier spectrum of the pressure signal with $P_{up}=800\text{bar}$ , $ET=700\mu s$ , FMV . . . . .	23
3.5	Fourier spectrum of the pressure signal with $P_{up}=1400\text{bar}$ , $ET=1000\mu s$ , PCV . . . . .	24
3.6	Fourier spectrum of the pressure signal $P_{up}=1800\text{bar}$ , $ET=1000\mu s$ , PCV . . . . .	24
3.7	Fourier spectrum of the pressure signal $P_{up}- \langle P_{up} \rangle$ with - $P_{up}=800\text{bar}$ , $ET=700\mu s$ , FMV regulation . . . . .	25
3.8	Fourier spectrum of the pressure signal $P_{up}- \langle P_{up} \rangle$ with - $P_{up}=1400\text{bar}$ , $ET=1000\mu s$ , PCV regulation . . . . .	26
3.9	Fourier spectrum of the pressure signal $P_{up}- \langle P_{up} \rangle$ with - $P_{up}=1800\text{bar}$ , $ET=1000\mu s$ , PCV regulation . . . . .	26

3.10	Instant flow graphs with MF from 1.1 to 0.9 with discretization step 0.05 ( $P_{up}$ =1400 bar, ET=1000 $\mu$ s, PVC regulation) . . . . .	27
3.11	Instant flow graphs with MF from 1.1 to 0.9 with discretization step 0.01 ( $P_{up}$ =1400 bar, ET=1000 $\mu$ s, PVC regulation) . . . . .	28
3.12	Instant flow graphs with MF from 1.1 to 0.9 with discretization step 0.005 ( $P_{up}$ =1400 bar, ET=1000 $\mu$ s, PVC regulation) . . . . .	28
3.13	Initial Flow-rate vs Final Flow rate with MF=0.9927 . . . . .	29
3.14	Spectra graph with MF from 1.1 to 0.9 with discretization step 0.01 ( $P_{up}$ =1400 bar, ET=1000 $\mu$ s, PVC regulation) . . . . .	30
3.15	Initial Spectrum vs Final Spectrum with MF=0.9927 . . . . .	30
3.16	Respectively graph of $P_{up}$ with reference value 1800 bar, pump equipped with 3 pumping elements, Fourier spectrum and flow rate graph with PCV regulation, n = 1000 rpm . . . . .	32
3.17	Respectively graph of $P_{up}$ with reference value 1400 bar, pump equipped with 3 pumping elements, Fourier spectrum and flow rate graph with PCV regulation, n = 1000 rpm . . . . .	33
3.18	reference value of pressure 1800 bar, regulation with FMV, 1000 $\mu$ s ET, respectively pressure measured by the upstream sensor and instantaneous flow rate . . . . .	34
3.19	Fourier spectrum of $\Delta p - \langle \Delta p \rangle$ with reference value of pressure 1800 bar, FMV . . . . .	35
3.20	Fourier spectrum of $P_{up} - \langle P_{up} \rangle$ with reference value of pressure 1800 bar, FMV . . . . .	35
3.21	Respectively graph of $P_{up}$ with reference value 1800 bar, pump equipped with 2 pumping elements, Fourier spectrum and flow rate graph with FMV regulation, n = 1000 rpm . . . . .	36
3.22	Pressure upstream the flowmeter (n=600rpm) . . . . .	37
3.23	Initial flow-rate (n=600rpm) . . . . .	38
3.24	Spectrum of the parameter $\langle \Delta p - \Delta p \rangle$ (n=600rpm) . . . . .	38
3.25	Spectrum of the parameter $P_{up} - \langle P_{up} \rangle$ (n=600rpm) . . . . .	39
3.26	Spectrum of the parameter $P_{up} - \langle P_{up} \rangle$ , reference pressure 1800 bar, 3 pumping elements of the pump (n=1000rpm) . . . . .	39
3.27	Respectively graph of $P_{up}$ with reference value 1300 bar, pump equipped with 2 pumping elements, Fourier spectrum and flow rate graph with FMV regulation, n = 600 rpm . . . . .	40
3.28	Pressure upstream the flow-meter (n=1500rpm) . . . . .	41
3.29	Initial flow-rate (n=1500rpm) . . . . .	41
3.30	Spectrum of the parameter $\Delta p - \langle \Delta p \rangle$ (n=1500rpm) . . . . .	42
3.31	Spectrum of the parameter $P_{up} - \langle P_{up} \rangle$ (n=1500rpm) . . . . .	42

3.32	Respectively graph of $P_{up}$ with reference value 1200 bar, pump equipped with 2 pumping elements, Fourier spectrum and flow rate graph with FMV regulation, $n = 1500$ rpm . . . . .	43
4.1	Fourier spectrum of pressure signal, PCV, reference pressure 1200 bar	45
4.2	Flow-rate's graph, PCV, reference pressure 1200 bar . . . . .	46
4.3	Initial spectrum with range of straight lines with corresponding points of intersection . . . . .	47
4.4	Line bundle of least squares with average value of the multiplicative coefficient MF equal to 1.03 . . . . .	48
4.5	Line bundle of least squares with average value of the multiplicative coefficient MF equal to 1.01 . . . . .	48
4.6	Line bundle of least squares with average value of the multiplicative coefficient MF equal to 0.952 . . . . .	49
4.7	Line bundle of least squares with average value of the multiplicative coefficient MF equal to 0.991 . . . . .	49
4.8	Spectrum associated to MF=0.9911, initial spectrum and fitting line	50
4.9	Flow-rate associated to MF=0.9911 and initial flow-rate . . . . .	51
4.10	Initial Spectrum and Spectra after first and second control . . . . .	52
4.11	Initial Flow-rate and Flow-rate after first and second control . . . . .	53
4.12	Initial spectrum and Spectra after first and second control, reference pressure 1000 bar, PCV regulation, 1000 $\mu s$ ET, 2 pumping elements	54
4.13	Initial flow-rate and flow-rate after first and second control, reference pressure 1000 bar, PCV regulation, 1000 $\mu s$ ET, 2 pumping elements	54
4.14	Initial spectrum and Spectra after first and second control, reference pressure 1500 bar, PCV regulation, 700 $\mu s$ ET, discretized step 0.0001, 3 pumping elements . . . . .	55
4.15	Initial flow-rate and flow-rate after first and second control, reference pressure 1500 bar, PCV regulation, 700 $\mu s$ ET, discretized step 0.0001, 3 pumping elements . . . . .	56
4.16	Initial Spectrum, Spectra and interpolating line . . . . .	57
4.17	Initial Spectrum and Final spectrum after the implementation of the algorithm . . . . .	58
4.18	Initial Flow-rate and Final flow-rate after the implementation of the algorithm . . . . .	59
4.19	Flow domain with discretization step 0.01, range of MF: from 1.1 to 0.97 . . . . .	60
4.20	Domain of spectra with discretization step 0.01, range of MF: from 1.1 to 0.97 . . . . .	61
4.21	Result of the algorithm with discretization step 0.01, range of MF: from 1.1 to 0.97 . . . . .	61

4.22	Flow domain with discretization step 0.001, range of MF: from 1.1 to 0.97 . . . . .	62
4.23	Domain of spectra with discretization step 0.001, range of MF: from 1.1 to 0.97 . . . . .	63
4.24	Result of the algorithm with discretization step 0.001, range of MF: from 1.1 to 0.97 . . . . .	63
4.25	Flow domain with discretization step 0.0001, range of MF: from 1.1 to 0.97 . . . . .	64
4.26	Domain of spectra with discretization step 0.0001, range of MF: from 1.1 to 0.97 . . . . .	65
4.27	Result of the algorithm with discretization step 0.0001, range of MF: from 1.1 to 0.97 . . . . .	65
5.1	Initial and final flow-rate, discretization step 0.001 . . . . .	67
5.2	Flow-chart of the first algorithm . . . . .	69
5.3	Matrix of multiplicative coefficients MF . . . . .	70
5.4	Matrix of the sum of the differences between the i-th spectra and the j-th line . . . . .	70
5.5	Example 1: Initial spectrum, final spectrum, intersection point and reference point for the initial algorithm . . . . .	71
5.6	Example 2: Initial spectrum, final spectrum, intersection point and reference point for the initial algorithm . . . . .	72
5.7	Example 3: Initial spectrum, final spectrum, intersection point and reference point for the initial algorithm . . . . .	73
5.8	Simplified algorithm: Spectrum identified by reference point following the intersection point . . . . .	74
5.9	Simplified algorithm: Spectrum identified by reference point fixed to 150 Hz . . . . .	75
5.10	Effect of the variation of the discretization step: first algorithm . . . . .	76
5.11	Effect of the variation of the discretization step: Simplified algorithm . . . . .	77
5.12	Initial Flow-rate, Reference pressure 1000 bar, 400 $\mu$ s ET, FMV regulation, n=1000 rpm . . . . .	78
5.13	Initial Flow-rate, Reference pressure 800 bar, 400 $\mu$ s ET, FMV regulation, n=1000 rpm . . . . .	79
5.14	Initial Flow-rate, Reference pressure 1200 bar, 400 $\mu$ s ET, FMV regulation, n=1000 rpm . . . . .	79
5.15	Initial Spectrum and Final spectrum, Reference pressure 1000 bar, 400 $\mu$ s ET, FMV regulation, n=1000 rpm . . . . .	80
5.16	Initial flow-rate and Correct Flow-rate, Reference pressure 1000 bar, 400 $\mu$ s ET, FMV regulation, n=1000 rpm . . . . .	80

5.17	Initial spectrum and final spectrum with the interval of the two controls fixed at $\pm 25\%$ . . . . .	81
5.18	Initial Flow-rate and final flow-rate with the interval of the two controls fixed at $\pm 25\%$ . . . . .	82
5.19	Initial Flow-rate and final flow-rate with the simplified algorithm . . . . .	83
A.1	Scheme of the flow-meter . . . . .	86
A.2	Pressure transducer . . . . .	87
A.3	3D model of the flowmeter . . . . .	89
A.4	Flow-meter connected to the circuit for diesel injection . . . . .	89
A.5	Rack of the device . . . . .	90
A.6	Injection circuit diagram [4] . . . . .	91



# Acronyms

**DFT**

Discrete Fourier transform

**FFT**

Fast Fourier transform

**HPP**

High pressure pump

**ET**

Energizing time

**FMV**

Flow-meter valve

**PCV**

Pressure control valve

**MF**

Multiplicative factor

**DS**

Discretization step

# Chapter 1

## Fourier Analysis

### 1.1 From the series to the Fourier transform

Let's consider a generic function  $F(t)$ .

Function  $F$  is defined **periodic** if there exists a real number  $\mathbf{T}$  (called **period** of the function) which satisfies the following expression:

$$F(t + T) = F(t) \quad (1.1)$$

In this way I can obtain  $F$  as an infinite sum of harmonic functions; I write  $F$  in **Fourier Series**:

$$F(t) = a_0 + \sum_{n=1}^{\infty} a_n \cos(n\Omega_0 t) + b_n \sin(n\Omega_0 t) \quad (1.2)$$

where:

$$\Omega_0 = \frac{2\pi}{T} \quad (1.3)$$

$\Omega_0$  is the fundamental frequency

$$a_0 = \frac{1}{T} \int_0^T F(t) dt = \frac{1}{T} \int_{-T/2}^{T/2} F(t) dt \quad (1.4)$$

$a_0$  is the mean value of the function  $F$

$$a_n = \frac{2}{T} \int_0^T F(t) \cos(n\Omega_0 t) dt = \frac{1}{T} \int_{-T/2}^{T/2} F(t) \cos(n\Omega_0 t) dt \quad (1.5)$$

$$b_n = \frac{2}{T} \int_0^T F(t) \sin(n\Omega_0 t) dt = \frac{1}{T} \int_{-T/2}^{T/2} F(t) \sin(n\Omega_0 t) dt \quad (1.6)$$

$a_0$ ,  $a_n$  and  $b_n$  are called **Fourier coefficients** and are a real numbers. Remembering this trigonometric expression:

$$a \cos \alpha + b \sin \beta = c \sin (\alpha + \beta) \tag{1.7}$$

I can rewrite the Fourier series in the following way:

$$F(t) = a_0 + \sum_{n=1}^{\infty} C_n \sin (n\Omega_0 t + \Phi) \tag{1.8}$$

$C_n$  is the amplitude of the  $n^{th}$  harmonic function.

The set of all  $C_n$  defined the **spectrum** of the function F.

An important concept to understand is that **I have moved from the time domain to the frequency domain** (this concept is extremely important when it'll be introduced the Fourier Transform and the Discrete Fourier Transform).

The difference between two consecutive spectral lines is called **frequency resolution** and it coincides with the fundamental frequency  $\Omega_0$ :

$$\Delta\Omega = \Omega_{n+1} - \Omega_n = \Omega_n - \Omega_{n-1} = n\Omega_0 - (n - 1)\Omega_0 = \Omega_0 \tag{1.9}$$

This because I describe the  $n^{th}$  frequency in this way:

$$\Omega_n = n\Omega_0 \tag{1.10}$$

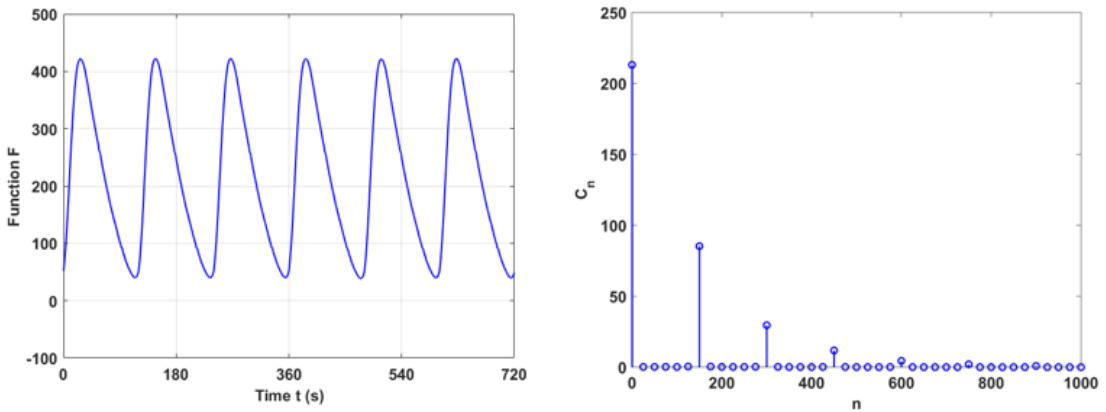


**Figure 1.1:** Example of Fourier Series of a generic periodic function F

It is possible to obtain the **exponential form of the Fourier series** by means of the Euler identity:

$$e^{i\alpha} = \cos \alpha + i \sin \alpha \tag{1.11}$$

(1.2) will become:

$$F(t) = a_0 + \sum_{n=1}^{\infty} \frac{(a_n - ib_n)}{2} e^{i\Omega_n t} + \frac{(a_n + ib_n)}{2} e^{-i\Omega_n t} \quad (1.12)$$

through some simple mathematical steps I obtain:

$$\frac{(a_n - ib_n)}{2} = \frac{1}{T} \int_0^T F(t)(\cos \Omega_n t - i \sin \Omega_n t) dt = \frac{1}{T} \int_0^T F(t) e^{-i\Omega_n t} dt = X_n \quad (1.13)$$

$$\frac{(a_n + ib_n)}{2} = \frac{1}{T} \int_0^T F(t) e^{-i\Omega_{-n} t} dt = X_{-n} \quad (1.14)$$

where:

$$\Omega_{-n} = -n\Omega_0 \quad (1.15)$$

Fourier series'll become:

$$F(t) = a_0 + \sum_{n=-\infty(n \neq 0)}^{\infty} (X_n e^{in\Omega_0 t} + X_{-n} e^{-in\Omega_0 t}) \quad (1.16)$$

$$F(t) = \sum_{n=-\infty}^{+\infty} X_n e^{in\Omega_0 t} \quad (1.17)$$

(1.17) is the **Fourier series in exponential form**

$X_n$  contains the amplitude and the phase because is a complex number:

$$X_n = \frac{1}{T} \int_0^T F(t) e^{-in\Omega_0 t} dt \quad (1.18)$$

The concept of the Fourier series finds space only in the field of periodic functions, but this can also be extended to non-periodic functions.

This can be done by considering the periodic non-periodic function with:

$$T \rightarrow +\infty \quad (1.19)$$

Doing this moves from the series to the **Fourier transform**

In this way the spectrum (before characterized by points as it was considered the  $n^{th}$  harmonic function) becomes a continuous function:

$$\Delta\Omega \rightarrow d\Omega (\rightarrow 0) \quad (1.20)$$

In this way:

$$n\Omega_0 \rightarrow \Omega \quad (1.21)$$

The resolution frequency tends to 0 and becomes fundamental frequency  $\Omega_0$  and this causes the spectrum to become continuous.

Through simple mathematical steps they will also change the shape of  $F(t)$  and  $X_n$ .

From (1.18):

$$\lim_{T \rightarrow \infty} (TX_n) = \int_{-\infty}^{+\infty} F(t)e^{-i\Omega t} dt = X(\Omega) \quad (1.22)$$

$X(\Omega)$  is the Fourier transform of the initial function  $F$  (note that the periodicity of the function is not required).

With the Fourier transform we pass from the time domain to the frequency domain, but the reverse passage it is allowed, infact with a few steps we can compute the **Inverse Fourier transform**:

$$F(t) = \frac{1}{2\pi} \int_{-\infty}^{+\infty} X(\Omega)e^{i\Omega t} d\Omega \quad (1.23)$$

With the inverse Fourier transform we pass from the frequency domain to the time domain.

The following table shows the differences between the Fourier series and the Fourier transform.

<b>Fourier Series</b>	<b>Fourier Transform</b>
Discrete Spectrum	Continuous Spectrum
Function with period $T$	Function with period $T \rightarrow +\infty$
Frequency resolution $\Delta\Omega = \Omega_0$	Frequency resolution $\Delta\Omega \rightarrow 0$
$F(t) = \sum_{n=-\infty}^{+\infty} X_n e^{in\Omega_0 t}$	$F(t) = \frac{1}{2\pi} \int_{-\infty}^{+\infty} X(\Omega) e^{i\Omega t} d\Omega$
$X_n = \frac{1}{T} \int_0^T F(t) e^{-i\Omega_n t} dt$	$X(\Omega) = \int_{-\infty}^{+\infty} F(t) e^{-i\Omega t} dt$

**Table 1.1:** Differences between the Fourier series and the Fourier transform

## 1.2 From the transform to the Discrete Fourier transform (DFT)

To better understand the concept of the Fast Fourier Transform (FFT) it is necessary to introduce the methodology with which one passes from an analog signal to a digital one.

An ADC is an electronic circuit capable of doing this, so it transforms a continuous signal (displacement, acceleration, voltage) into a series of discrete values with particular properties.

Identify a generic function  $G(t)$  in the time domain.

The analog to digital converter performs a sampling of the function, the distance between two sampled points is called **sampling period**  $\Delta t$ .

It's possible to introduce the **sampling frequency**:

$$f_s = \frac{1}{\Delta t} [Hz] \quad (1.24)$$

If the sampling frequency is very large the frequency resolution gets large, which is not positive to build the signal.

It's necessary to introduce the **Shannon theorem** (or Nyquist theorem): the theorem guarantees that an analog signal can be perfectly recovered as long as the sampling rate is at least twice of the highest-frequency component of the analog signal to be sampled.

The condition is:

$$f_s \geq 2f_{max} \quad (1.25)$$

where  $f_{max}$  is the maximum-frequency of the analog signal to be sampled.

If this theorem is not respected, there is a subsampling of the analog signal in the time domain; in the frequency domain there is the production of frequencies that are not inherent to the original signal (This phenomenon is called **aliasing**) and vice versa from the frequency domain to the time domain a distortion of the original signal is generated.

The process is complicated by the fact that the frequency of the signal to be digitized is not known, therefore it is necessary to use appropriate filtering to identify a cut off frequency.

The most important digital filters are identified:

- **low pass-filter**: the spectrum (or Frequency Response Function) after the  $f_{cutoff}$  is canceled.
- **high pass-filter**: the spectrum before the  $f_{cutoff}$  is canceled.
- **band pass-filter**: a range of frequencies is identified  $[f_{min}, f_{max}]$  where the spectrum is not canceled

The steps for identifying DFT are now analyzed.

It is necessary to pass from the transform to the DFT because:

- The continuous function is unknown;
- By means of the analog-digital converter the discrete signal is available and it is not possible to carry out the Fourier transform of a discrete signal;
- The hypothesis of an infinite period cannot be found in reality;

It is therefore necessary to return to the Fourier series (and to its hypothesis of periodic function) and integrate with all the sampling discourse developed above. From (1.18), sampled time history:

$$t = k\Delta t \tag{1.26}$$

$$F(t) = F(k\Delta t) = F_k \tag{1.27}$$

$$T = N\Delta t \tag{1.28}$$

With the following modifications we obtain the **Discrete Fourier Transform**:

$$X_n = \frac{1}{N} \sum_{k=0}^{N-1} F_k e^{-i2\pi n \frac{k}{N}} \tag{1.29}$$

Some of the properties of the DFT are as follows:

- it replaces  $K'=n+N$

$$X_{K'} = \frac{1}{N} \sum_{k=0}^{N-1} F_k e^{-i2\pi(n+N)\frac{k}{N}} = \frac{1}{N} \sum_{k=0}^{N-1} F_k e^{-i2\pi n \frac{k}{N}} e^{-i2\pi k} \tag{1.30}$$

By Euler's identity:

$$e^{-i2\pi k} = \cos 2\pi k - i \sin 2\pi k = 1 \tag{1.31}$$

because  $n \in \mathbb{N}$ .

It can say that the coefficients of the DFT are periodic because:

$$X_{N+n} = X_n \tag{1.32}$$

- In the same way, if it replaces  $K'=N-n$ , it is obtain:

$$X_{N-n} = X_n^* \tag{1.33}$$

Where  $X_n^*$  is the conjugate complex.

(1.33) is valid for  $n=1,2,3\dots N/2$ , therefore it is not necessary to sample the whole domain, but only half of it.

In reality, modern software does not implement DFT, but FFT (Fast Fourier Transform).

**The Fast Fourier Transform** is an implementation of the DFT which produces almost the same results as the DFT, but it is incredibly more efficient and much faster which often reduces the computation time significantly.

It is just a computational algorithm used for fast and efficient computation of the DFT [1].

# Chapter 2

## Test bench

All experimental tests were conducted in the laboratory of the Energy Department of the Polytechnic.

Using the measuring instruments it is possible to detect the quantity of fuel injected by the individual injectors, the time histories of the pressures and temperatures in operation.

The signals are acquired through a program that analyzes the current signal coming from the control unit.

### 2.1 Hydraulic circuit

Figure 2.1 shows the diagram of the hydraulic circuit used in the test bench. The following circuits are identified in the figure:

- Low pressure hydraulic circuit;
- High pressure circuit tools ;
- Continuous meters of medium injected flow KMM;
- EMI2 flow-meter
- Meter of instantaneous flow-rate EVI;

**High-pressure pump (HPP)** is driven by a three-phase asynchronous motor, controlled by an inverter, whose nominal characteristics are, depending on the star / delta switching of the power supply:

- Speed 2000/4000 rpm;
- Power 37/34 kW;

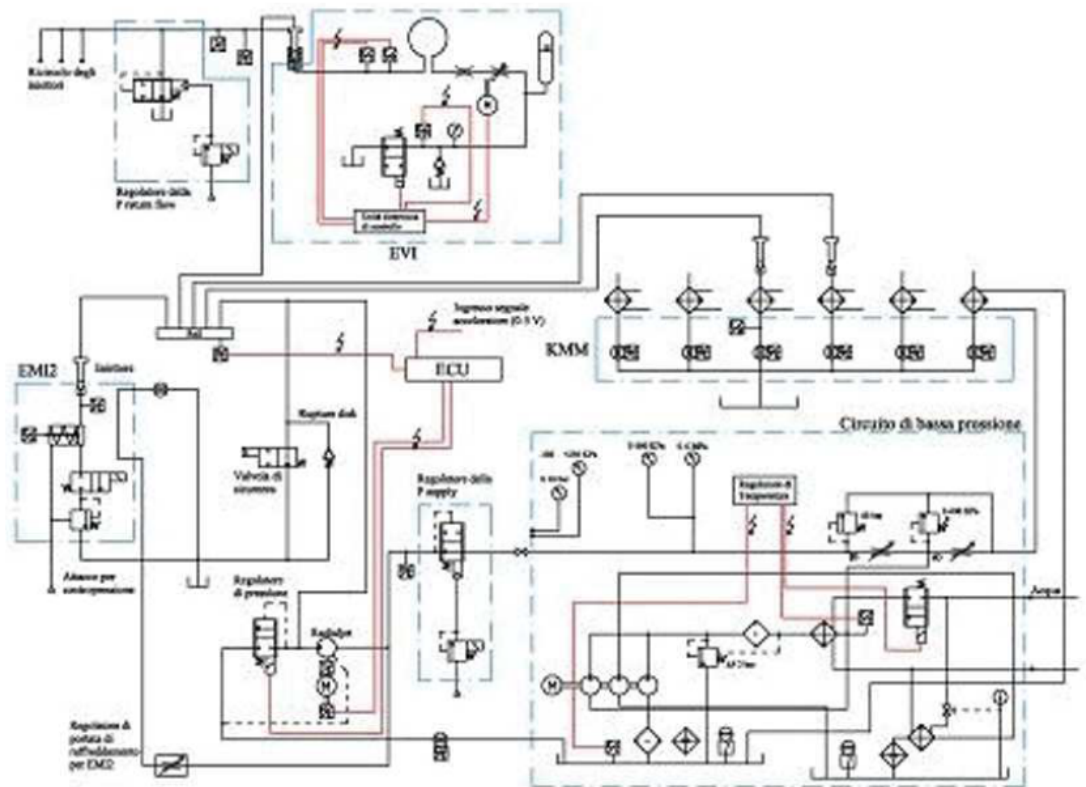


Figure 2.1: Hydraulic circuit of the test bench

- Torque 175/82 Nm.

For protection of the counter from any **torque overloads** caused by injection system malfunctions, a safety **joint** is mounted between the pump and the electric motor.

To avoid explosions the test stand is not powered directly with diesel fuel, but with oil with characteristics that comply with the ISO 4113 standard.

**Low pressure circuit** consists of three priming pumps and a system of sensors and heat exchangers that feed the HPP with a fluid controlled in pressure and temperature and cool the motor that drives the pump itself.

The fluid itself is tapped to cool the EMI2 meter.

Two pneumatically operated solenoid valves are present on the low pressure circuit to regulate the HPP and to regulate the back pressure on the recirculation of the injector pilot stages.

## 2.2 Oil tank

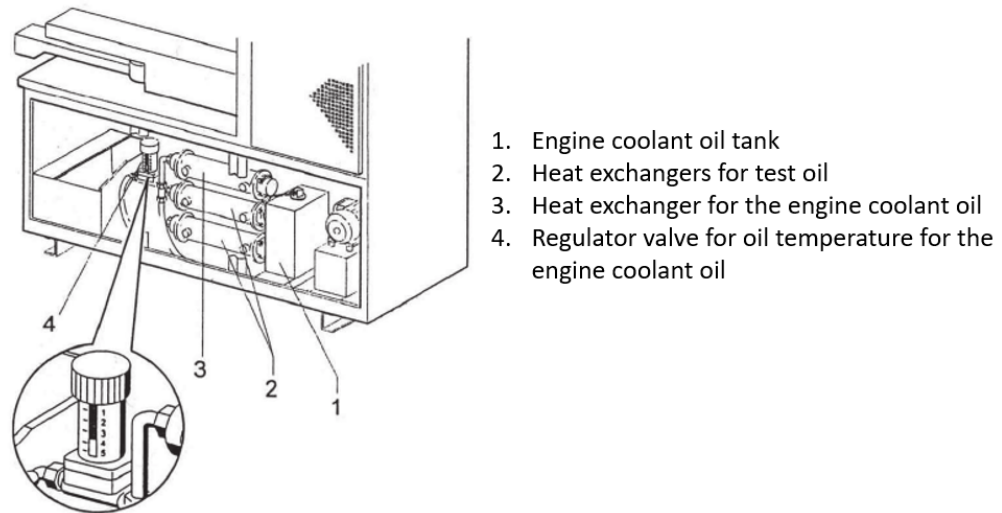


**Figure 2.2:** Oil refrigeration system

The test oil tank has a capacity of 50 liters and is equipped with a thermal probe through which the temperature of the liquid present in it is detected and there is also a coil heater.

A minimum oil level is guaranteed thanks to a float switch.

An additional thermal protection probe is also inserted in this switch, which deactivates the entire bench in the event that the temperature of the test oil, following operating anomalies, exceeds 80°C.

As long as the HPP is not activated, the heating device, if activated, raises the temperature of the oil contained in the tank to the desired value.

The temperature is continuously monitored by means of the thermal probe integrated in the tank.

When the HPP is activated the entire regulation system is controlled in feedback by a second thermal probe, placed at the inlet of the HPP and the coil heater in the tank keeps the HPP suction temperature constant.

## 2.3 Feed pumps and cooling circuits

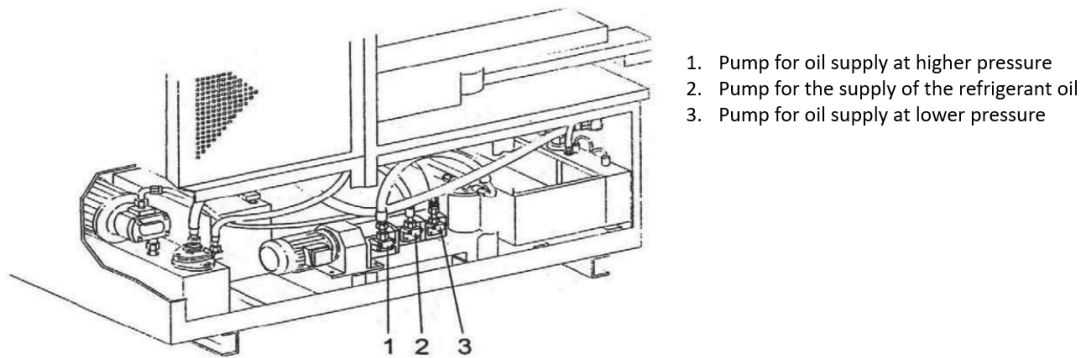


**Figure 2.3:** Feed and cooling pumps

In the **low pressure circuit** there are three pumps mounted in parallel on the shaft of a direct current electric motor.

Pump 2 is the one that makes the oil flow into the cooling circuit of the HPP drive motor.

Pump 2 sucks the oil from the 16-liter tank and discharges it into it at a higher temperature, after the oil has fulfilled its function as engine coolant.

The two remaining pumps are used to supply the HPP and are connected to a device that regulates the pressure and causes pump 1 to reach a maximum pressure of 60 bar and pump 3 to a pressure of up to 6 bar.

**The test oil** is cooled by means of a heat exchanger positioned on the feed pump delivery, downstream of the filter.

The fluid flows through the cooling pipes and transfers its heat to the water that laps them.

The test bench also houses a second 16-liter tank for the refrigeration circuit of the electric motor driving the bench.

The oil in this circuit is cooled in a water heat exchanger, the flow rate of which is selected, this time manually, through an appropriate proportional valve (Item 4 figure 2.2).

Also in this device there is a float switch for safety reasons.

Through a variable throttle the exchanger is fed with an appropriate quantity of water taken from the water mains; regulation of the throttle is carried out in closed loop by an electronic control unit.

## 2.4 KMM flow-meter

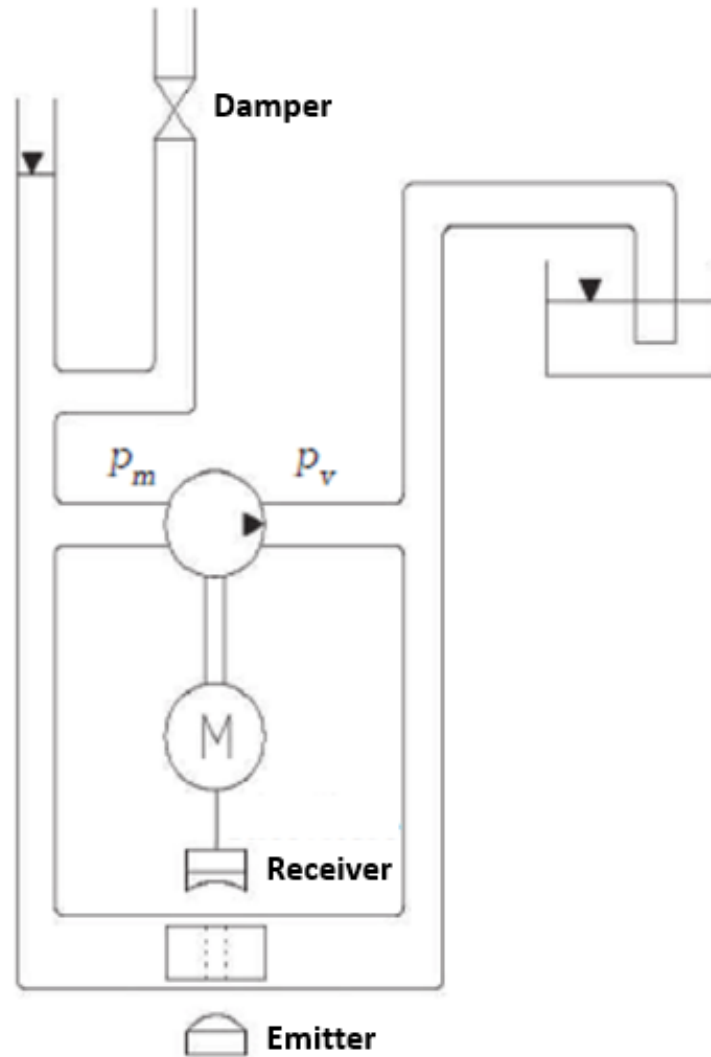


**Figure 2.4:** KMM meter's scheme

KMM meters have the same operation as traditional volumetric flow meters, but have the difference of having a mechanical-optical device which increases the accuracy of the measurement.

The injected flow rate (in this case in the chamber) is directed towards a damper

which reduces the pressure oscillations of the fluid.

There is, therefore, an accumulation of fluid on the left side of the circuit.

The right side is directly connected to the tank.

Other elements present in the KMM system are a positive displacement pump driven by an electric motor and a floating plunger.

The plunger has a radial through hole through which a light beam from an emitter passes (as seen in the figure 2.4) which is intercepted by a receiver.

A signal is generated which is then sent to the engine.

**In the rest situation (no injection)** the pressures in the two branches  $p_m$  and  $p_v$  are equal to those of the tank, the plunger is also in equilibrium with the hole positioned so as to give the receiver the entire light beam projected by the emitter. Following the accumulation of fluid, the value of  $p_m$  increases with respect to  $p_v$ , the floating piston moves and the receiver does not take on the entire light beam. This is transformed into a signal that is sent to the motor which drives the pump with a rotation speed proportional to the degree of obscuring of the sensor.

In this way  $p_m$  begins to decrease and the plunger returns to the equilibrium position and the pump begins to decrease its rotation speed.

The servo system installed in the meter tries to keep  $p_m$  and  $p_v$  equal, therefore by means of the mechanical-optical feedback device it correlates the number of revolutions carried out by the pump to the injected volume flow.

## 2.5 EMI2 meter

The EMI2 measuring instrument senses the displacement of a piston which limits the cylindrical chamber on which the injector is mounted.

In this way the injected volume is calculated. Using a thermocouple, the temperature in the injection chamber is measured and based on the counter pressure value used, the meter also gives an indication of the injected mass.

For the correct functioning of the EMI2 meter it is necessary:

- An encoder;
- A nitrogen bottle to guarantee the required back pressure (nitrogen is used rather than compressed air to avoid the formation of an air-oil mixture);
- Cooling oil;

For each engine cycle it is possible to measure the preliminary, main and final injected quantity, in addition to the overall and cumulative quantities.

When the piston reaches the end of its stroke, the normally closed two-position solenoid valve allows the fluid to be evacuated from the chamber.

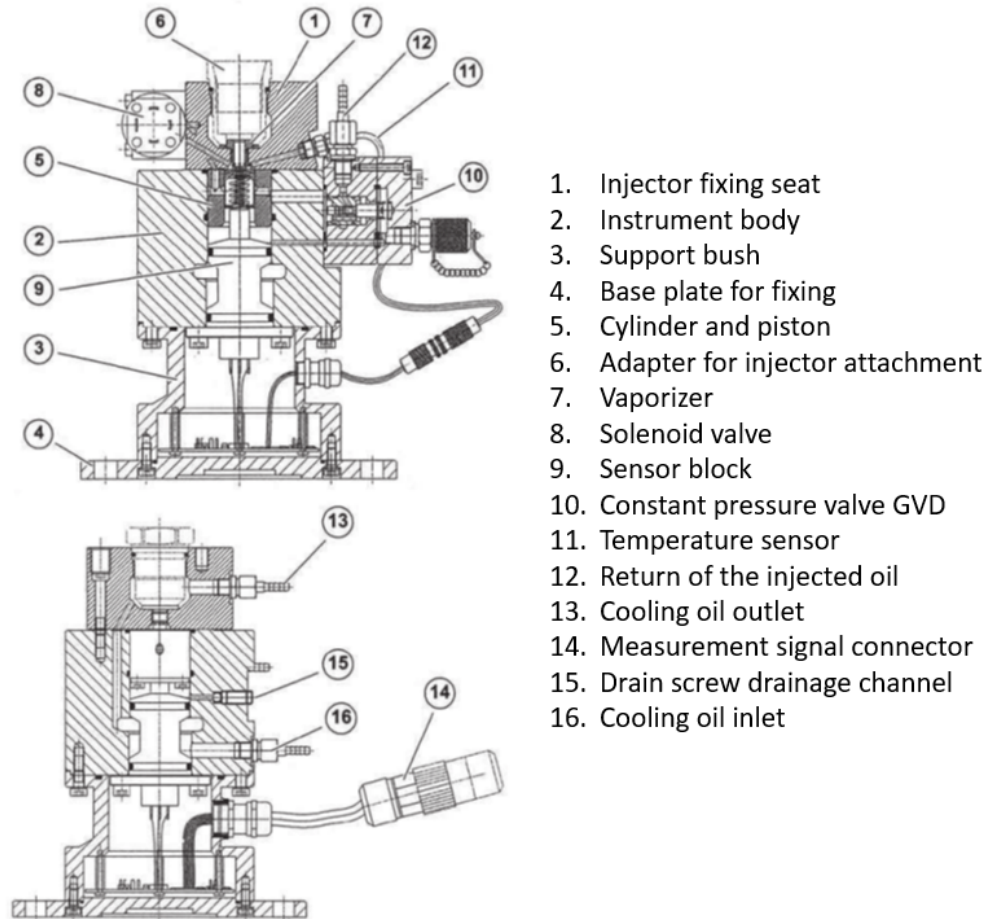
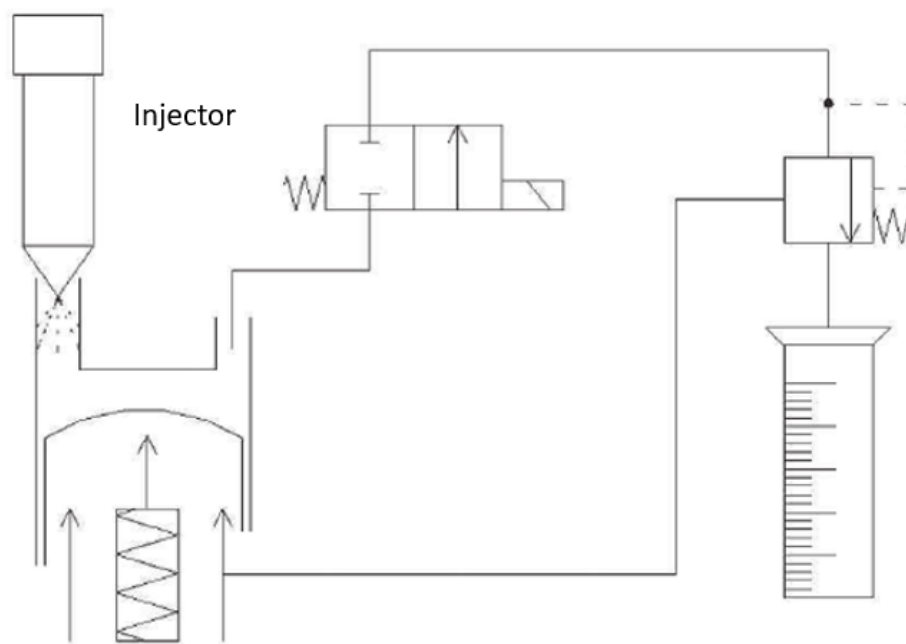


Figure 2.5: Structure of EMI2 meter

During the injection phase, the solenoid valve remains closed and the piston descends due to the filling of the chamber placed above it. The volume of injected liquid is associated with the displacement of the piston. The piston position is always controlled by a position transducer. The pressure in the chamber is known as it must be such as to counterbalance the back pressure in order to guarantee the balance of the piston. At the end of the injection the solenoid valve opens and the piston, under the action of the spring, releases the liquid from the measuring chamber. The next figure (2.6) shows an operational diagram of the EMI2 meter:



**Figure 2.6:** Operating diagram of EMI2 meter

The meter controls the solenoid valve so that the chamber never empties completely and the liquid that remains in the chamber is called liquid stop and its value is adjustable.

When the injections are small enough not to guarantee the permanence of the liquid stop, the emptyings themselves do not take place at each injection, but periodically and the instrument communicates this to the user by means of a flashing signal.

In this way, correct functioning is guaranteed in every possible situation.

The graduated burette is used in the calibration phase, the liquid is collected and

is used as a term of comparison for the cumulative quantity detected in a certain number of injections.

In the mechanical configuration used, the maximum measurable single injection quantity is  $600 \text{ mm}^3$  with an accuracy of  $\pm 0.1\%$  of full scale which corresponds to an absolute precision of  $\pm 0.6 \text{ mm}^3$ .

## 2.6 EVI meter

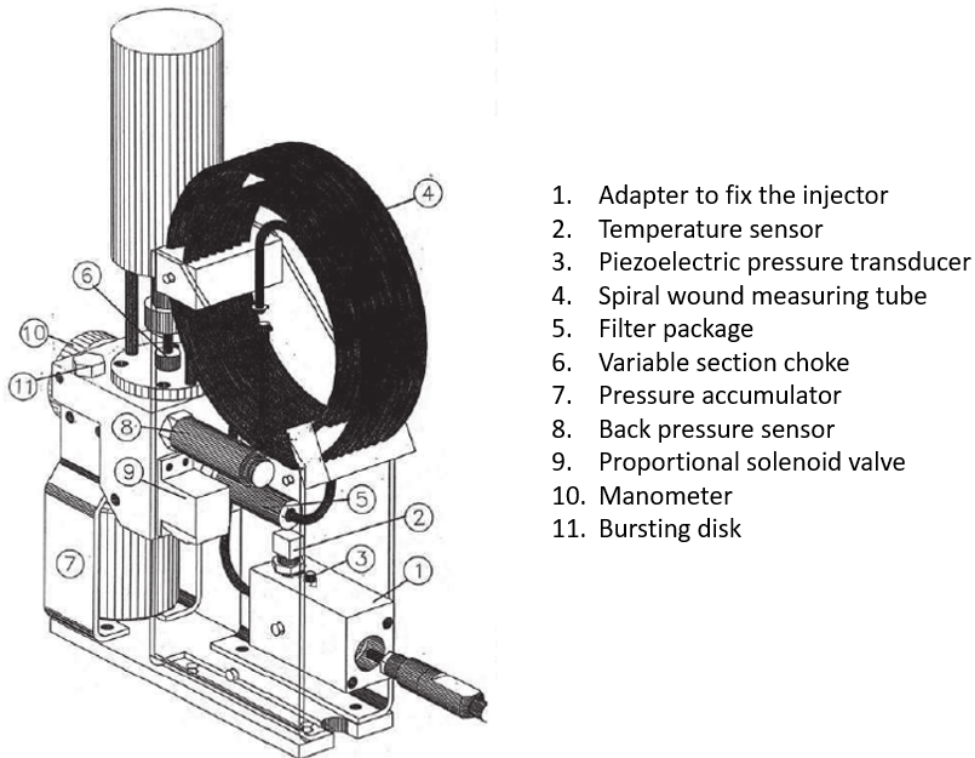


**Figure 2.7:** Structure of EVI meter

EVI meter detects the pressure increase due to the injection of the fluid into a capacity consisting of a spiral-wound tube.

The measured pressure increase leads to the injected flow rate.

The damper section is varied by a stepping electric motor; the variation of the section determines a variation of the damping of the system and, therefore, of the perturbation of the pressure wave of the fluid.

The filter package attenuates the pressure wave, so it has the same effect as the damper.

The bursting disk is an overpressure protection device in the event of a malfunction of the back pressure regulator valve.

To understand how the meter works it is necessary to see the next figure (Figure 2.8).

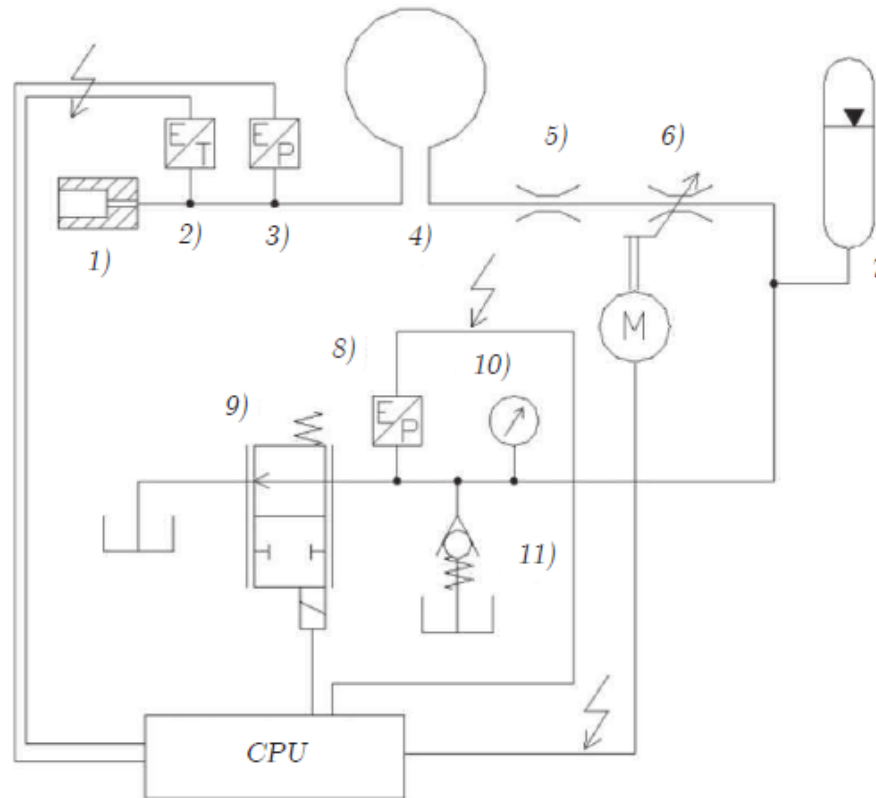


**Figure 2.8:** Operating diagram of EVI meter

The injector injects the fluid into the spiral measuring tube, this causes an increase in pressure in the tube, directly proportional to the mass of the fluid entering.

The piezoelectric pressure sensor detects the pressure increase as a variation with respect to the average pressure value (piezoelectric sensors do not detect the absolute pressure value).

The acquired value is sent to the electronic acquisition system.

The injection generates a pressure wave that propagates on the spiral wound tube and this wave is attenuated thanks to the damper and thanks to the filter package.

When the perturbation is completely damped, the entire quantity of injected fluid passes through the choke.

Downstream of the throttle, through the solenoid valve, it is possible to adjust the

back pressure to simulate all the conditions of our interest.

By means of physical and mathematical considerations it can be shown that:

$$du = \frac{dp}{\rho a} \quad (2.1)$$

- $du$  is the speed increase due to the pressure wave perturbation;
- $dp$  is the pressure variation;
- $\rho$  is the density of the fluid;
- $a$  is the speed of sound in the fluid at rest.

Through the piezoelectric pressure sensor the EVI measures the pressure variation  $dp$ , therefore it is possible to calculate the velocity of the inlet fluid through the numerical integration of the above-mentioned equation.

The initial speed condition can be zero because between two consecutive injections the measuring tube and the variable throttle completely dampen the pressure wave. The volumetric flow rate can be calculated as follows:

$$Q = u \times A \quad (2.2)$$

$A$  is the section of the injection chamber of the EVI.

Mass flow rate can be calculated:

$$\dot{m} = \rho u A \quad (2.3)$$

By integrating equation (2.3), the total injected mass is obtained:

$$M = \int_{t_0}^{t_1} \dot{m} dt \quad (2.4)$$

$t_0$  and  $t_1$  are the initial and final instants of the injection.

This procedure presents measurement uncertainties.

It is necessary to calibrate the procedure by comparing the injected fluid volume values calculated with the EVI with those measured by EMI2 with the same injector.

It should be remembered that EVI provides an indication of the injection characteristic and EMI2 provides an indication of the volume injected.

Therefore, the calibration procedure mentioned above has rather the purpose of ensuring that the measurements performed by the EVI, and the procedure to compute the instantaneous flow rate are congruent with the indications provided by EMI2, and that therefore they can ultimately be deemed reliable. [2]

# Chapter 3

## Before algorithms

### 3.1 Presentation of the problem

Goal of the algorithm is to improve the flow diagram obtained by means of a fluid dynamic model which allows to compute the instantaneous flow rate of fuel entering the combustion chamber of a common rail diesel engine.

The fluid dynamic model allows to calculate the flow rate in this way:

$$G(t) = \frac{A}{l} \left( \int_0^t \Delta p dt - \langle \Delta p \rangle \right) \quad (3.1)$$

where:

- A is the Area of the flow-meter;
- l is the distance between the two pressure sensors;
- $\Delta p$  is the pressure drop calculated by the two sensors.

The experimental tests performed allow to compute the flow rate considering pressure variations ranging from 600 bar to 2000 bar.

It is possible to note that by diagramming what has been obtained from the experimental points, the graph of the flow presents errors that have no physical value.

After the injector fires into the combustion chamber the fuel should have a flow rate value equal to 0 (precisely it will not be 0 because the mechanical system being analyzed is highly dynamic, therefore it will continuously show variations in flow rate between positive values and negative values), but this does not happen because we work with very high pressure variations and the sensors will not be able to provide an accurate estimate at all.

It should be emphasized that more than 100 tests have been analyzed at different

pressures, at different ET (energizing times), so the same experimental test will not be proposed.

The next figures show 3 examples (low, intermediate and high pressure) to better understand the problem:

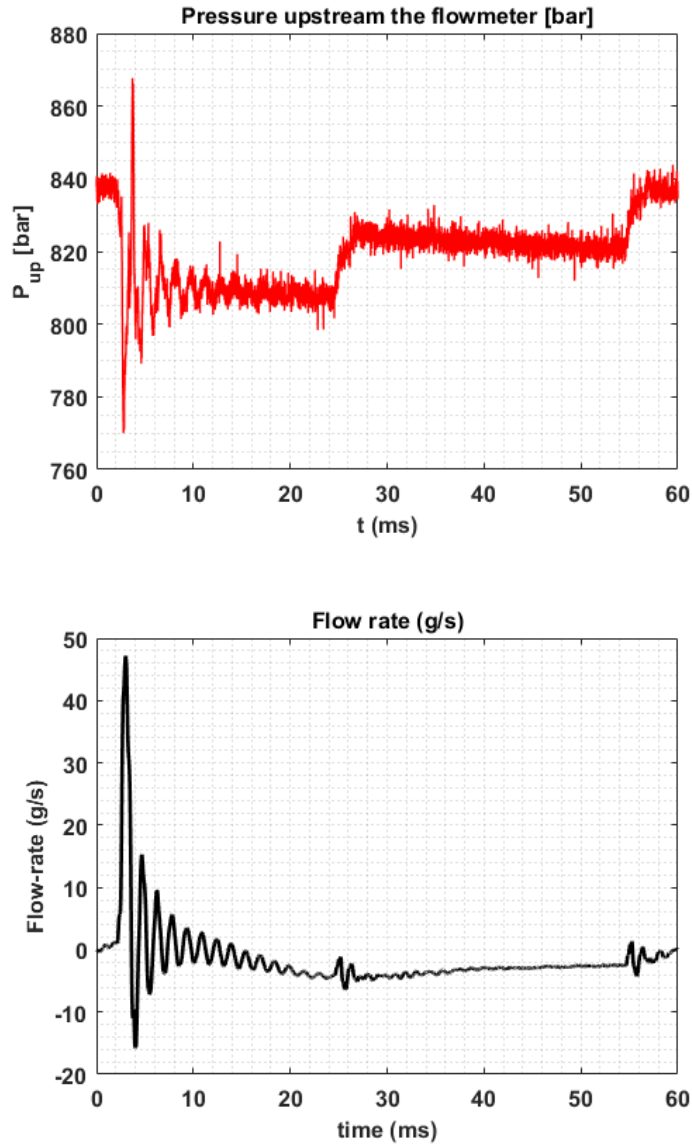


**Figure 3.1:** Low pressure: 800 bar, regulation with FMV,  $700 \mu\text{s}$  ET, respectively pressure measured by the upstream sensor and instantaneous flow rate

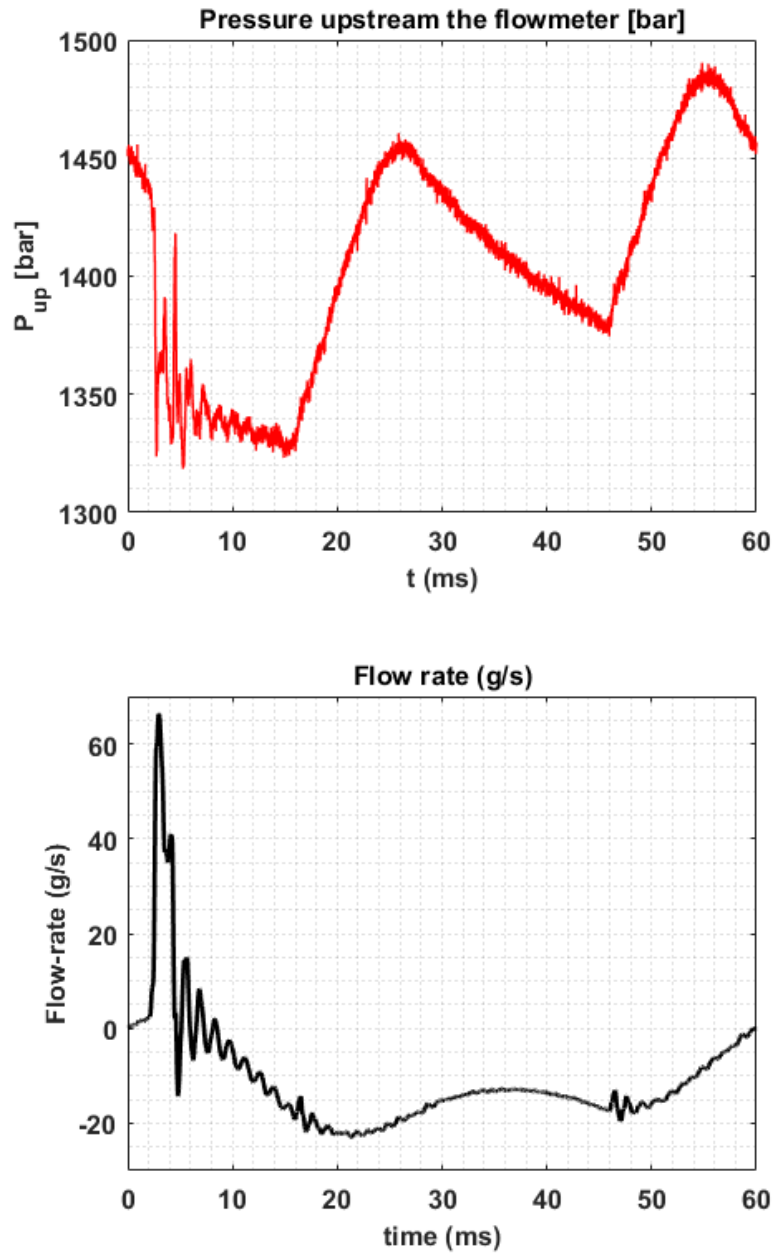


**Figure 3.2:** Intermediate pressure: 1400 bar, regulation with PVC, 1000  $\mu$ s ET, respectively pressure measured by the upstream sensor and instantaneous flow rate

It is emphasized that all the calculations carried out refer only to the pressure upstream of the flow meter and that most of the experimental tests refer to the

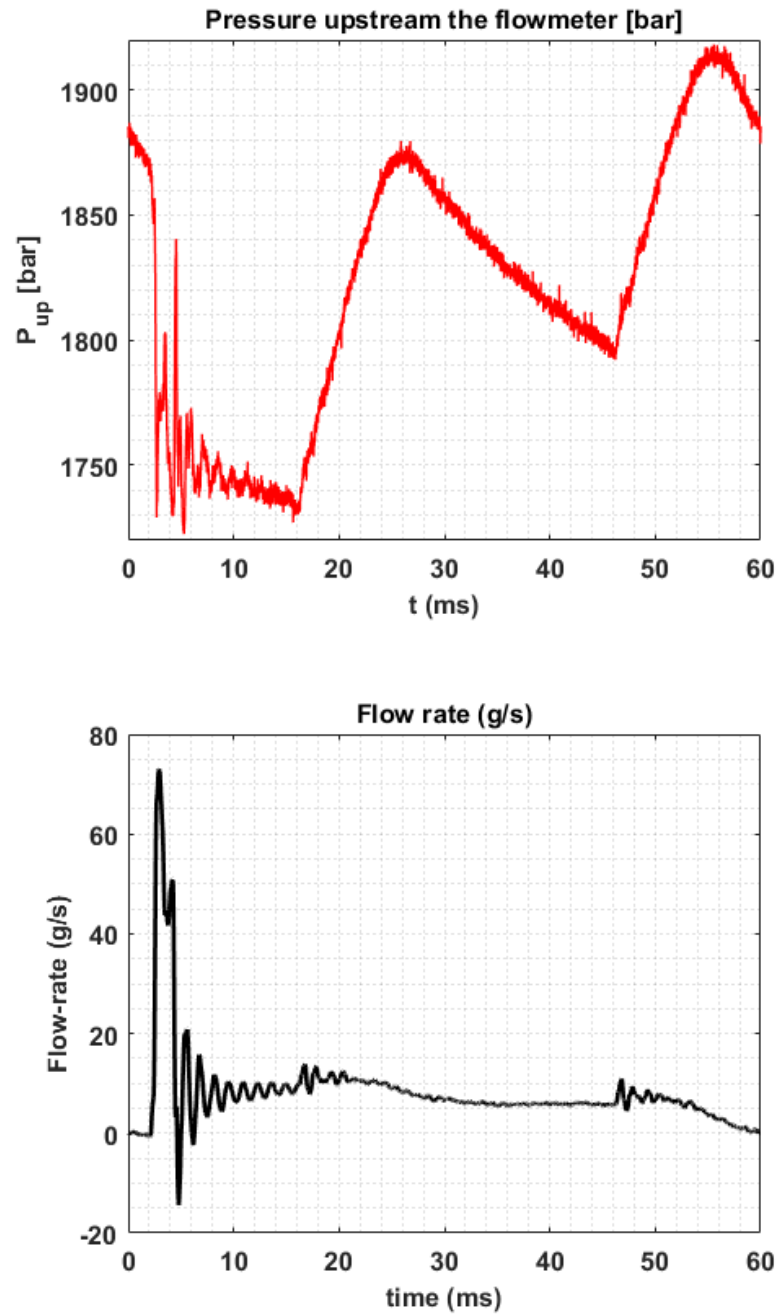


**Figure 3.3:** High pressure: 1800 bar, regulation with PVC, 1000  $\mu$ s ET, respectively pressure measured by the upstream sensor and instantaneous flow rate

rotation speed of the pump of 1000 rpm.

From the graphs highlighted it is evident that the output flow rate is wrong, therefore it is necessary to introduce a methodology to solve the problem.

By carefully analyzing the Fast Fourier Transform of the pressure signal upstream of the flow meter, in all experimental tests, at different rotation speeds, for different conditions, a common point is noted: **a peak at a significant frequency for each test.**

Paying attention to this effect, the respective 3 Fourier spectra of the pressure signals represented above are reported:

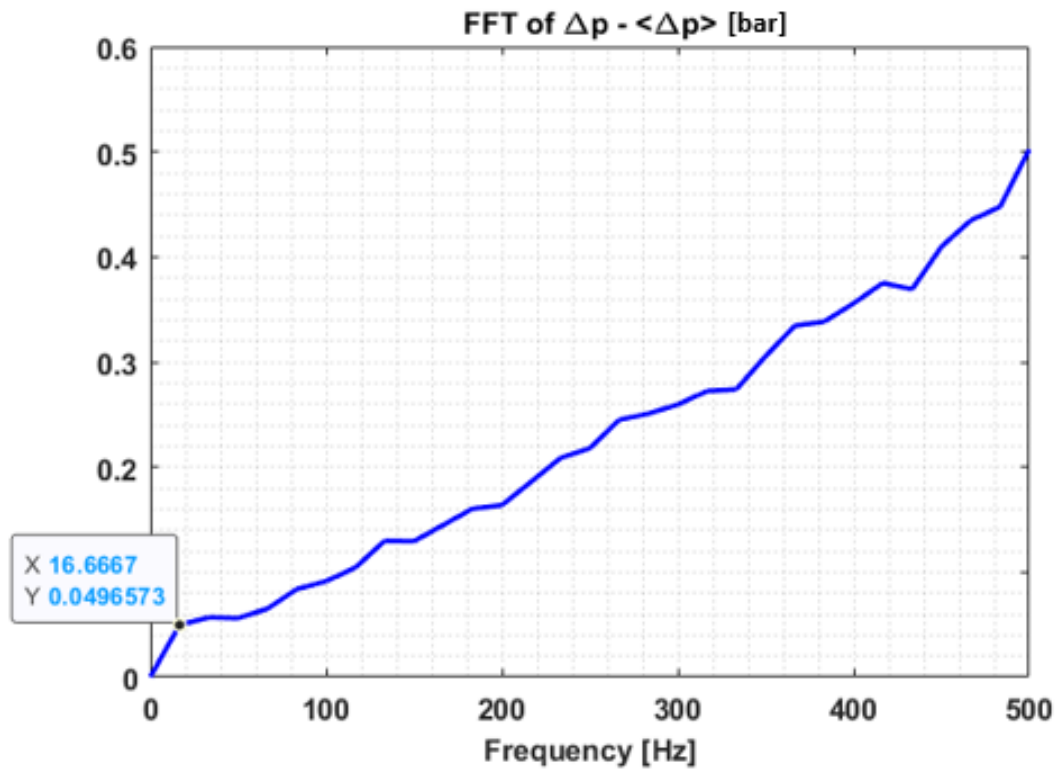


**Figure 3.4:** Fourier spectrum of the pressure signal with  $P_{up}=800\text{bar}$ ,  $ET=700\mu\text{s}$ , FMV

It is necessary to note that for each spectrum a frequency can be identified which must be identified (in the cases that have been seen 16.67 Hz and 33.33 Hz).

The idea is therefore to carry out some operation on the Fourier spectrum of the parameter  $\Delta p - \langle \Delta p \rangle$ , but to make everything computerized it is necessary to identify, for each spectrum, this remarkable frequency.

The next step is to do just that.

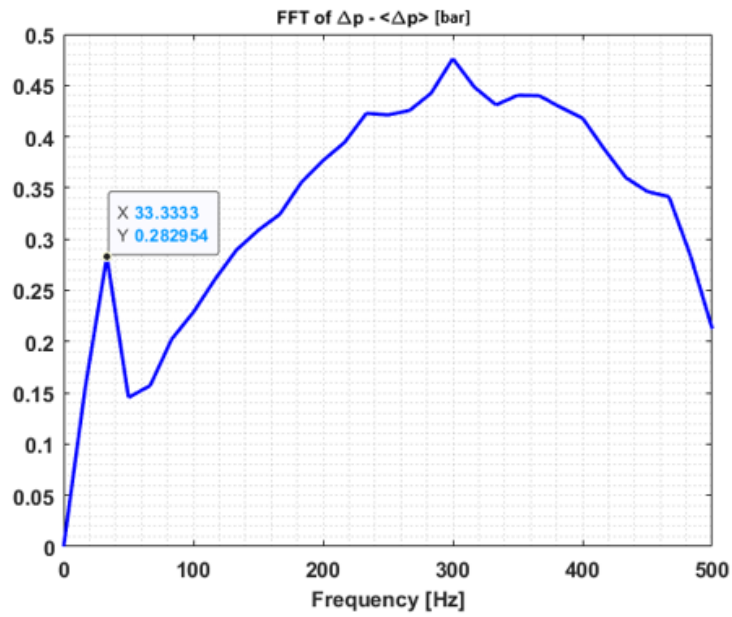


**Figure 3.5:** Fourier spectrum of the pressure signal with  $P_{up}=1400$ bar,  $ET=1000$   $\mu s$ , PCV

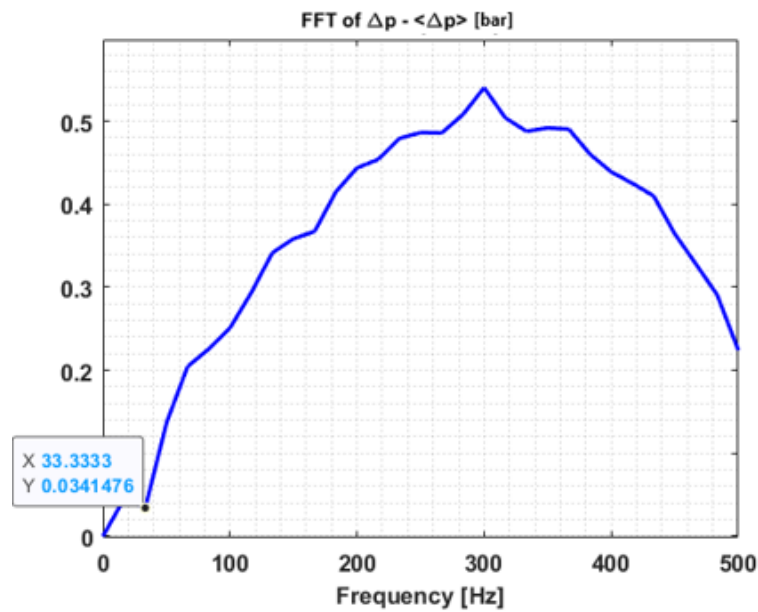


**Figure 3.6:** Fourier spectrum of the pressure signal  $P_{up}=1800$ bar,  $ET=1000$   $\mu s$ , PCV

## 3.2 Multiplicative factor MF and linearization of the spectrum

By doing the FFT of the parameter  $P_{up} - \langle P_{up} \rangle$  it's possible to identify the frequency on which we have to work (in the previous cases we expect a peak at 16.67 Hz and two peaks at 33.33 Hz).

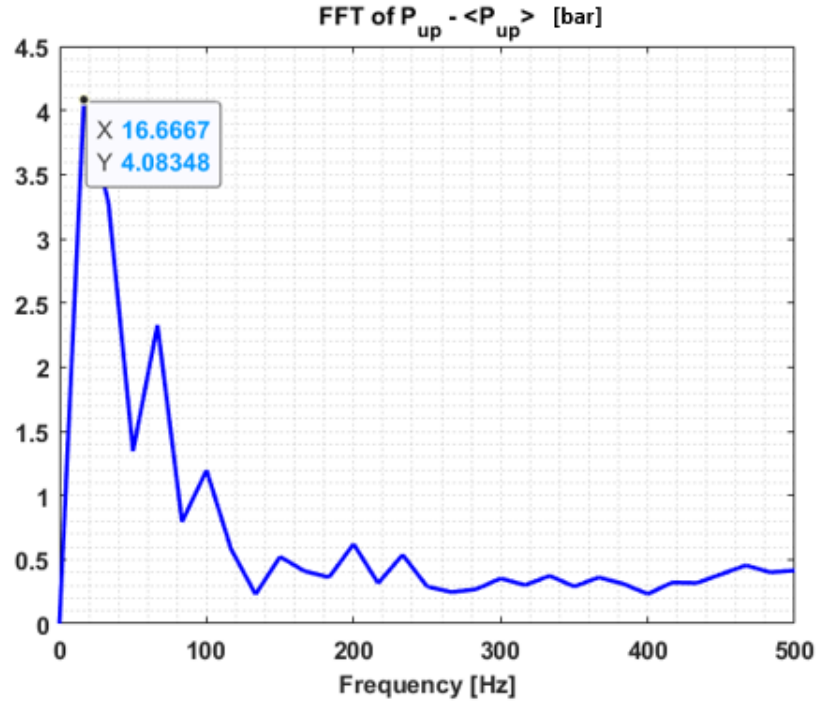


**Figure 3.7:** Fourier spectrum of the pressure signal  $P_{up} - \langle P_{up} \rangle$  with  $P_{up} = 800$  bar,  $ET = 700 \mu s$ , FMV regulation

Now it's possible to identify the remarkable frequency and identify a methodology to solve the problem.

The other 2 spectra (Figure 3.8 and Figure 3.9) are reported for completeness to clarify the results.

After careful analysis, it was understood that the goal is not to cancel the contribution of the spectrum at the considerable frequency, but to linearize the spectrum locally, in order to eliminate the peak.

It has been noted that multiplying  $P_{up}$  with an adequate multiplication factor MF (totally random) results in convergence, the contribution of the spectrum is eliminated and the range seems to stabilize.

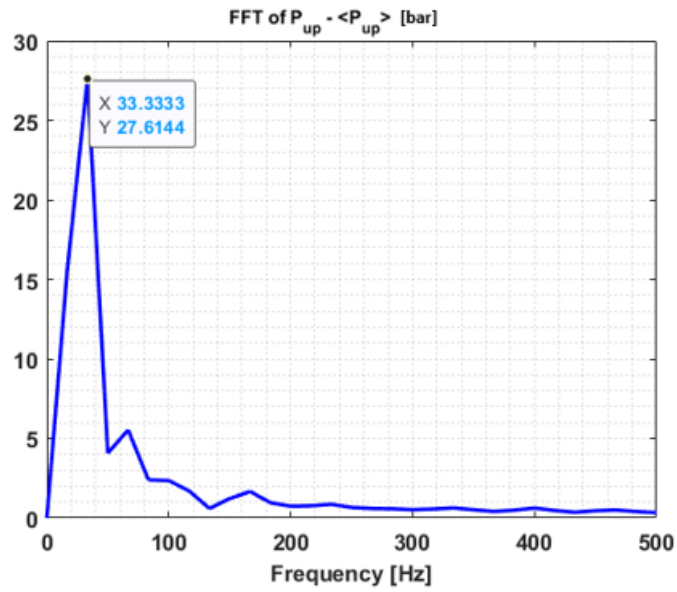


**Figure 3.8:** Fourier spectrum of the pressure signal  $P_{up} - \langle P_{up} \rangle$  with  $P_{up}=1400\text{bar}$ ,  $ET=1000 \mu\text{s}$ , PCV regulation

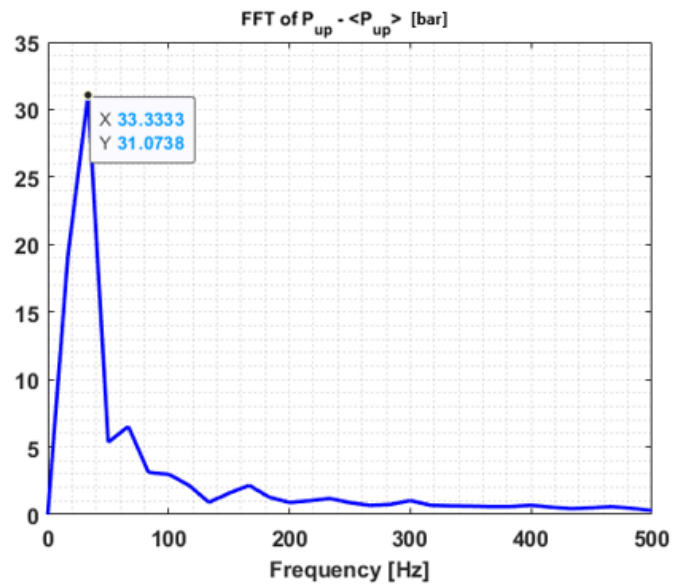


**Figure 3.9:** Fourier spectrum of the pressure signal  $P_{up} - \langle P_{up} \rangle$  with  $P_{up}=1800\text{bar}$ ,  $ET=1000 \mu\text{s}$ , PCV regulation

Now let's analyze the behavior of the different graphs when the different MFs change; it is necessary to take into account the order of magnitude of the various multiplying factors (Figures 3.10 and Figure 3.11).

In figure 3.10 we have constructed the graph of the instantaneous flow rate considering a range of MF from 1.1 to 0.9 with step 0.05, while in figure 3.11 the same range, but with a smaller discretization step 0.01. None of the graphs converge

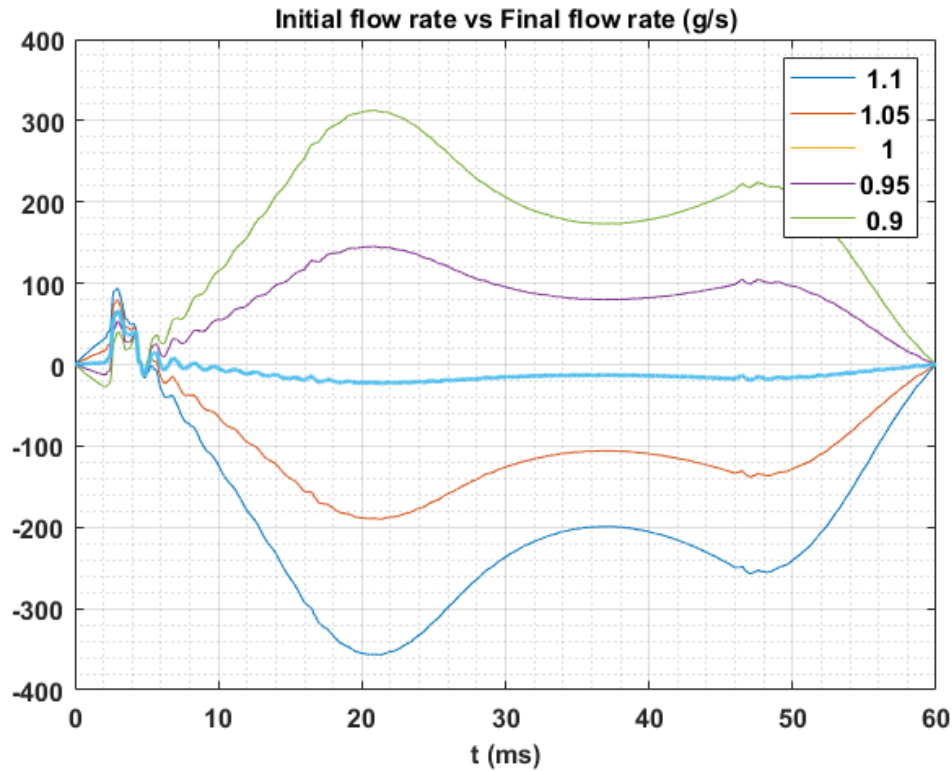


**Figure 3.10:** Instant flow graphs with MF from 1.1 to 0.9 with discretization step 0.05 ( $P_{up}=1400$  bar,  $ET=1000 \mu s$ , PVC regulation)

because the unit of measurement of the multiplicative coefficient is wrong, so for each diagram that is taken into consideration, the correct MF value must be considered.

Obviously it is possible, at the limit, to use an infinitesimal multiplicative coefficient, but this implies a very high computation burden.

Another property that the algorithm must take into account is that the execution time of the program must be as low as possible: **having a really efficient algorithm, but slow in terms of computational burden is a poor result.**

With a lower discretization step it is obtained:

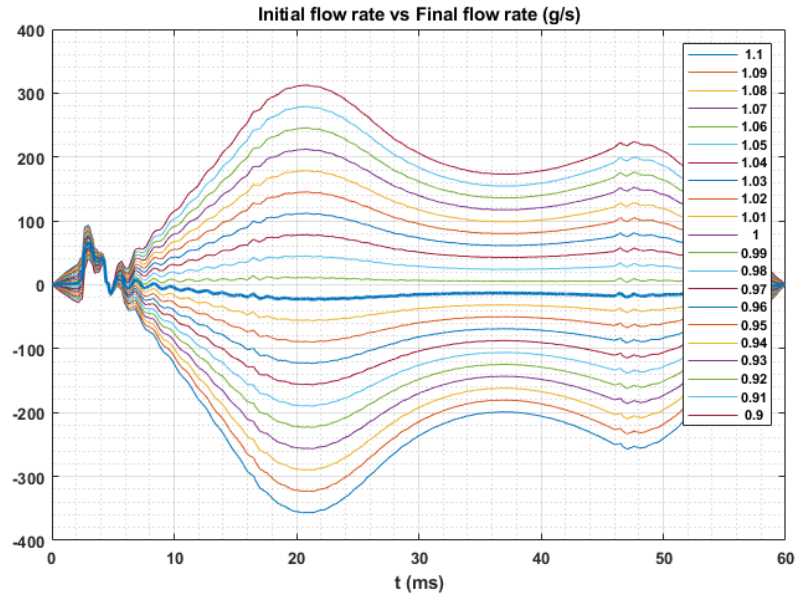


**Figure 3.11:** Instant flow graphs with MF from 1.1 to 0.9 with discretization step 0.01 ( $P_{up}=1400$  bar,  $ET=1000 \mu s$ , PVC regulation)

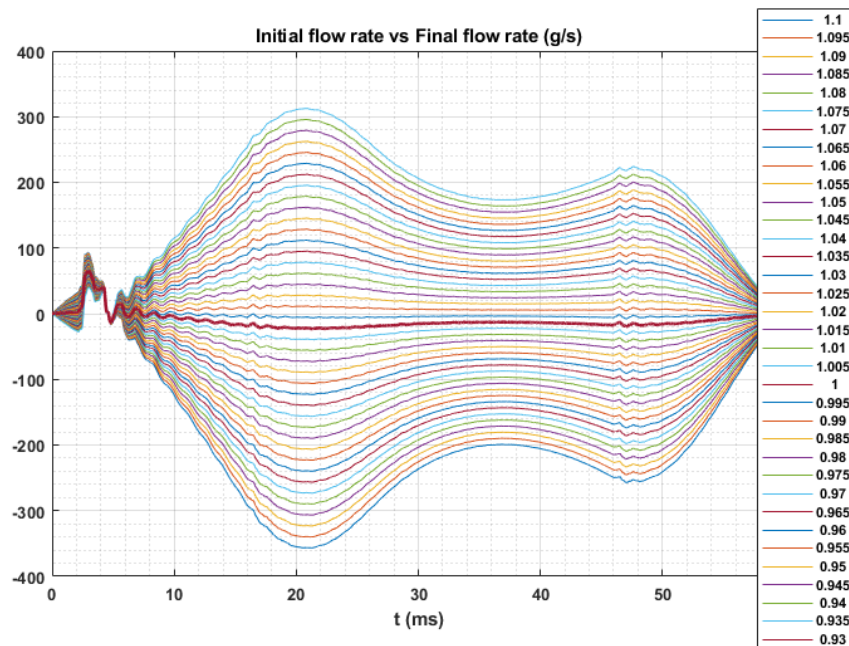


**Figure 3.12:** Instant flow graphs with MF from 1.1 to 0.9 with discretization step 0.005 ( $P_{up}=1400$  bar,  $ET=1000 \mu s$ , PVC regulation)

The result with figure 3.11 is 0.99, but decreasing the discretization step we see that it converges on 0.9927.

The comparison is now made between the initial and final flow rate with MF corrected and identified by means of the implemented algorithms. .

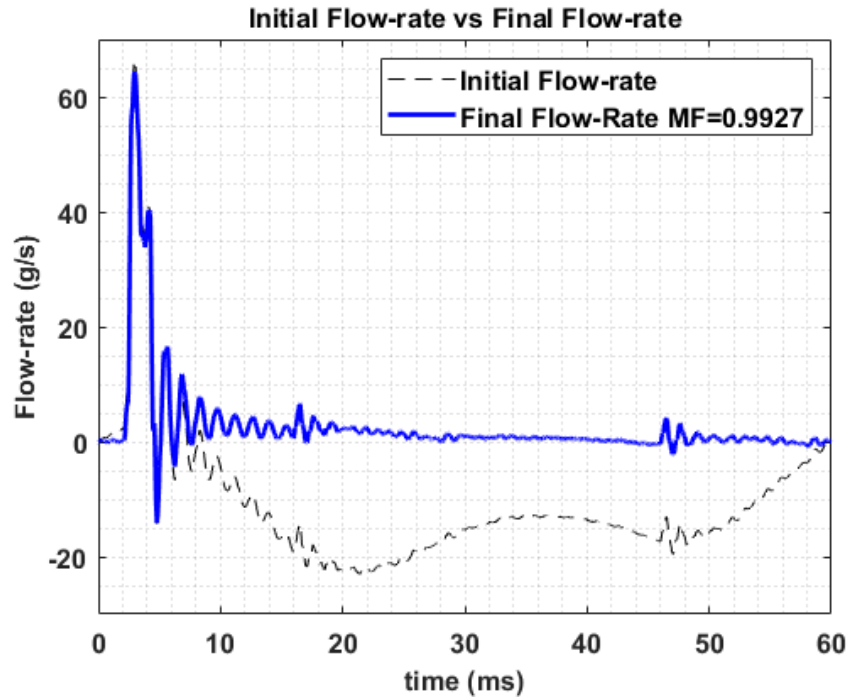


**Figure 3.13:** Initial Flow-rate vs Final Flow rate with MF=0.9927

From the behavior of the spectra it is possible to notice some fundamental characteristics that will be taken into consideration during the implementation of the algorithm.

Obviously, all the discourse made about the discretization step, the computational burden applies to the spectra and we must take this into account. From figure 3.14 it's possible to notice that the spectrum corresponding to 0.99 has the lowest slope, but making the comparison between the initial one and the one to which  $MF = 0.9927$  corresponds there is a clear and precise correspondence.

From figure 3.15 it is perfectly clear that a **linearization of the Fourier spectrum must be performed**.

it is therefore necessary to define an intersection frequency that will serve as a control parameter (in addition to MF) to make the spectrum diagram fit well and, consequently, the flow rate one.

In conclusion it can be stated that, from all the considerations made, to solve the problem there are 2 parameters that influence the methodology: the intersection

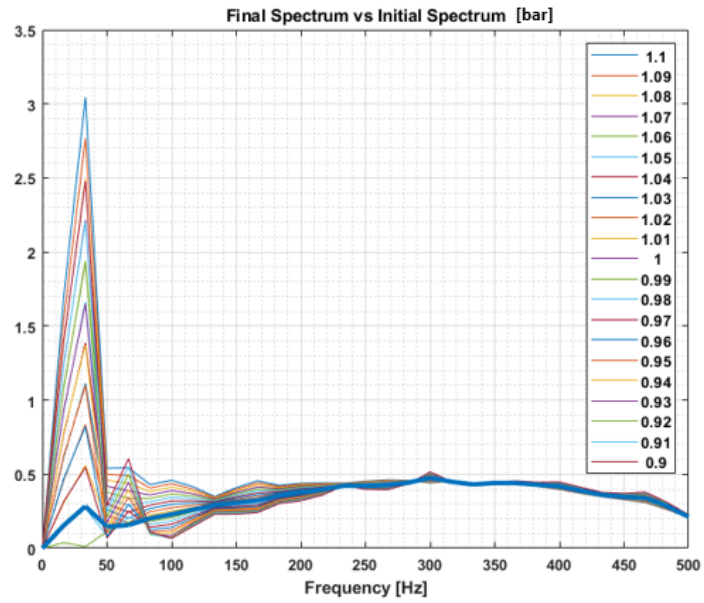


**Figure 3.14:** Spectra graph with MF from 1.1 to 0.9 with discretization step 0.01 ( $P_{up}=1400$  bar,  $ET=1000 \mu s$ , PVC regulation)

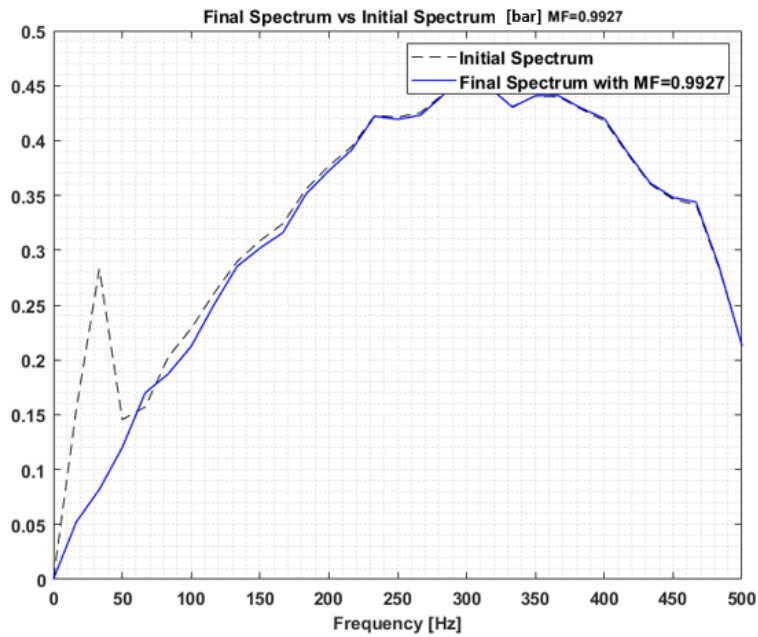


**Figure 3.15:** Initial Spectrum vs Final Spectrum with MF=0.9927

frequency which allows to linearize the spectrum and eliminate the peak and the MF coefficients that correct the flow rate.

These two must be connected and everything will be explained in the following paragraphs when the algorithm is explained in depth.

### 3.3 Extension to all situations

A characteristic that the algorithm must have is **generality**, all possible situations must be considered and, obviously, in all cases it must work.

Up to now it has been considered a classic mechanical system, with a fixed rotation speed (1000rpm), with precise regulation techniques, but we must get away from all this.

The following changes will be considered:

- Different pump rotation speed;
- Different pressure levels and different ET;
- Injection that is not for  $t = 0$ , therefore also intermediate injection.

**Figure 3.16** analyzes a different situation.

The pumping elements of the pump used in the mechanical system are no longer 2, but 3. The rotation speed is always the same (1000 rpm), but a total transformation of the Fourier spectrum is noted.

The results of the algorithm (in blue) make the correction.

It is possible to note, again in the Fourier spectrum diagram, the interpolating line that has the intersection at a frequency that respects certain requirements of the algorithm (concept explained in the previous paragraph and which will be deepened in the following paragraphs).

It is possible to note that the linearization resulted has a beneficial effect on the flow rate graph which was initially completely wrong.

**Figure 3.17** analyzes a different situation.

The pumping elements, also this time, are 3.

The rotation speed is always the same (1000 rpm), but the injection no longer takes place in the initial instant, but in an instant of intermediate time.

It is always possible to note that the spectrum always assumes a strange shape, but the goal is always to linearize it at the frequency recognized by the Fourier spectrum of the magnitude  $P_{up-} < P_{up} >$ .

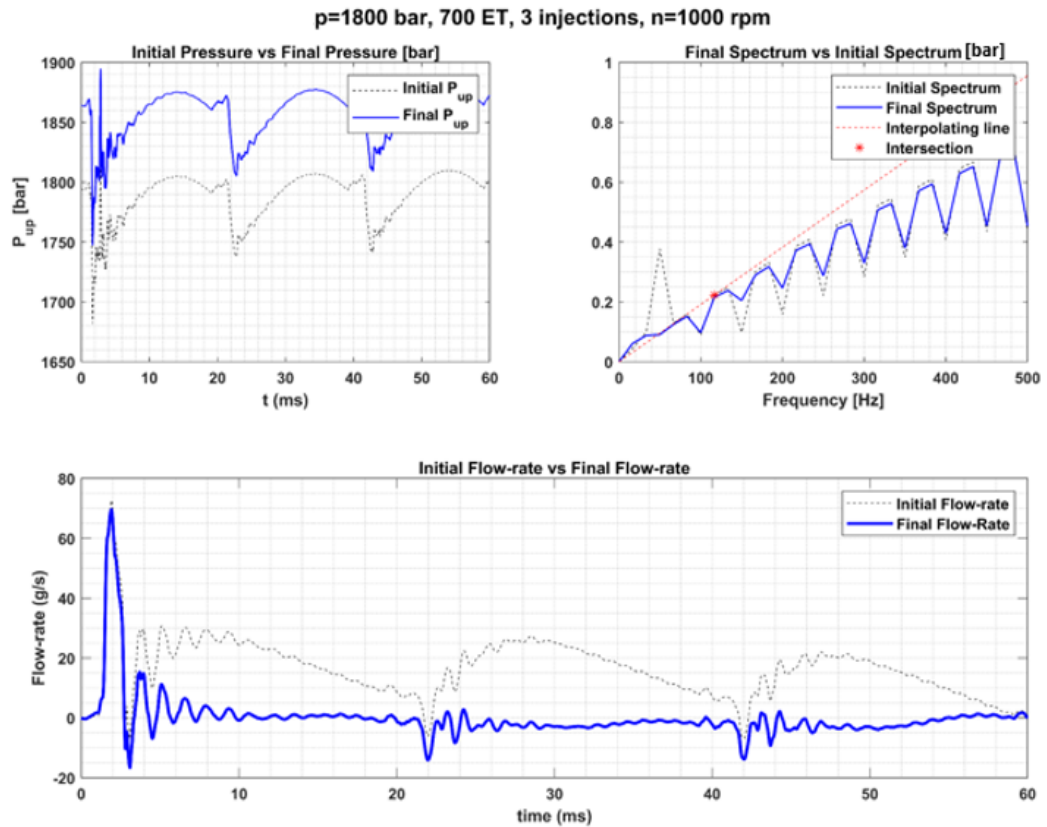


**Figure 3.16:** Respectively graph of  $P_{up}$  with reference value 1800 bar, pump equipped with 3 pumping elements, Fourier spectrum and flow rate graph with PCV regulation,  $n = 1000$  rpm

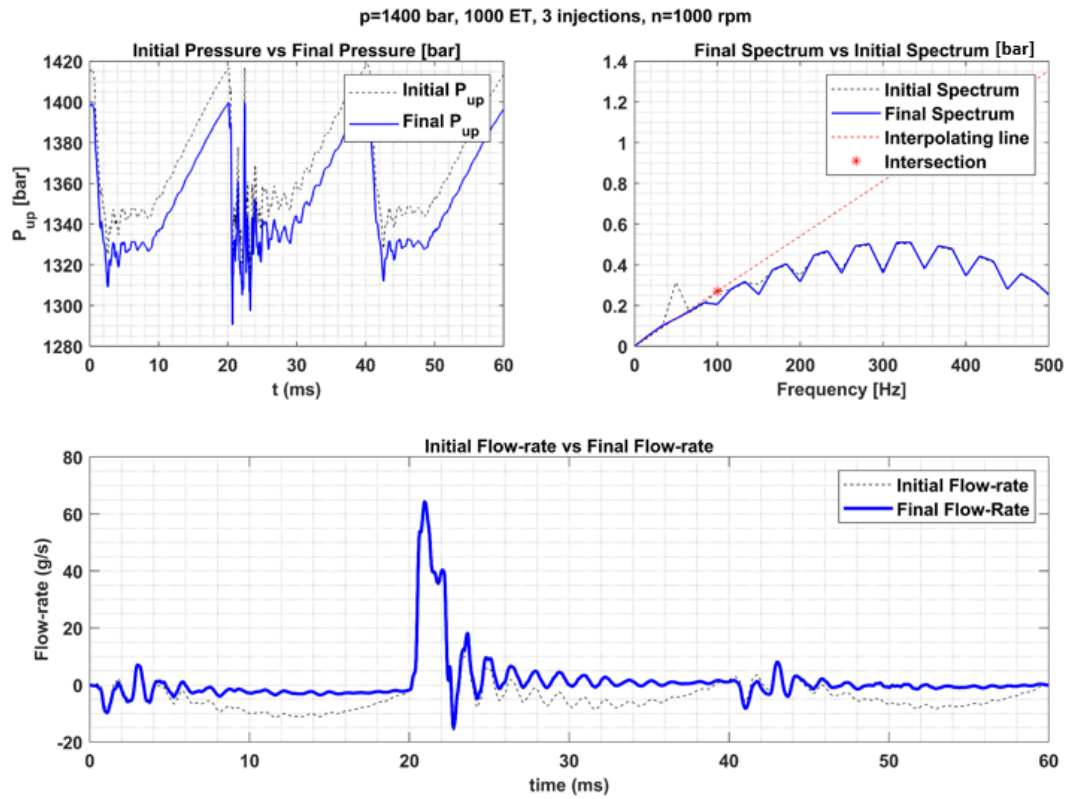


**Figure 3.17:** Respectively graph of  $P_{up}$  with reference value 1400 bar, pump equipped with 3 pumping elements, Fourier spectrum and flow rate graph with PCV regulation,  $n = 1000$  rpm

Consider another situation: FMV regulation, average pressure value upstream of the flow meter 1800 bar, 1000  $\mu\text{s}$  ET. Consider the initial pressure, flow and Fourier spectrum graphs.

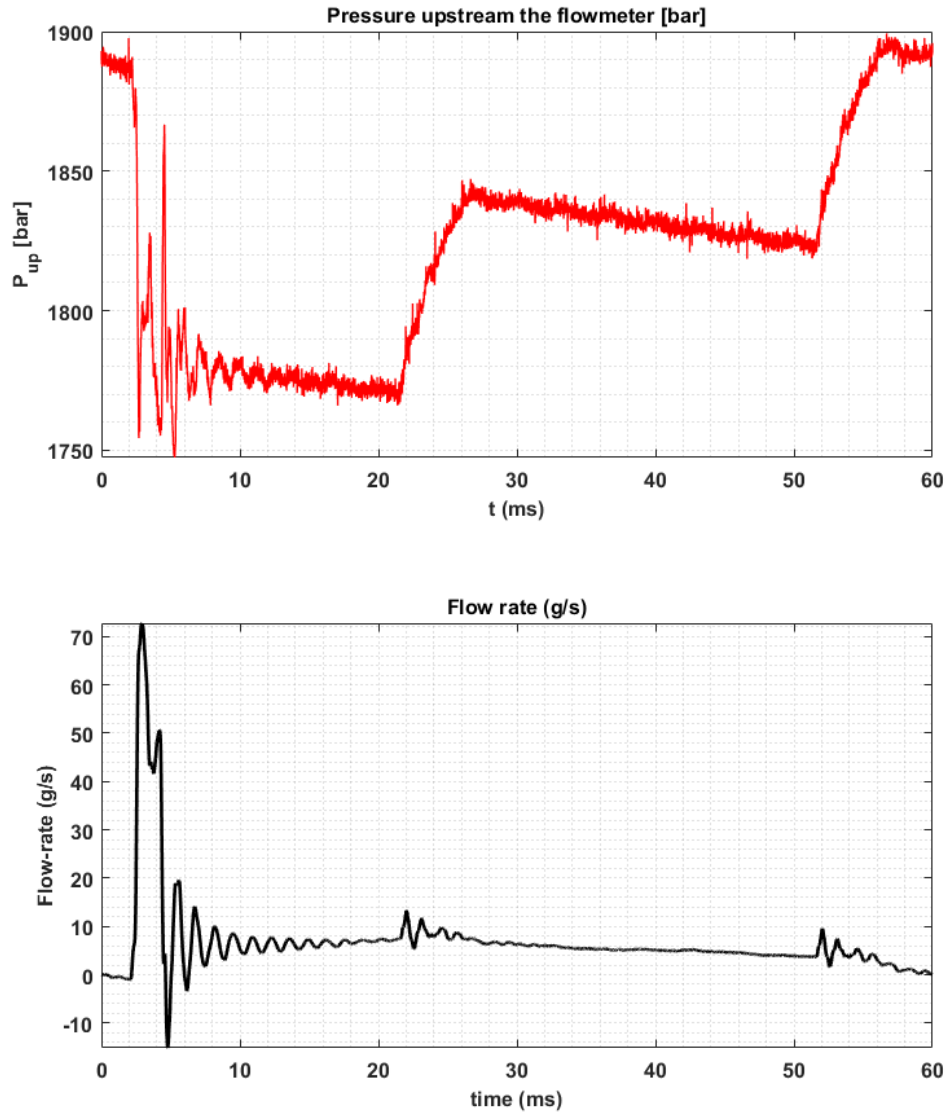


**Figure 3.18:** reference value of pressure 1800 bar, regulation with FMV, 1000  $\mu\text{s}$  ET, respectively pressure measured by the upstream sensor and instantaneous flow rate

In this case, unlike what happened previously, there is no presence of the frequency peak, therefore, at first glance, one could say that there is no need to linearize the

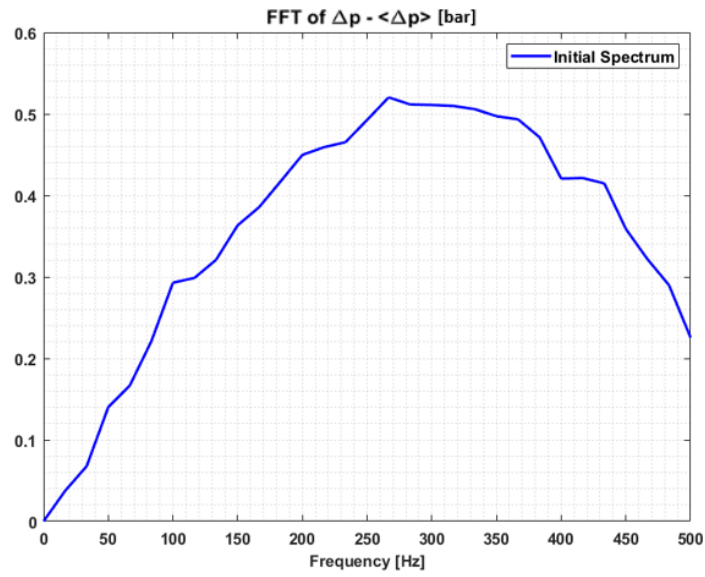


**Figure 3.19:** Fourier spectrum of  $\Delta p - \langle \Delta p \rangle$  with reference value of pressure 1800 bar, FMV

spectrum.

See what happens to the FFT of parameter  $P_{up} - \langle P_{up} \rangle$  and see if there is a correspondence with what was said before.

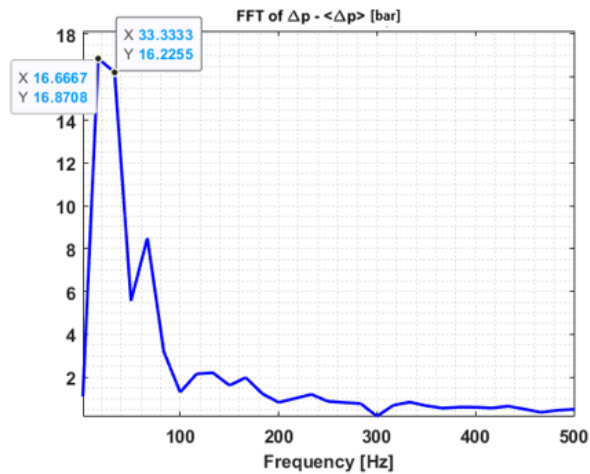


**Figure 3.20:** Fourier spectrum of  $P_{up} - \langle P_{up} \rangle$  with reference value of pressure 1800 bar, FMV

The peak is always present, therefore the methodology for solving the problem remains unchanged.

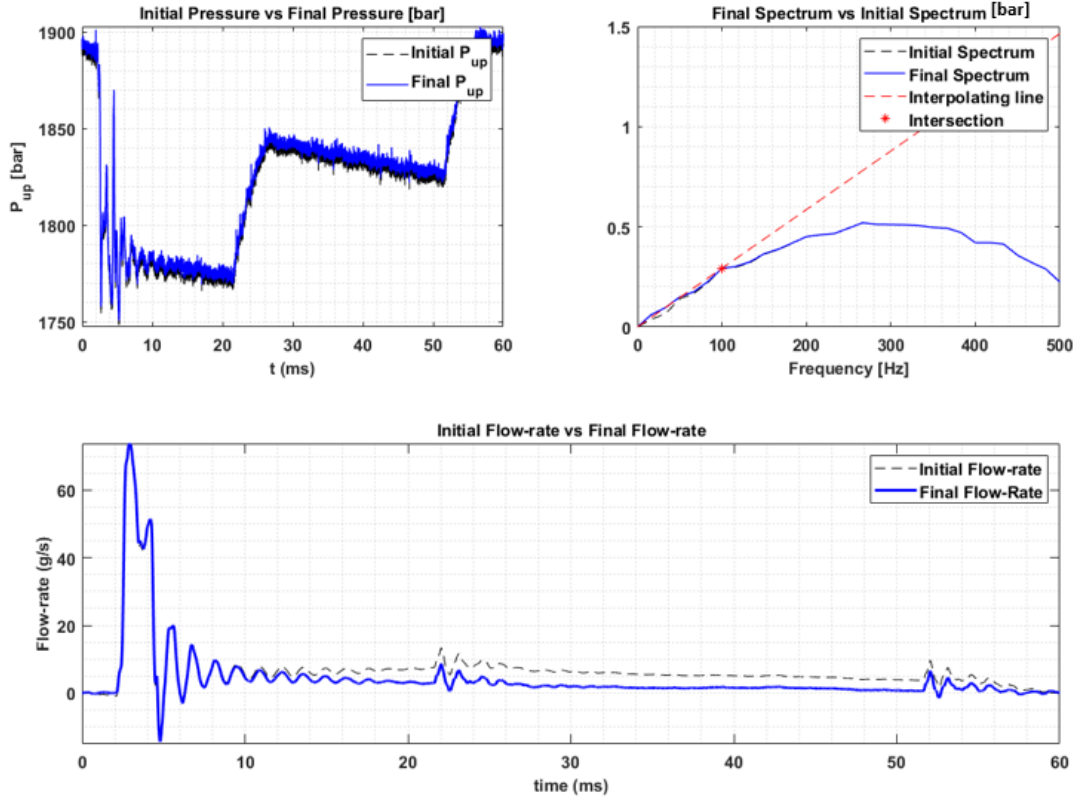


**Figure 3.21:** Respectively graph of  $P_{up}$  with reference value 1800 bar, pump equipped with 2 pumping elements, Fourier spectrum and flow rate graph with FMV regulation,  $n = 1000$  rpm

It's possible to notice that the algorithm is efficient in solving this problem.

### 3.4 Different speeds of rotation

To implement the algorithm, the different rotation speeds to which the motor will be subjected must be taken into account.

It is limiting to consider only the rotation speed of 1000 rpm, therefore, experimental tests were carried out at other speeds: 1500 rpm and 600 rpm.

#### 3.4.1 Experimental tests with rotation speed $n = 600$ rpm

Consider the usual diagrams for the study of the problem and for the research of the methodology of resolution.

Let's consider PCV regulation, reference value of pressure 1300 bar,  $1000 \mu\text{s}$  ET,  $n=600$  rpm.

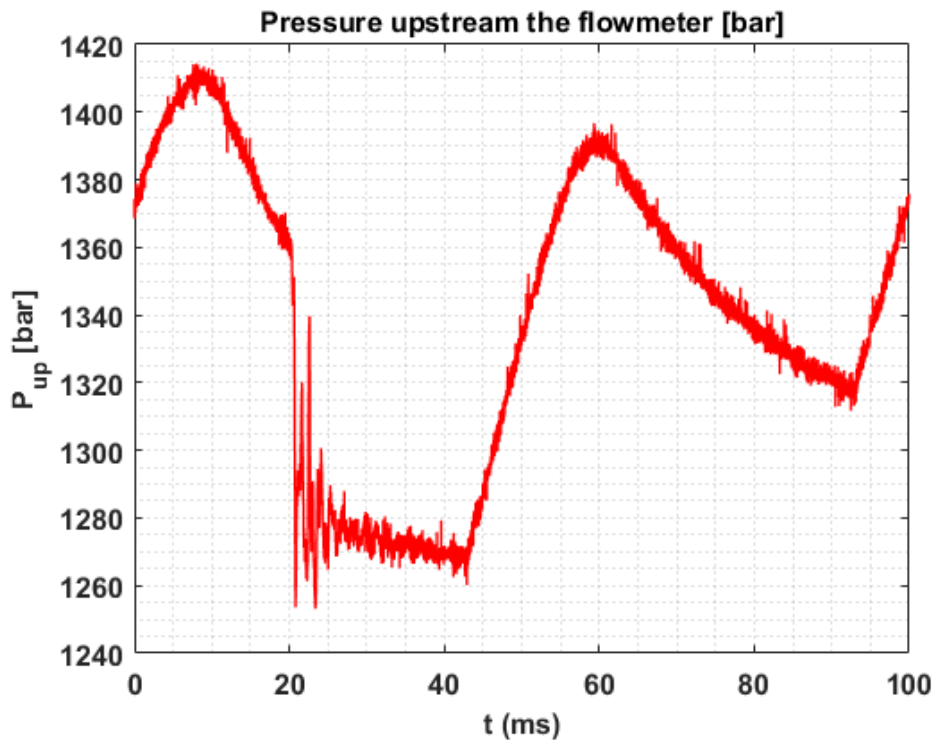


Figure 3.22: Pressure upstream the flowmeter ( $n=600$ rpm)

The initial flow diagrams and the associated spectra are shown respectively. The problem is still the same, but it is possible to notice that the peak frequency takes on a different value than 16.67 Hz and 33.33 Hz (cases for  $n = 1000$ rpm) and this time it is 20 Hz.

There seems to be, at least in PCV regulation, a well-known correspondence

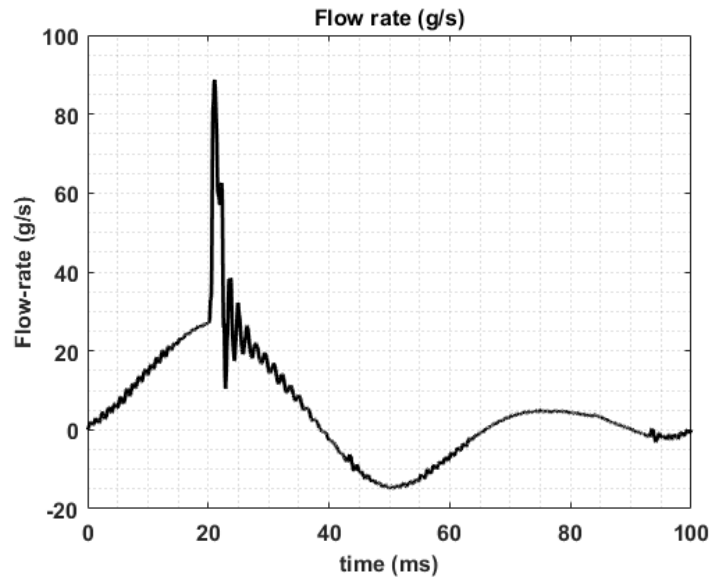


Figure 3.23: Initial flow-rate (n=600rpm)

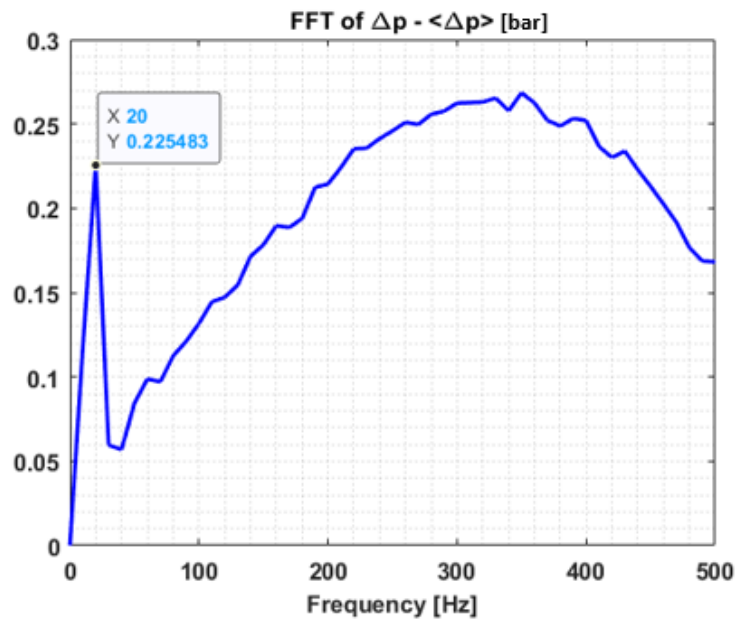
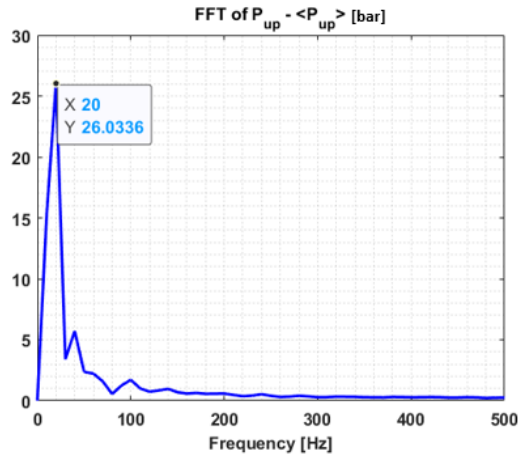


Figure 3.24: Spectrum of the parameter  $\langle \Delta p - \Delta p \rangle$  (n=600rpm)



**Figure 3.25:** Spectrum of the parameter  $P_{up} - \langle P_{up} \rangle$  ( $n=600\text{rpm}$ )

between the peak frequency, the geometric characteristics of the pump and its rotation speed.

Reconsidering the previous case (figure 3.16) consider the Fourier spectrum of the parameter  $P_{up} - \langle P_{up} \rangle$

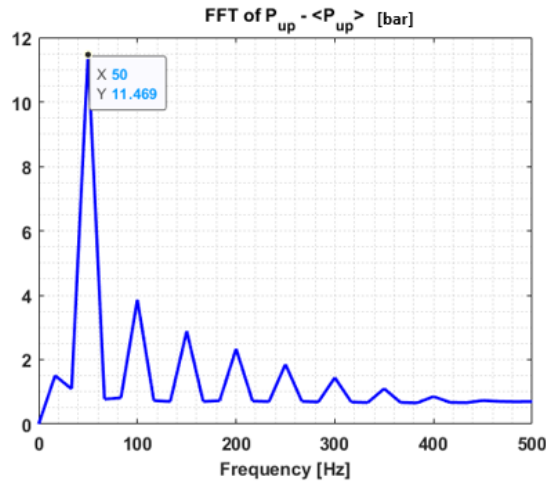


**Figure 3.26:** Spectrum of the parameter  $P_{up} - \langle P_{up} \rangle$ , reference pressure 1800 bar, 3 pumping elements of the pump ( $n=1000\text{rpm}$ )

The algorithm solves the problem and gives a coherent solution (Figure 3.27).

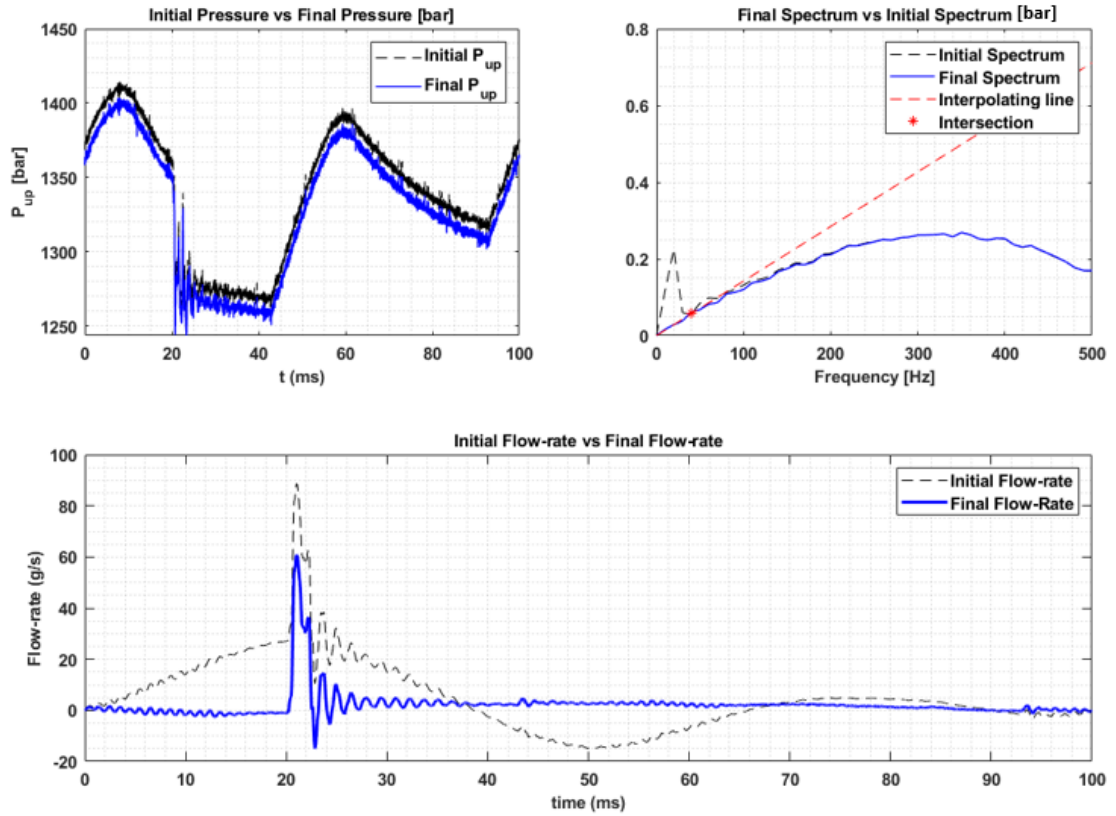


**Figure 3.27:** Respectively graph of  $P_{up}$  with reference value 1300 bar, pump equipped with 2 pumping elements, Fourier spectrum and flow rate graph with FMV regulation,  $n = 600$  rpm

### 3.4.2 Experimental tests with rotation speed $n = 1500$ rpm

Let's consider PCV regulation, reference value of pressure 1200 bar,  $1000 \mu\text{s}$  ET,  $n=1500$  rpm.

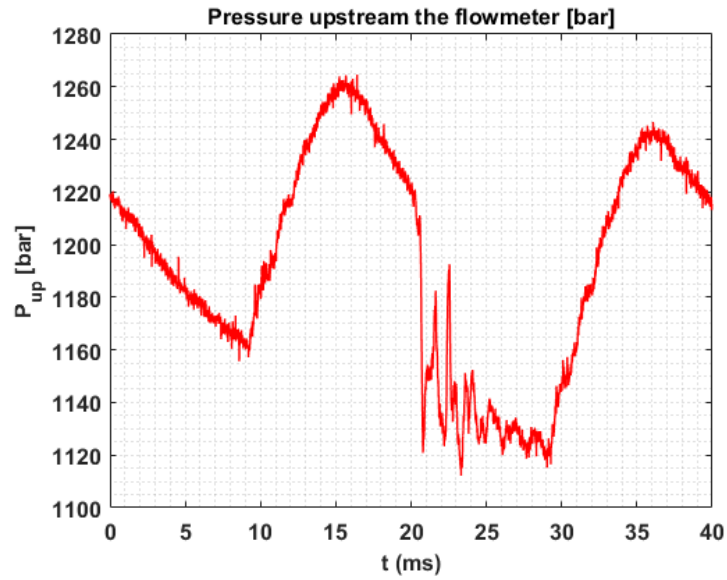


Figure 3.28: Pressure upstream the flow-meter ( $n=1500$ rpm)

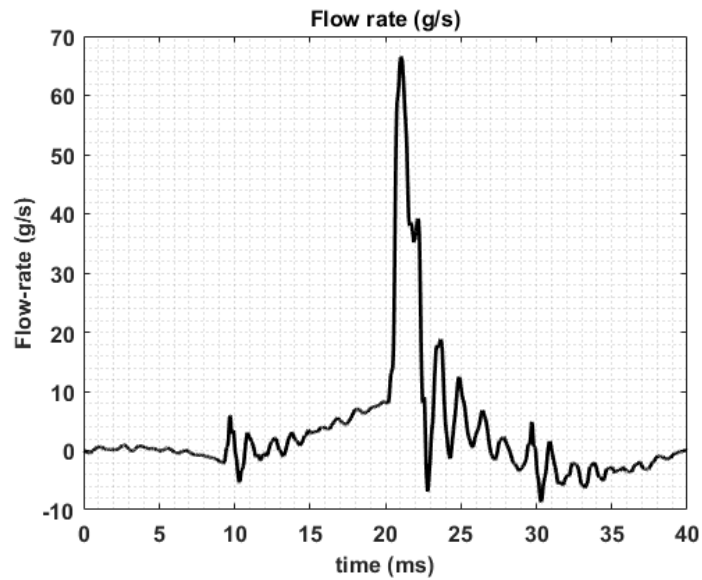


Figure 3.29: Initial flow-rate ( $n=1500$ rpm)

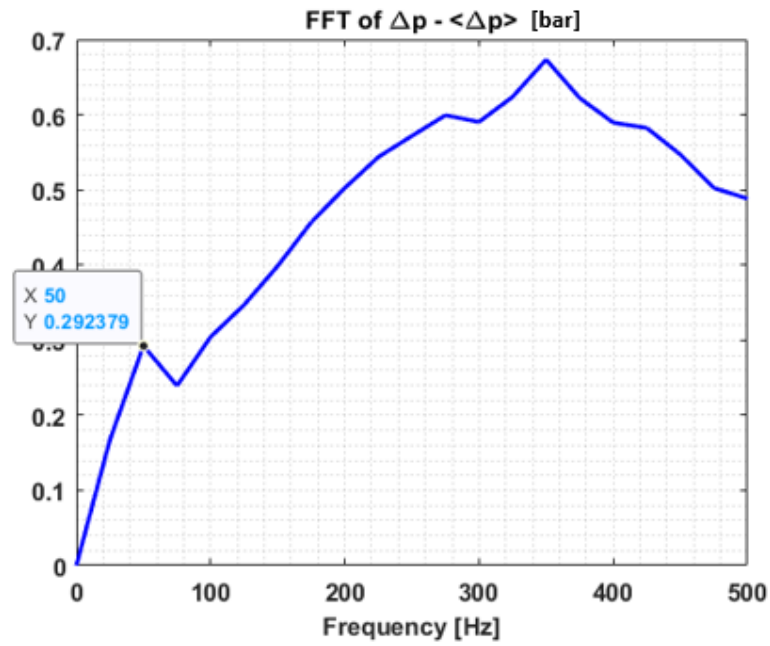


Figure 3.30: Spectrum of the parameter  $\Delta p - \langle \Delta p \rangle$  (n=1500rpm)

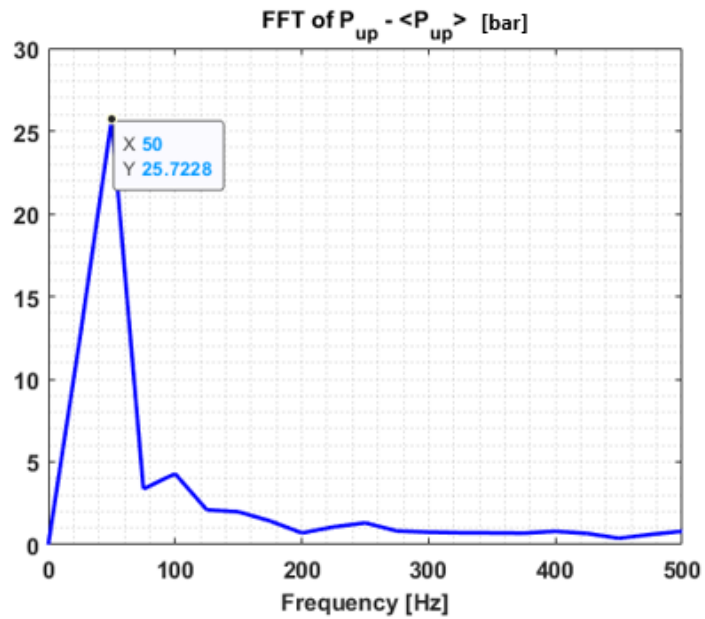
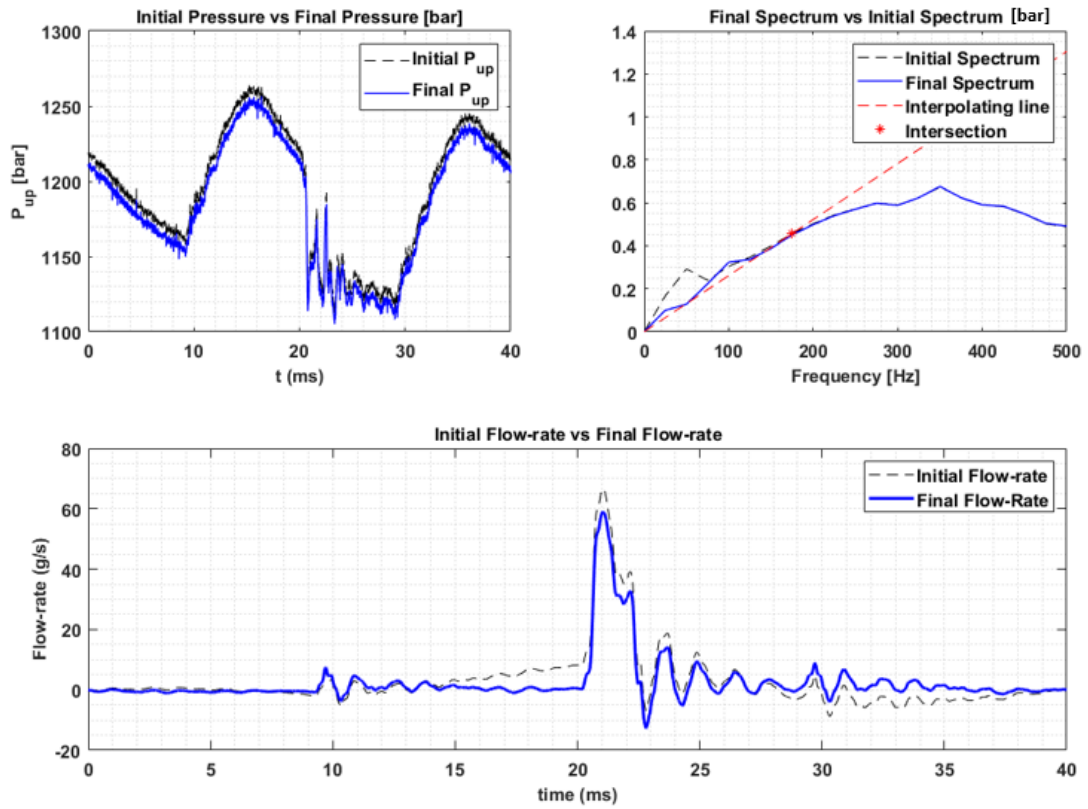


Figure 3.31: Spectrum of the parameter  $P_{up} - \langle P_{up} \rangle$  (n=1500rpm)

The solution of the algorithm is as follows:



**Figure 3.32:** Respectively graph of  $P_{up}$  with reference value 1200 bar, pump equipped with 2 pumping elements, Fourier spectrum and flow rate graph with FMV regulation,  $n = 1500$  rpm

In this case the frequency to be cut down is 50 Hz.

Through all the examples seen it is possible, for the PCV regulation, to identify a correlation between the peak frequency and the operating (rotation speed) and geometric (number of pumping elements) properties.

Before doing this we summarize the results obtained with the following table:

600 rpm	1000 rpm	1500 rpm
2 pumping elements	2 pumping elements	2 pumping elements
$f_{peak} = 20Hz$	$f_{peak} = 33.3Hz$	$f_{peak} = 50Hz$
	3 pumping elements	
	$f_{peak} = 50Hz$	

**Table 3.1:** PCV regulation, data to derive analytical equation between peak frequency, pump rotation speed and number of pumping elements

$$f_{peak} = N \frac{n}{60} \quad (3.2)$$

where:

- N is the number of the pumping elements of the pump;
- n is the rotation speed of the pump;

Unfortunately, experimental tests are not enough to be able to find an analytical relationship also for the FMV regulation (no tests have been developed with the 3 pumping pump with FMV regulation).

This result can be really interesting as it is possible to link the peak frequency with the frequency between the intersection of the interpolating line and the initial spectrum.

# Chapter 4

## Implementation of the algorithms

### 4.1 Introduction to the first check

For the study of the algorithm we will consider a test in particular: PCV regulation, reference pressure: 1200 bar,  $n = 1000\text{rpm}$ , 400 ET.

The corresponding Fourier spectrum is as follows:

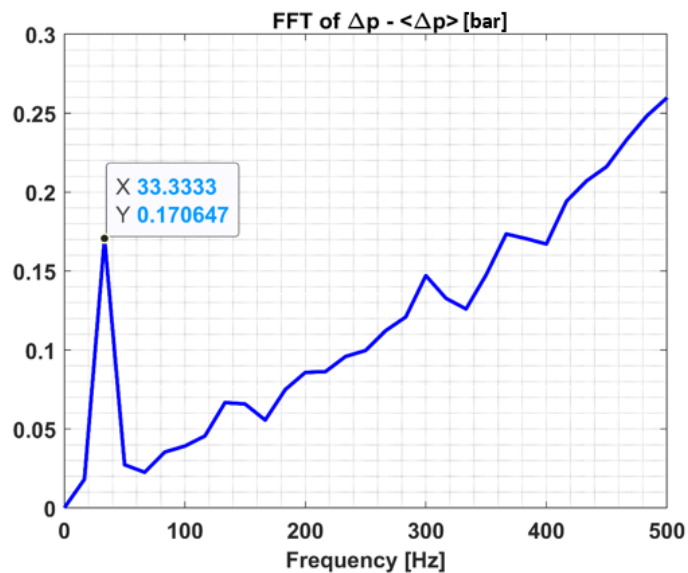


**Figure 4.1:** Fourier spectrum of pressure signal, PCV, reference pressure 1200 bar

to which it corresponds the flow-rate:

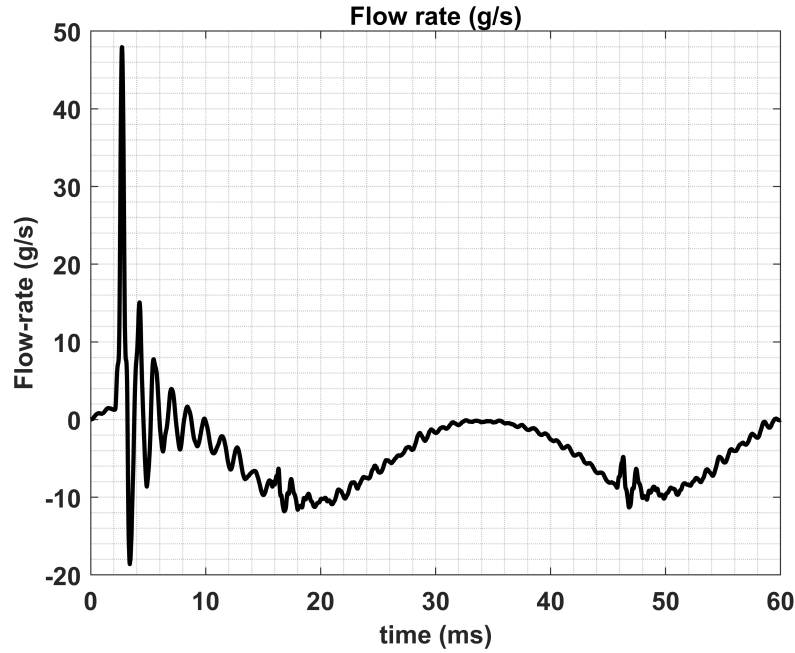


**Figure 4.2:** Flow-rate's graph, PCV, reference pressure 1200 bar

The idea of the first control is to create a vector of frequencies following the peak frequency identified by the Fourier spectrum (of the other quantity).

Each frequency will determine a point of intersection with the initial spectrum and, considering the origin, **a series of straight lines that will form a fan** (Figure 4.3).

**The goal is to identify which of the following lines allows a better linearization of the Fourier spectrum, then associate the multiplicative coefficient MF to these lines.**

For each line, a cycle will be carried out and a vector of multiplicative coefficients MF will be associated with it, appropriately spaced with a discretization step.

The line leading to the solution of the algorithm is the one that intersects the spectrum at 83.33 Hz (it is the one that best approximates the linearization of the spectrum); for this reason we will proceed with the description taking into account only the latter.

Once the vector of the multiplicative coefficients has been built, I start a cycle where I carry out, each time, the following steps:

- Calculate  $\Delta p$  in this way:

$$\Delta p = P_{up} \times MF - P_{down} \quad (4.1)$$

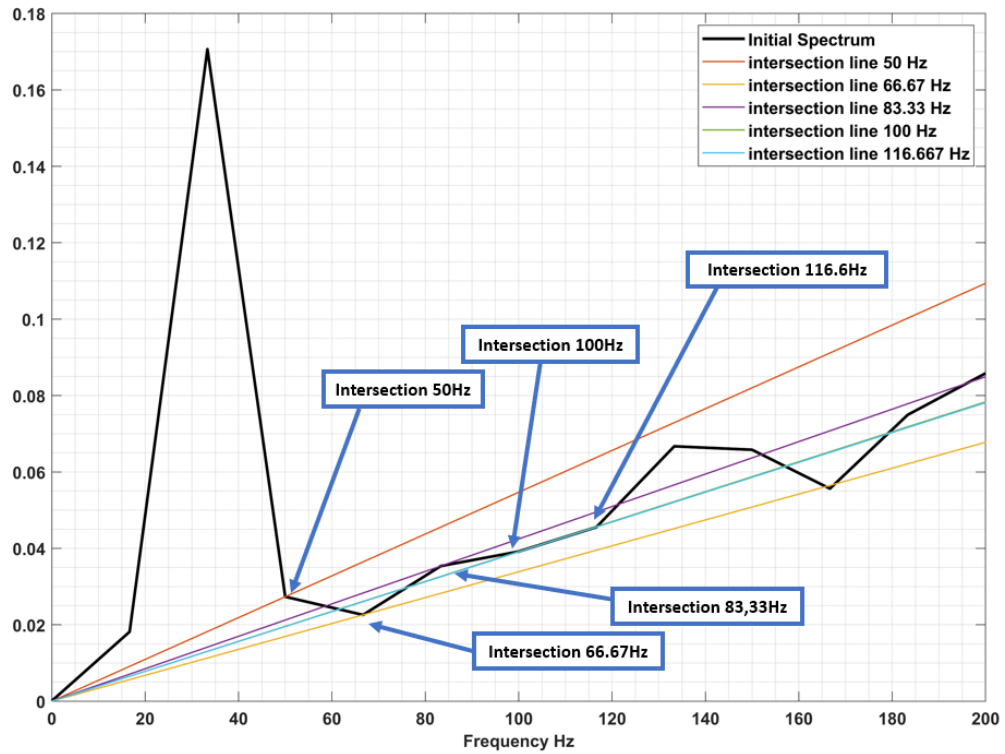


**Figure 4.3:** Initial spectrum with range of straight lines with corresponding points of intersection

- Calculate the integral, do the difference with his mean value;
- Calculate the flow-rate;
- Compute the Fourier spectrum of this new signal;
- For each multiplicative factor the relative spectrum is constructed and for each spectrum a **least square line** is constructed (with an appropriate range).

Now notice how the least squares lines converge going around the solution identified by the algorithm ( $MF = 0.922$ ).

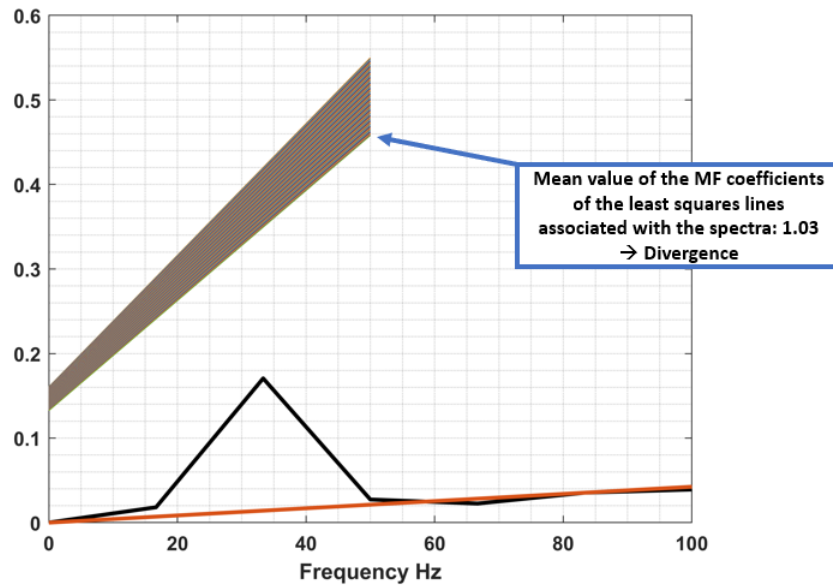


**Figure 4.4:** Line bundle of least squares with average value of the multiplicative coefficient MF equal to 1.03

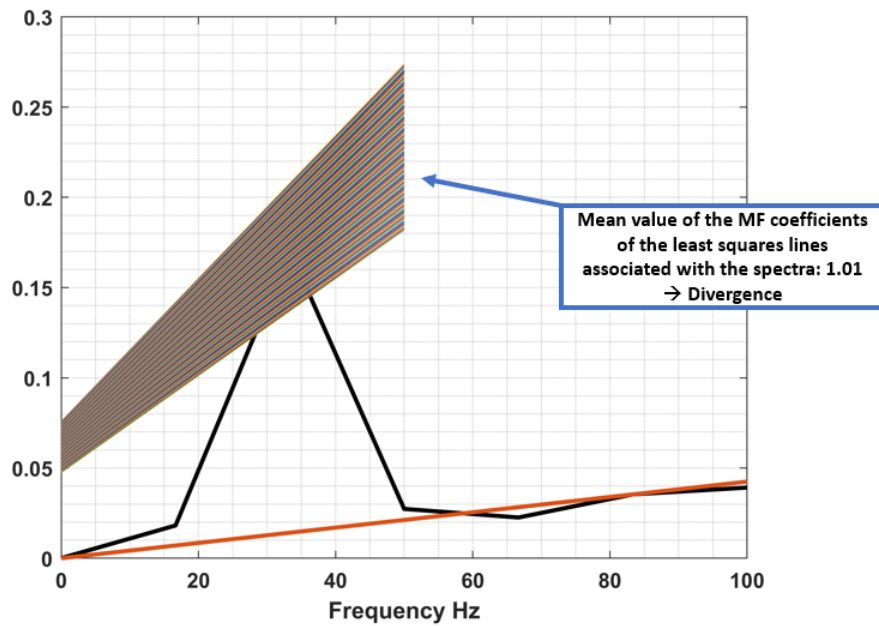


**Figure 4.5:** Line bundle of least squares with average value of the multiplicative coefficient MF equal to 1.01

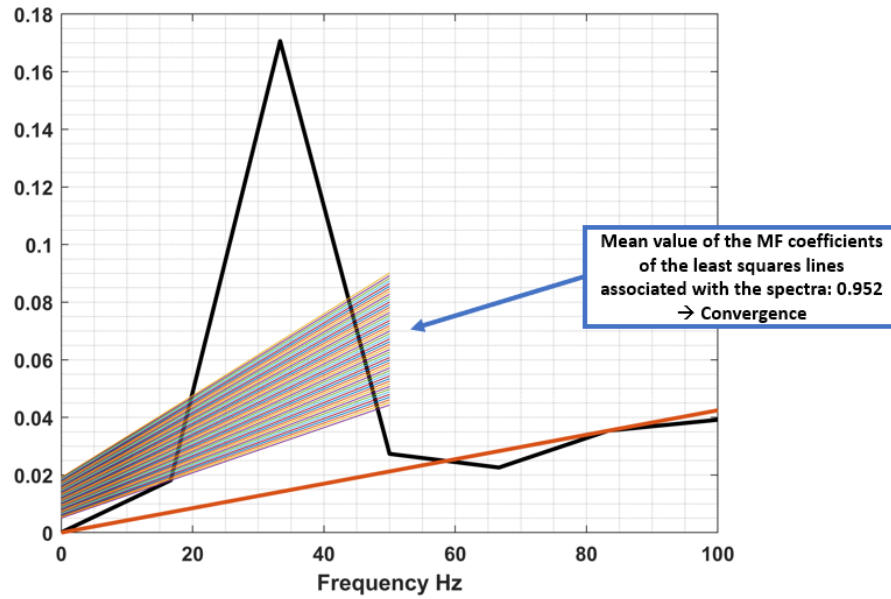


**Figure 4.6:** Line bundle of least squares with average value of the multiplicative coefficient MF equal to 0.952

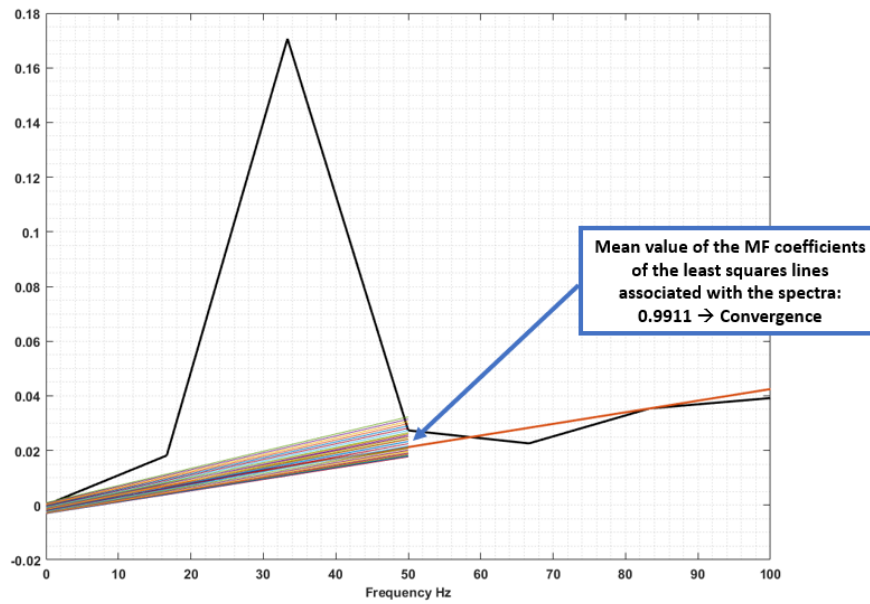


**Figure 4.7:** Line bundle of least squares with average value of the multiplicative coefficient MF equal to 0.991

The first check consists in respecting a certain slope of the least squares lines with respect to the intersection line.

For each Spectrum analyzed we've to compare the angular coefficient of the first line and the angular coefficient of the fitting line.

## 4.2 Second check

This first control isn't enough because each test has its own behaviour, therefore some lines that satisfy the imposed condition have a spectrum that is not good for the application, we need a second control.

The first check may not be enough because a solution in which the spectrum has a jump from 16.67 Hz to 33.33 Hz would be correct because the fitting line would not notice this.

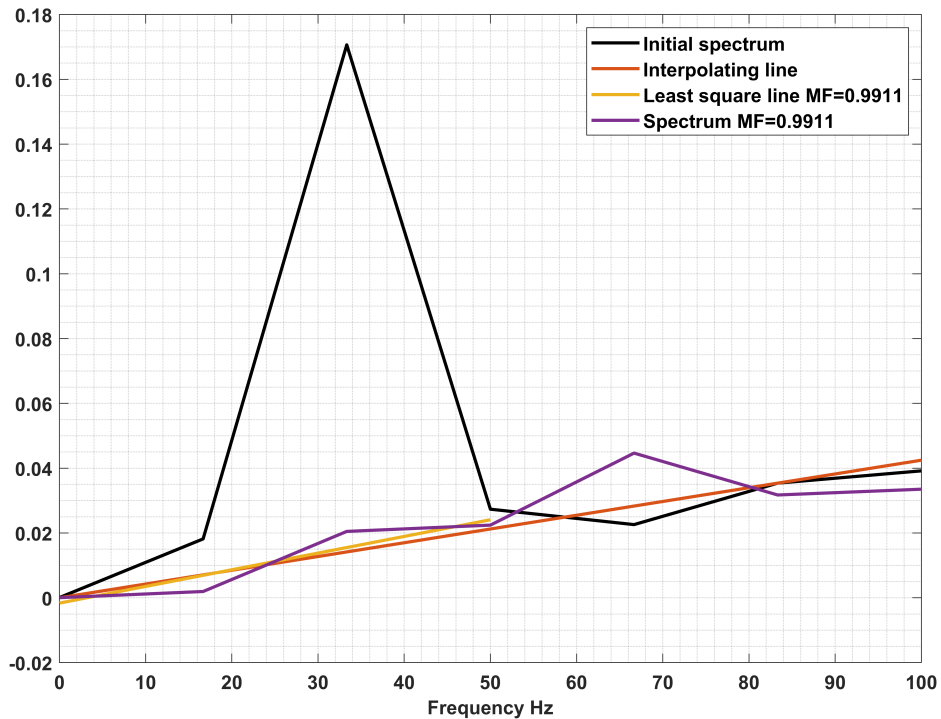
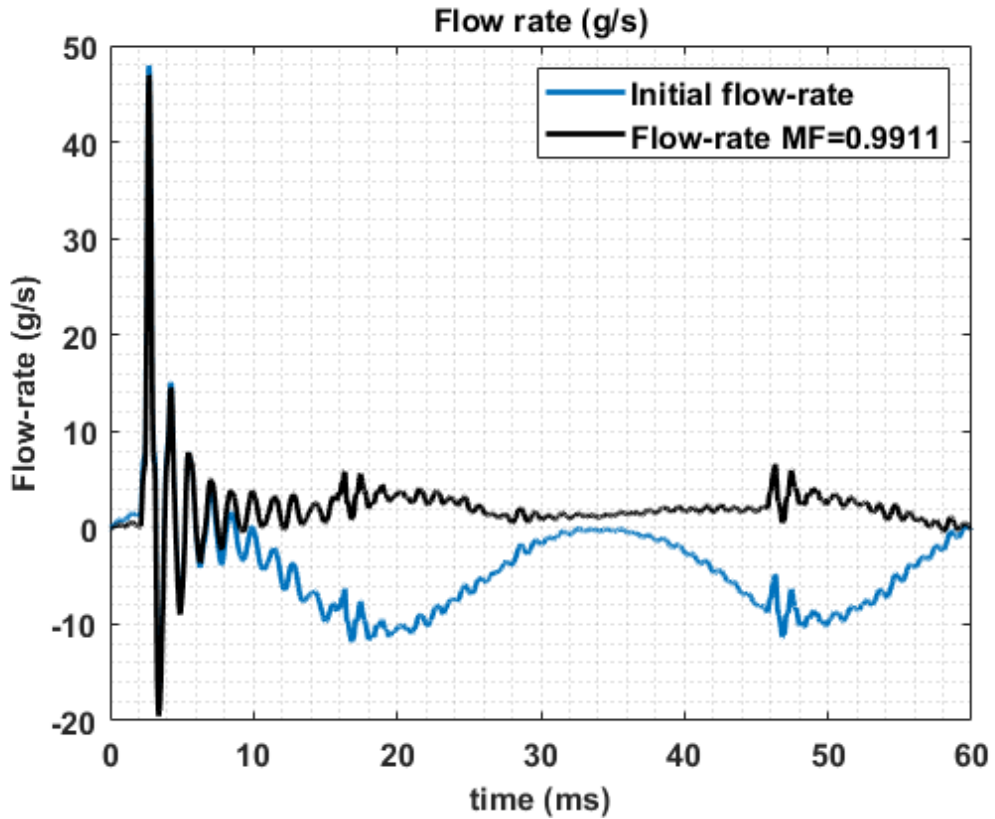


Figure 4.8: Spectrum associated to MF=0.9911, initial spectrum and fitting line

In addition to a control of the inclination of the lines, I need a control for a correct distribution of the spectra in the considered neighborhood (In this case 16.67 Hz, 50 Hz, 66.67 Hz and 100 Hz, but every n will have his neighborhood).

The corresponding flow diagrams are as follows: To solve this problem the discretized



**Figure 4.9:** Flow-rate associated to MF=0.9911 and initial flow-rate

integration between the fitting line and the reference line were compared; in this way'll have a better distribution of the spectra.

**The discretized integration of the reference line (straight line) will be:**

$$S = \sum_{i=1}^N m_1 f(x_i) \quad (4.2)$$

**The discretized integration of the fitting line'll be:**

$$R = \sum_{i=1}^N m_2 f(x_i) \quad (4.3)$$

N is the number of samples on which we want to do this integration (it represents the range of the least square line).

**After making these checks it is necessary to connect the multiplicative**

coefficients MFs with the correct slope of the line that best linearizes the spectrum (this is done by applying the least squares method between the spectrum corresponding to the MF coefficient and the line in an appropriate interval).

First and second checks are not yet satisfactory for solving the problem because there are wrong spectra that respect the conditions of the checks.

Let's see the situation after these two checks: For the experimental test taken into

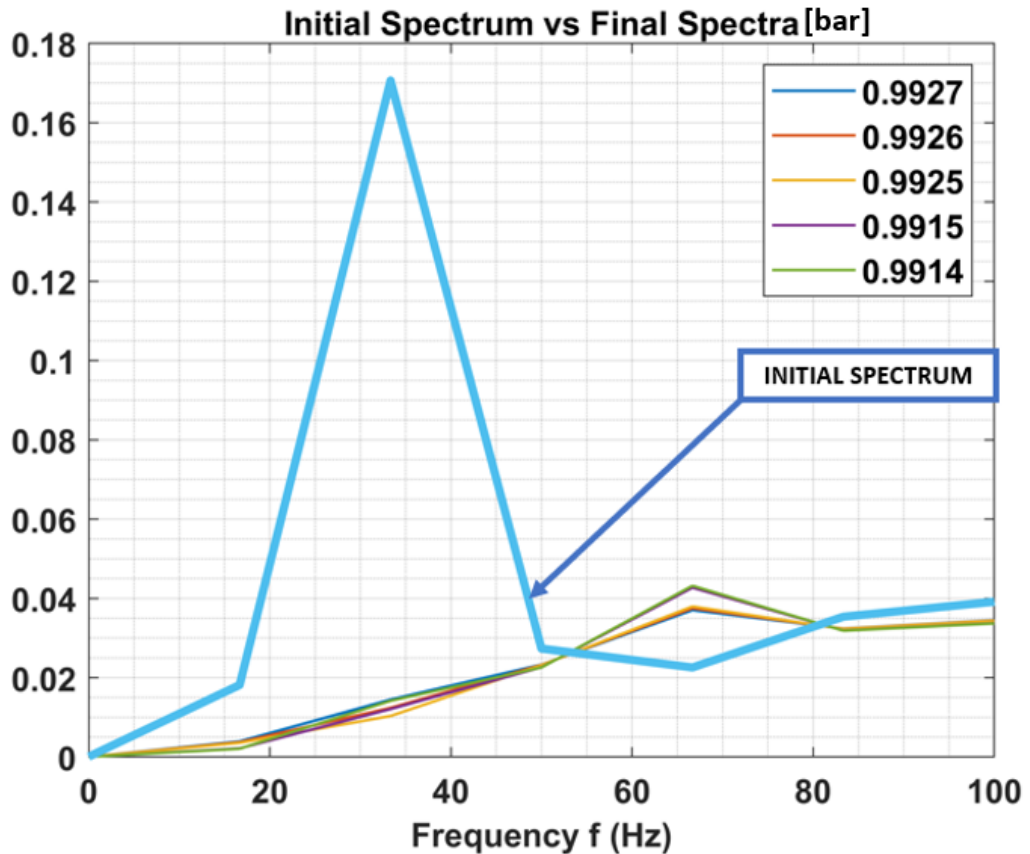


Figure 4.10: Initial Spectrum and Spectra after first and second control

consideration (1200 bar, PCV, 400 ET  $\mu s$ ) we do not see a real divergence of the solution, but we propose a series of images that make it clear that after the two checks the result does not exactly converge.

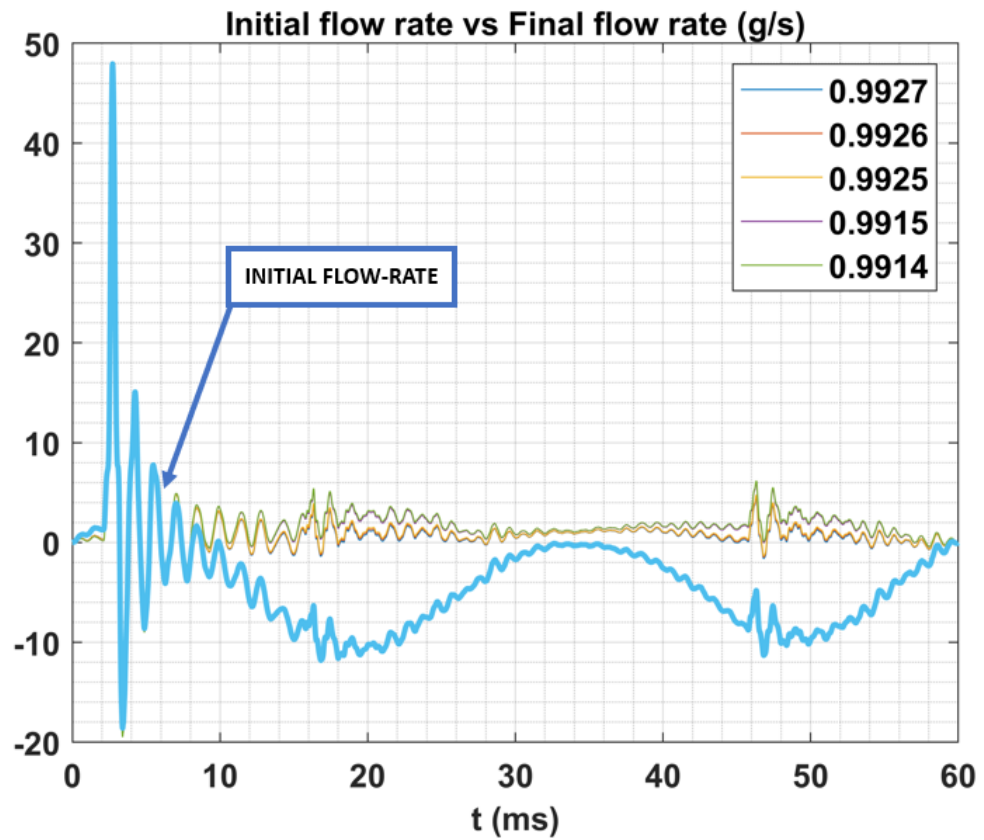
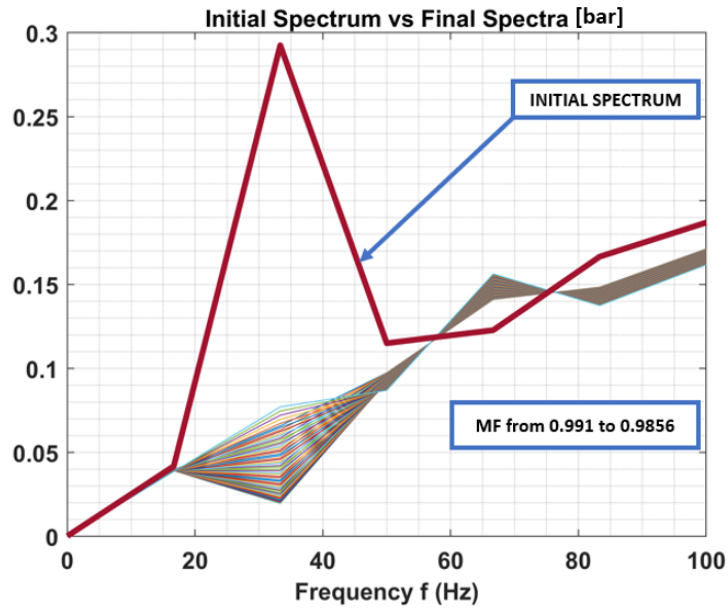
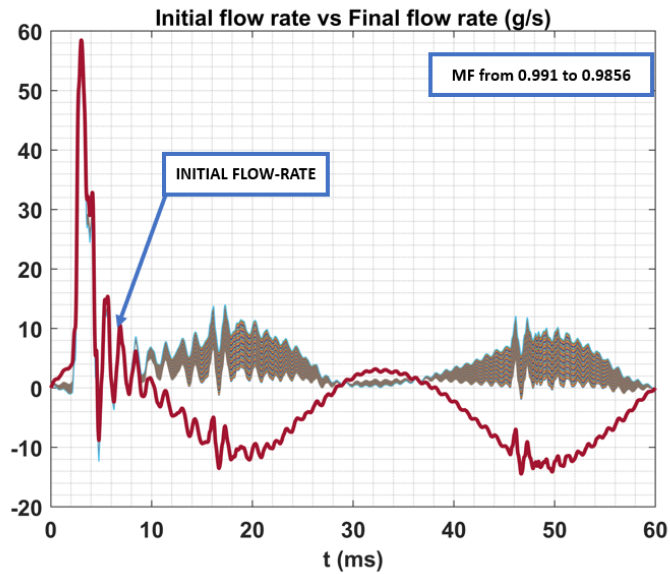


Figure 4.11: Initial Flow-rate and Flow-rate after first and second control



**Figure 4.12:** Initial spectrum and Spectra after first and second control, reference pressure 1000 bar, PCV regulation, 1000  $\mu$ s ET, 2 pumping elements



**Figure 4.13:** Initial flow-rate and flow-rate after first and second control, reference pressure 1000 bar, PCV regulation, 1000  $\mu$ s ET, 2 pumping elements

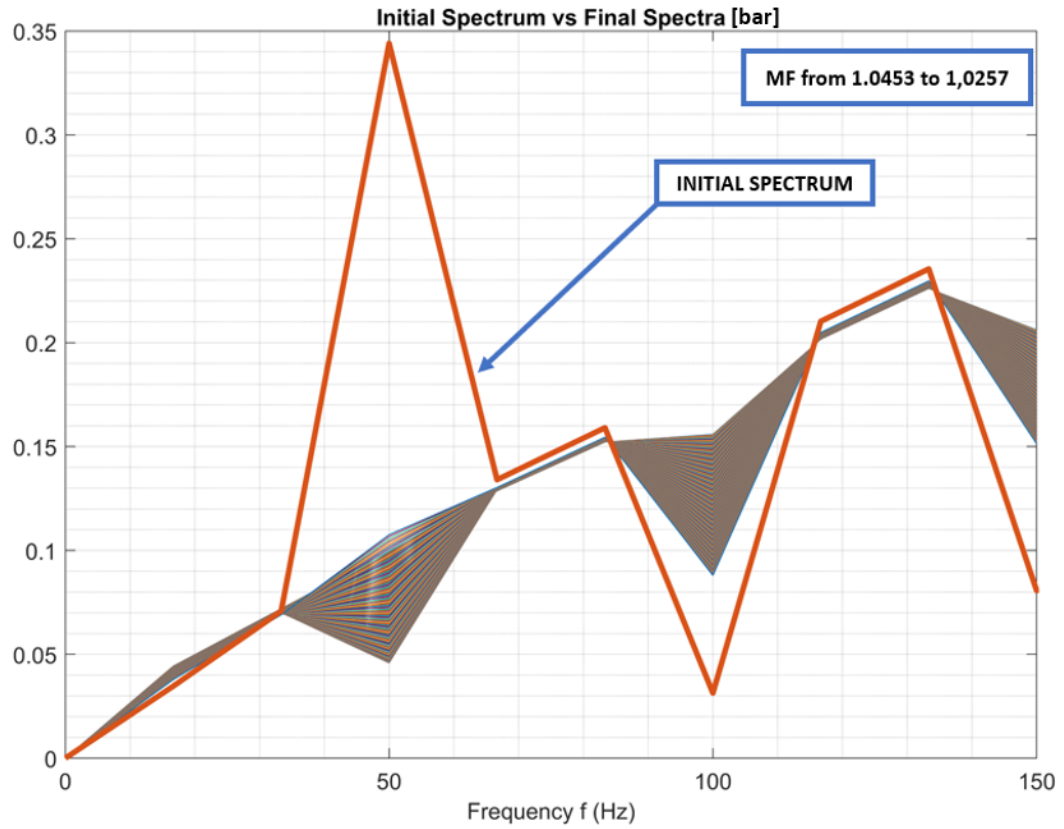


**Figure 4.14:** Initial spectrum and Spectra after first and second control, reference pressure 1500 bar, PCV regulation, 700  $\mu$ s ET, discretized step 0.0001, 3 pumping elements

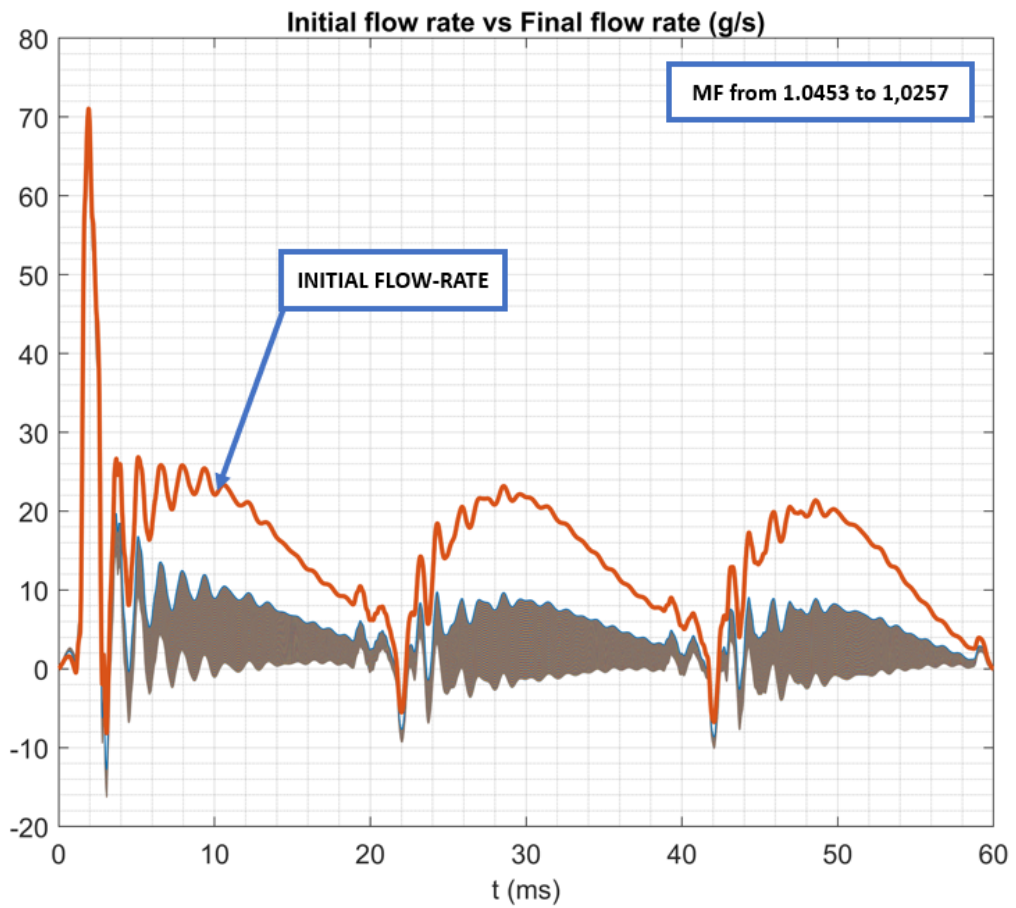


**Figure 4.15:** Initial flow-rate and flow-rate after first and second control, reference pressure 1500 bar, PCV regulation, 700  $\mu$ s ET, discretized step 0.0001, 3 pumping elements

### 4.3 Third check

Returning to the example of paragraphs 1 and 2 (reference pressure 1200 bar, 400  $\mu$ s ET, PCV, 2 pumping elements) let's analyze the situation after the controls. After the first checks, **the line that best linearizes the spectrum was identified:**

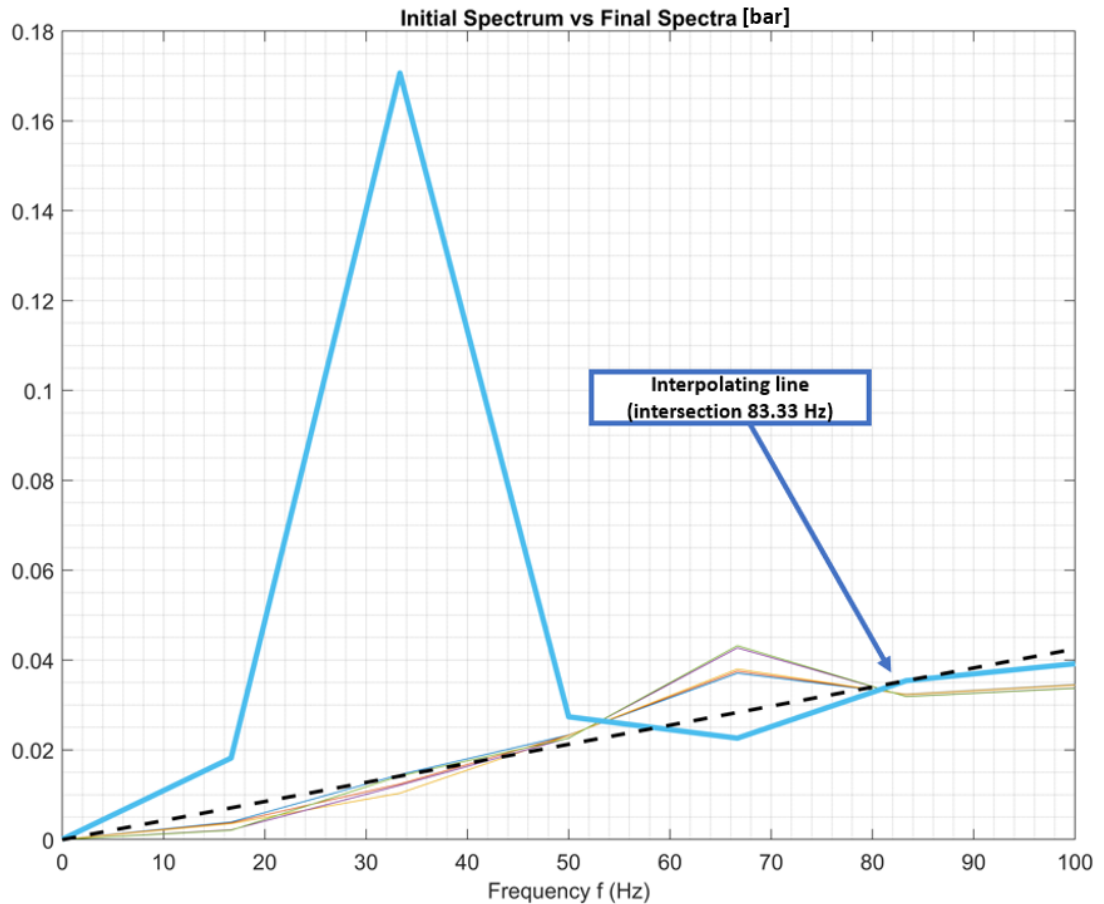


**Figure 4.16:** Initial Spectrum, Spectra and interpolating line

It is easy to understand that the third check will be done on the spectrum closest to the straight line obtained initially.

In this way we will have only one result and it will be the solution to our problem. The range to be considered is from 0 to the next point of the intersection between the initial spectrum and the identified line (in this case 100 Hz).

The final results are reported:

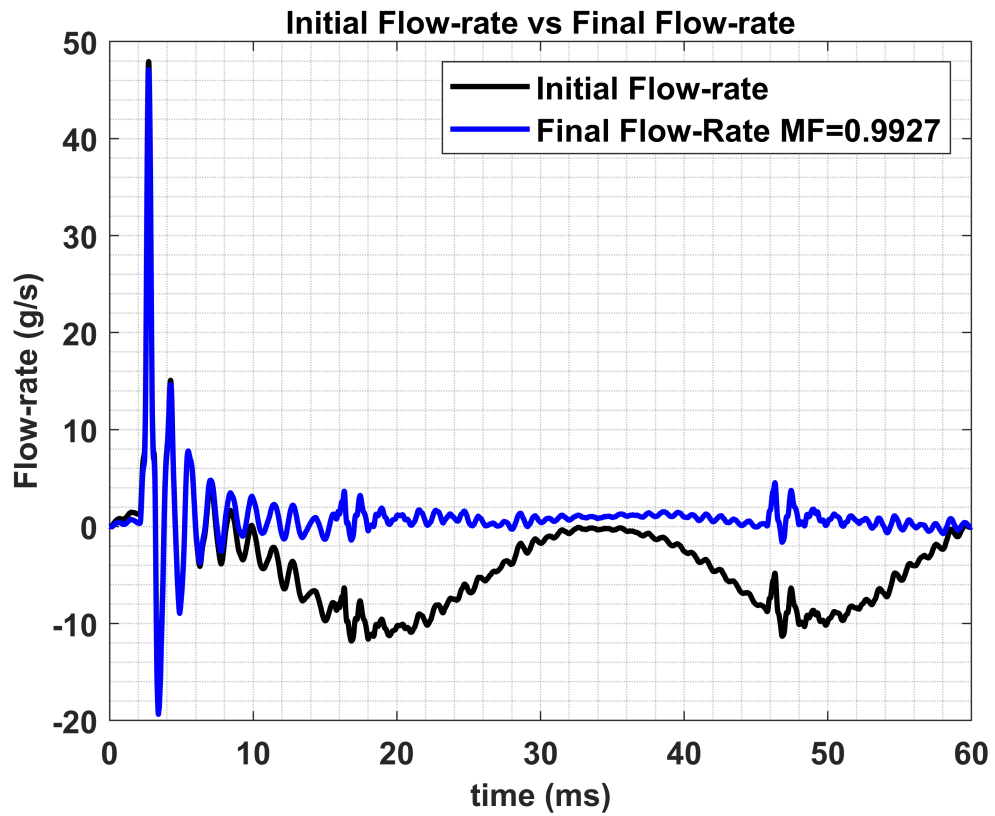
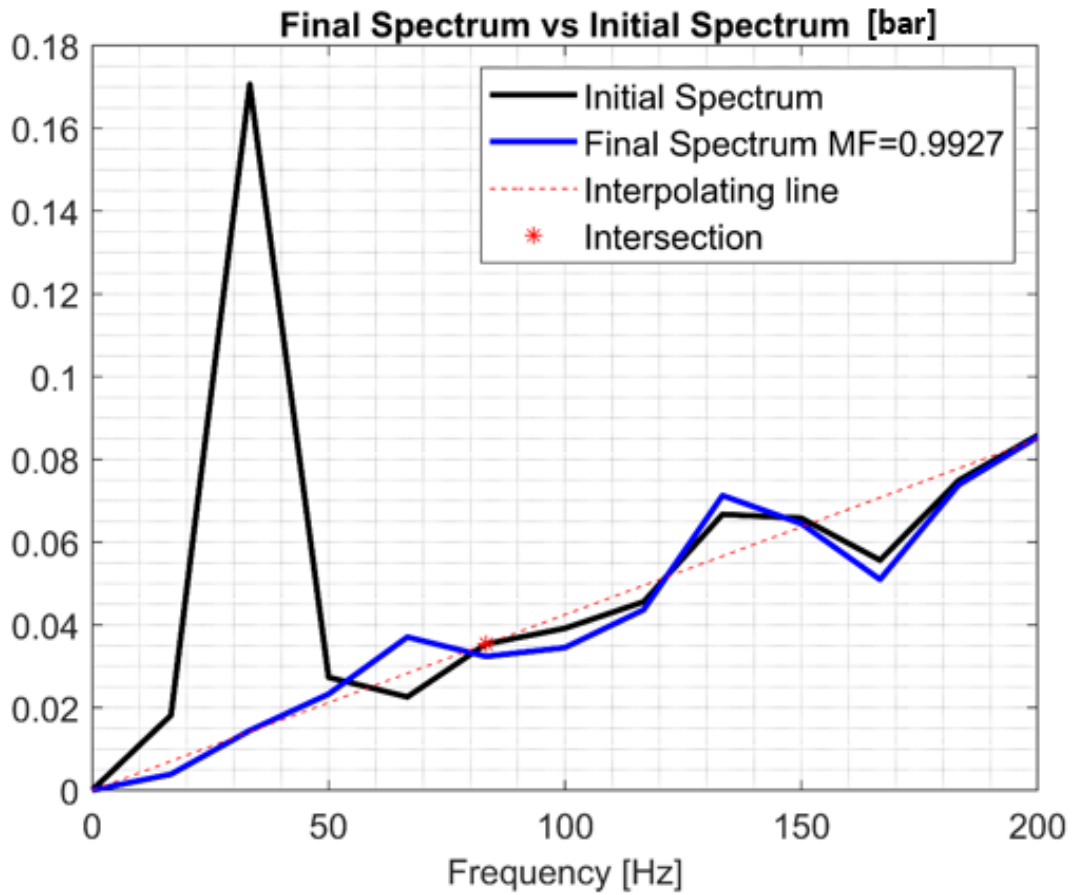


Figure 4.17: Initial Spectrum and Final spectrum after the implementation of the algorithm



**Figure 4.18:** Initial Flow-rate and Final flow-rate after the implementation of the algorithm

## 4.4 Introduction to the simplified algorithm

It is necessary to reduce the processing time of the algorithm (the 3 controls are efficient, but entail a high computational burden).

It has been noticed that the logic of the third control is a good choice to implement the new algorithm.

**In the first algorithm the discretization step was not fundamental because the first two controls eliminated the spectra that were wrong and at the last control the spectra remained at best correct, so inserting a smaller step did not change the algorithm that much.**

Now the discretization step is fundamental because the first two controls have been removed.

Some examples follow (Consider reference pressure 1400 bar, 3 pumping elements,  $400 \mu\text{s}$  ET, PCV regulation):

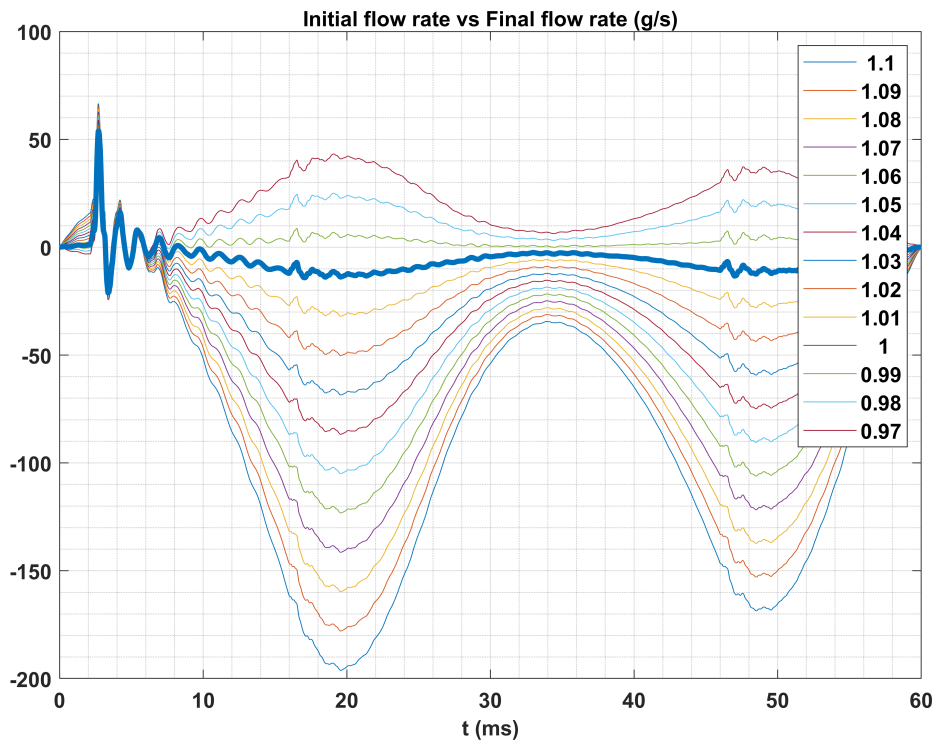


**Figure 4.19:** Flow domain with discretization step 0.01, range of MF: from 1.1 to 0.97

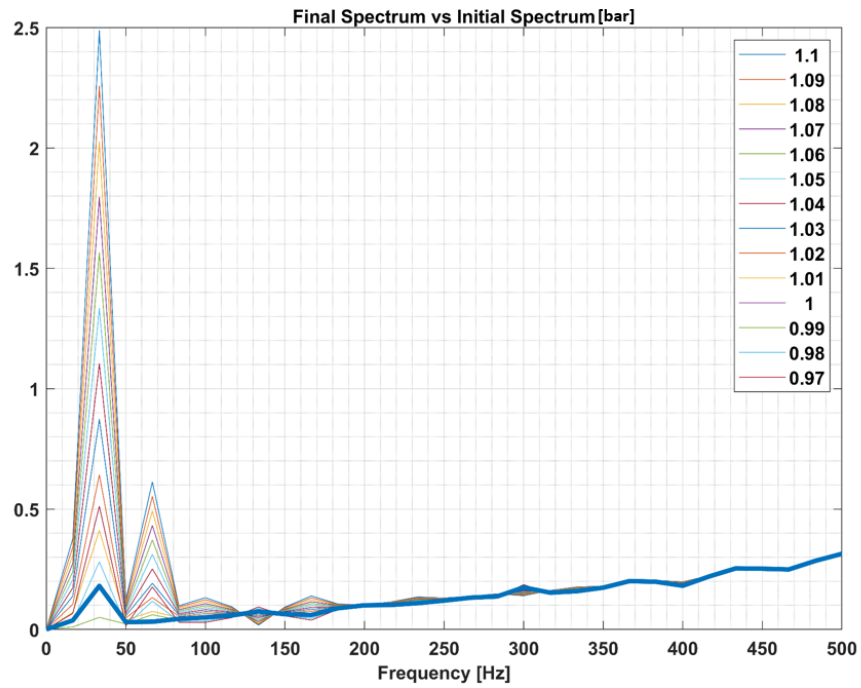


**Figure 4.20:** Domain of spectra with discretization step 0.01, range of MF: from 1.1 to 0.97

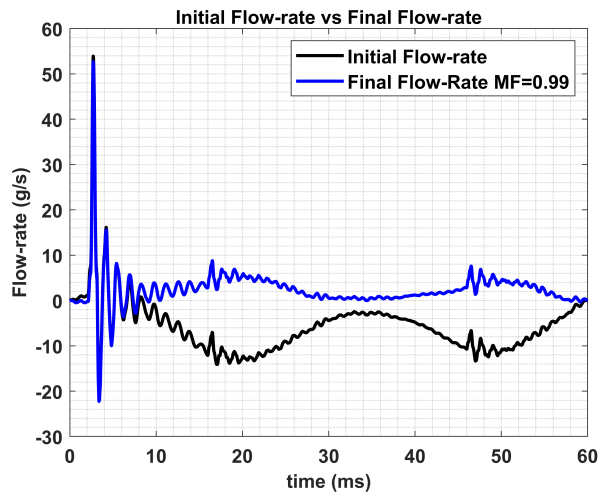


**Figure 4.21:** Result of the algorithm with discretization step 0.01, range of MF: from 1.1 to 0.97

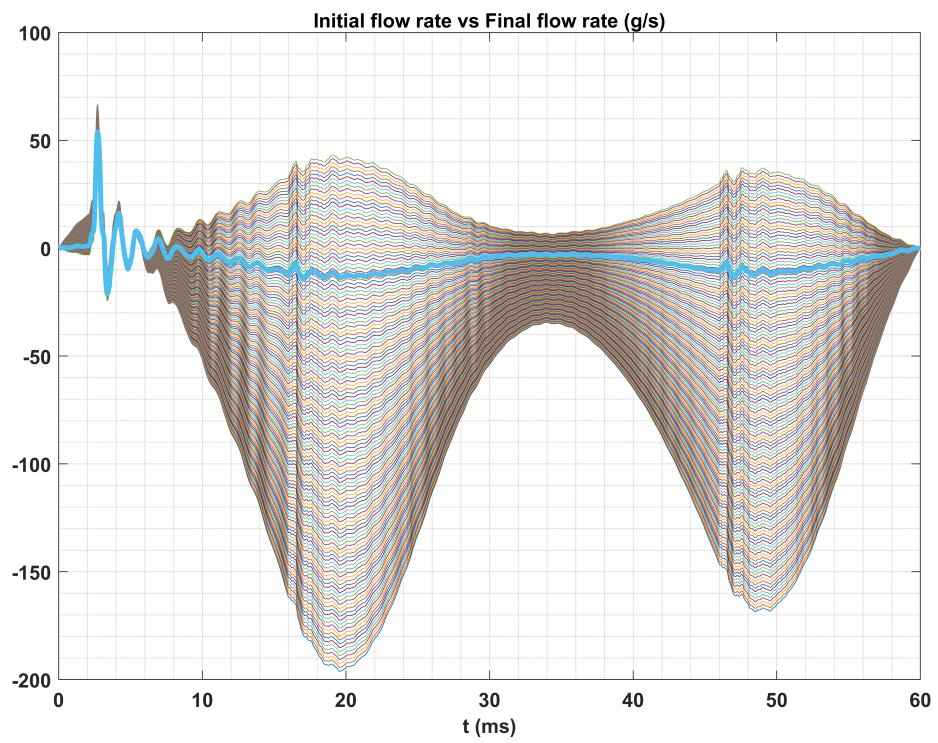


**Figure 4.22:** Flow domain with discretization step 0.001, range of MF: from 1.1 to 0.97

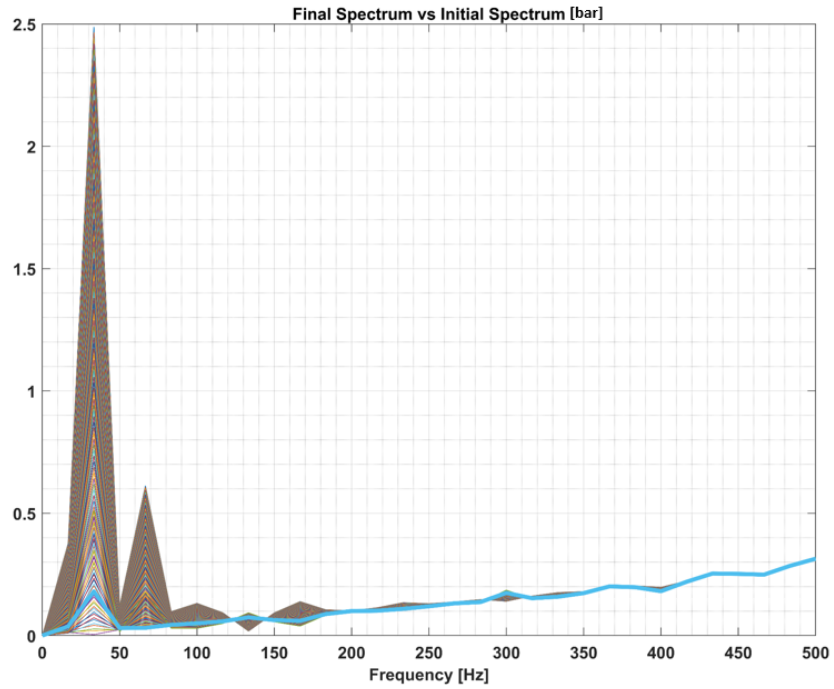


**Figure 4.23:** Domain of spectra with discretization step 0.001, range of MF: from 1.1 to 0.97

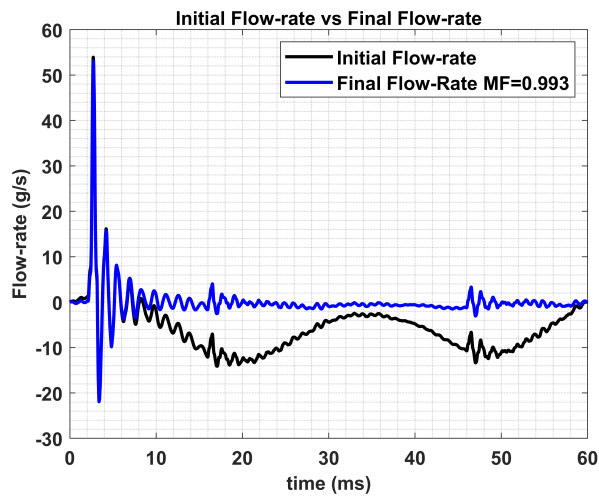


**Figure 4.24:** Result of the algorithm with discretization step 0.001, range of MF: from 1.1 to 0.97

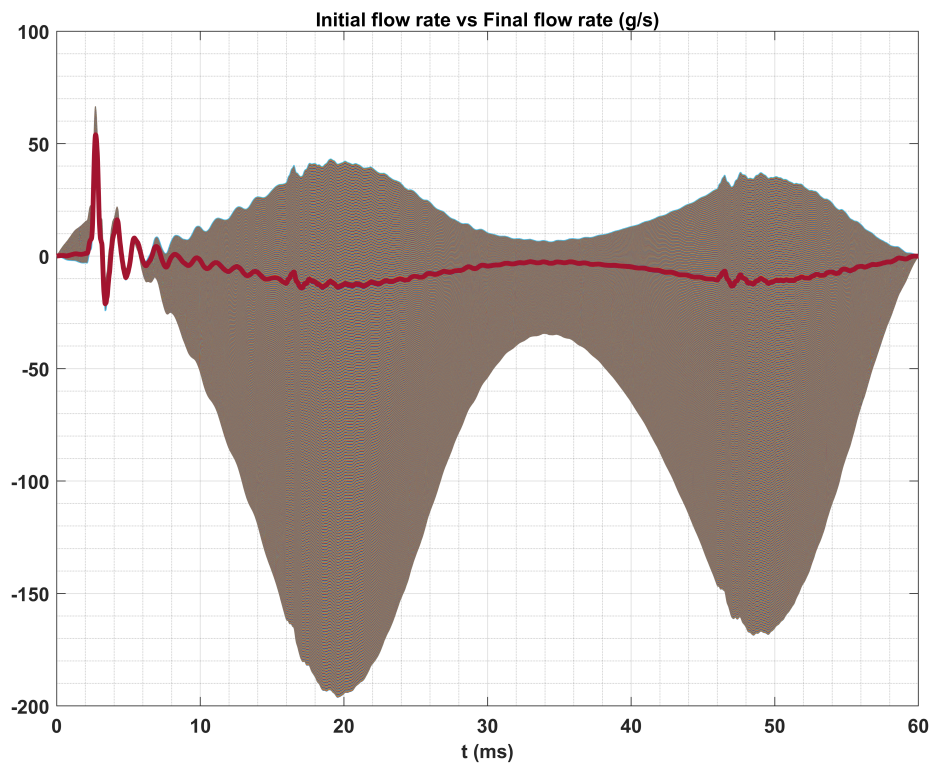


**Figure 4.25:** Flow domain with discretization step 0.0001, range of MF: from 1.1 to 0.97

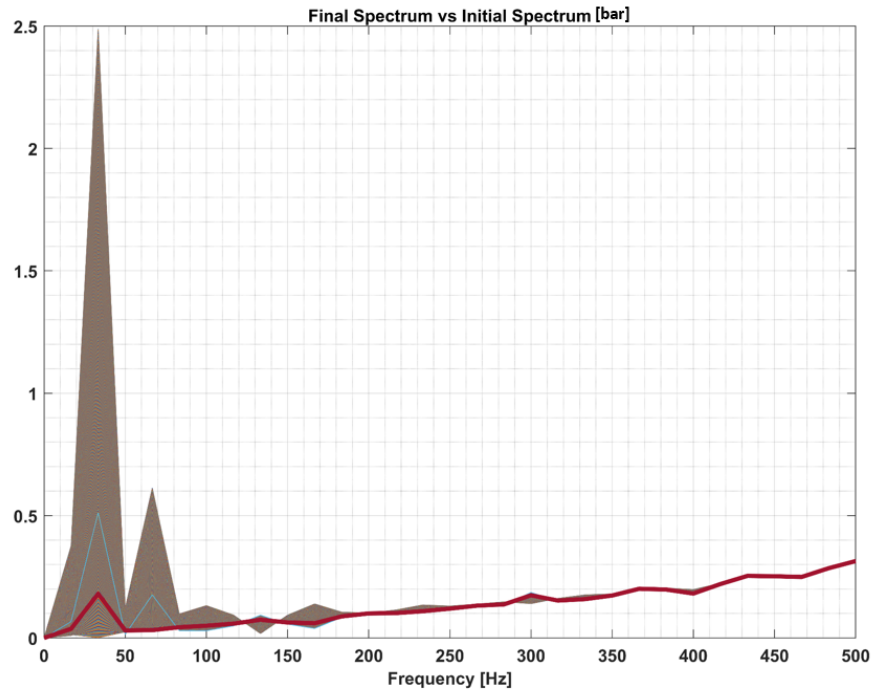


**Figure 4.26:** Domain of spectra with discretization step 0.0001, range of MF: from 1.1 to 0.97

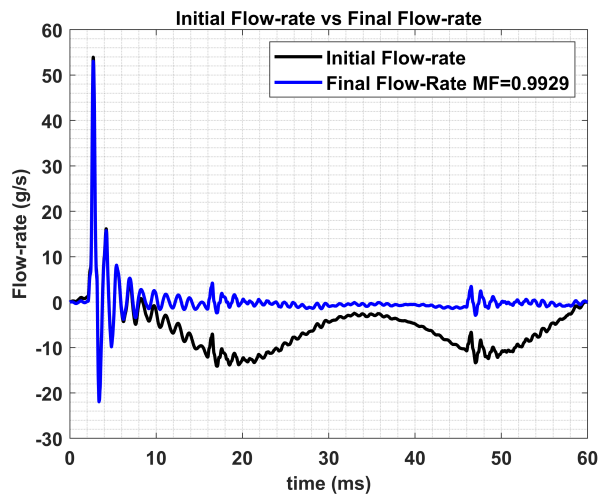


**Figure 4.27:** Result of the algorithm with discretization step 0.0001, range of MF: from 1.1 to 0.97

# Chapter 5

## Comparison of algorithms

### 5.1 A brief summary

Making a small summary it can say that:

- The first algorithm performs three checks (least squares line, discretized integral and sum of the differences between the  $i$ -th spectrum and the reference line) to identify the spectrum that best linearizes the Fourier spectrum.

**The advantage of the algorithm is efficiency**, in fact it is able to identify the best spectrum and, consequently, the correct flow-rate.

Another advantage (which was not discussed previously) **is that in the third check the sum of the differences between the  $e$ -th spectrum and the identified line is carried out up to a very precise point (the point after the intersection found).**

**The disadvantage should be the computational time.**

- The second algorithm (**simplified algorithm**) foresees a single control which corresponds to the third control of the first algorithm, but the logic is different because this time the control is applied on the whole family of spectra that are considered.

The Fourier spectra analyzed in this control are many compared to those of the first algorithm, therefore the trends will not be as ordered as before (in the first algorithm the first two controls gave a certain order of the remaining spectra) and, consequently, **the point up where to check is not easy to identify.**

**One of the disadvantages** has already been mentioned: difficulty in identifying the final point of the control (it no longer coincides with the point after the intersection).

**The main advantage should be the low computational time** (unlike the other algorithm there is now only one check to be performed)

However, the two algorithms have several differences and you have to compare them to understand which one can be the best.

The differences that will be analyzed are the following:

- Processing time;
- Identification of the intersection line with the initial spectrum;
- Final point to check the sum of the differences between the straight line and the  $i$ -th spectra;
- Accuracy and efficiency;
- Comparison of results.

## 5.2 Processing time

The processing time is the time it takes to make the algorithm work, that is the time it takes for the algorithm to give the result.

Consider a generic test and compare the processing times for both (FMV regulation, reference pressure 1400 bar, 700  $\mu$ s ET):

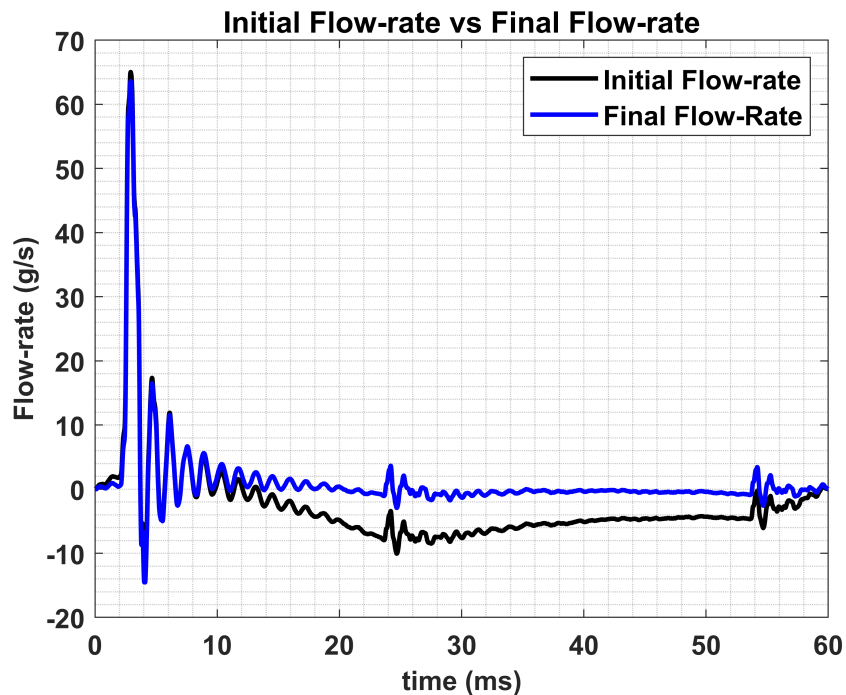


Figure 5.1: Initial and final flow-rate, discretization step 0.001

Both algorithms give MF=0.994 as result.

The algorithm of the 3 controls gives as processing time a value of 0.58 s (including the time to plot the graph) while the simplified algorithm 0.61s.

Only the processing times are considered (excluding the times to have the graphs):

$$t_{1^{st}algorithm} = 0.18s \quad (5.1)$$

$$t_{2^{nd}algorithm} = 0.21s \quad (5.2)$$

First algorithm appears to have the lowest time, but see a table where a list of times is made. with all certainty it can be said that:

Experimental test	Processing time first algorithm	Processing time second algorithm
PCV, 600 bar, ET=400 $\mu$ s	0,12 s	0,17 s
PCV, 600 bar, ET=700 $\mu$ s	0,13 s	0,15 s
PCV, 600 bar, ET=1000 $\mu$ s	0,137 s	0,148 s
PCV, 800 bar, ET=400 $\mu$ s	0,126 s	0,161 s
PCV, 800 bar, ET=700 $\mu$ s	0,131 s	0,152 s
PCV, 800 bar, ET=1000 $\mu$ s	0,138 s	0,146 s
PCV, 1000 bar, ET=400 $\mu$ s	0,16 s	0,17 s
PCV, 1000 bar, ET=700 $\mu$ s	0,142 s	0,17 s
PCV, 1000 bar, ET=1000 $\mu$ s	0,125 s	0,15 s
PCV, 1200 bar, ET=400 $\mu$ s	0,11 s	0,162 s
PCV, 1200 bar, ET=700 $\mu$ s	0,13 s	0,165 s
PCV, 1200 bar, ET=1000 $\mu$ s	0,125 s	0,15 s
PCV, 1400 bar, ET=400 $\mu$ s	0,172 s	0,181 s
PCV, 1400 bar, ET=700 $\mu$ s	0,123 s	0,15 s
PCV, 1400 bar, ET=1000 $\mu$ s	0,125 s	0,17 s
PCV, 1600 bar, ET=400 $\mu$ s	0,126 s	0,169 s
PCV, 1600 bar, ET=700 $\mu$ s	0,136 s	0,152 s
PCV, 1600 bar, ET=1000 $\mu$ s	0,136 s	0,154 s
PCV, 1800 bar, ET=400 $\mu$ s	0,12 s	0,169 s
PCV, 1800 bar, ET=700 $\mu$ s	0,123 s	0,158 s
PCV, 1800 bar, ET=1000 $\mu$ s	0,119 s	0,145 s

**Table 5.1:** Comparison of times for all the tests listed, PCV regulation, n=1000 rpm

$$t_{1^{st}algorithm} < t_{2^{nd}algorithm} \quad (5.3)$$

**The processing time of the algorithm of the three controls is lower than that of the simplified algorithm**

### 5.3 Identification of the intersection line with the initial spectrum

A flow-chart is introduced to understand the logic of the first algorithm:

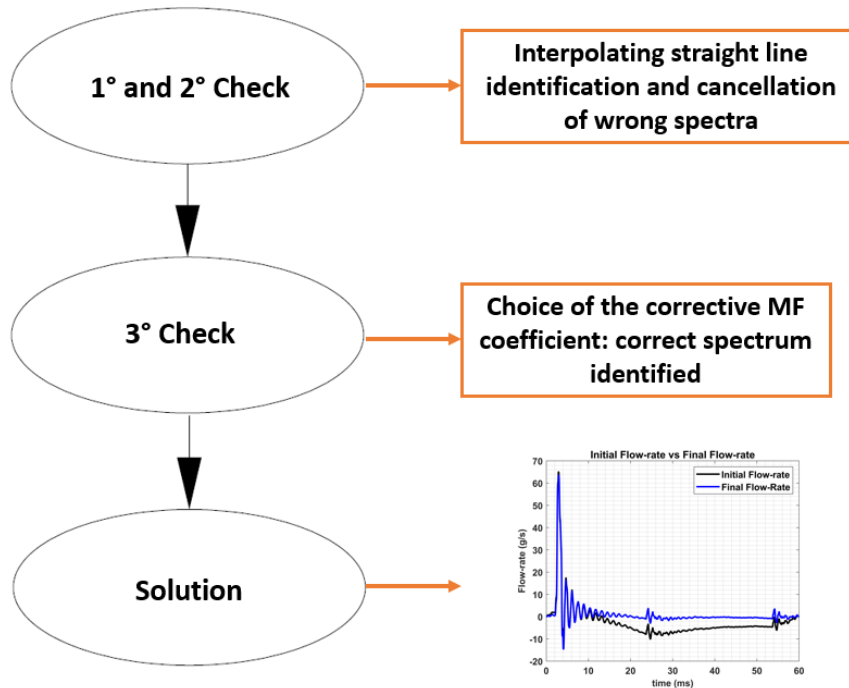


Figure 5.2: Flow-chart of the first algorithm

The  $i$ -th spectrum associated with the  $j$ -th frequency is checked, the spectrum is passed in the first two controls; if the spectrum respects the controls, a summation is performed and the associated value is inserted into a matrix, instead if it does not respect it, the value 0 will be associated.

There will be two similar matrices with values other than 0 and with many 0s.

**The minimum of the matrix of figure 5.4 is identified and the frequency is extracted from the column and the remaining multiplicative coefficients will go into the third control.**

It can be said that everything is quite complex, while in the simplified algorithm everything happens in one fell swoop: both the identification of the frequency and the multiplicative coefficient MF.

**The simplified algorithm is more compact than the first algorithm.**



## 5.4 Final point

For 'final point' it means the point up to where to compute the sum of the differences between the intersection line and the  $i$ -th spectrum.

In the algorithm of the 3 controls this point has been identified as the point following the intersection between the intersection line and the initial spectrum.

**The important thing to emphasize is that this point applies to all experimental tests that have been analyzed.**

**This happens because the first two controls destroy the wrong spectra and thus give a certain order of the remaining spectra.**

Let's see a series of examples for the first algorithm:

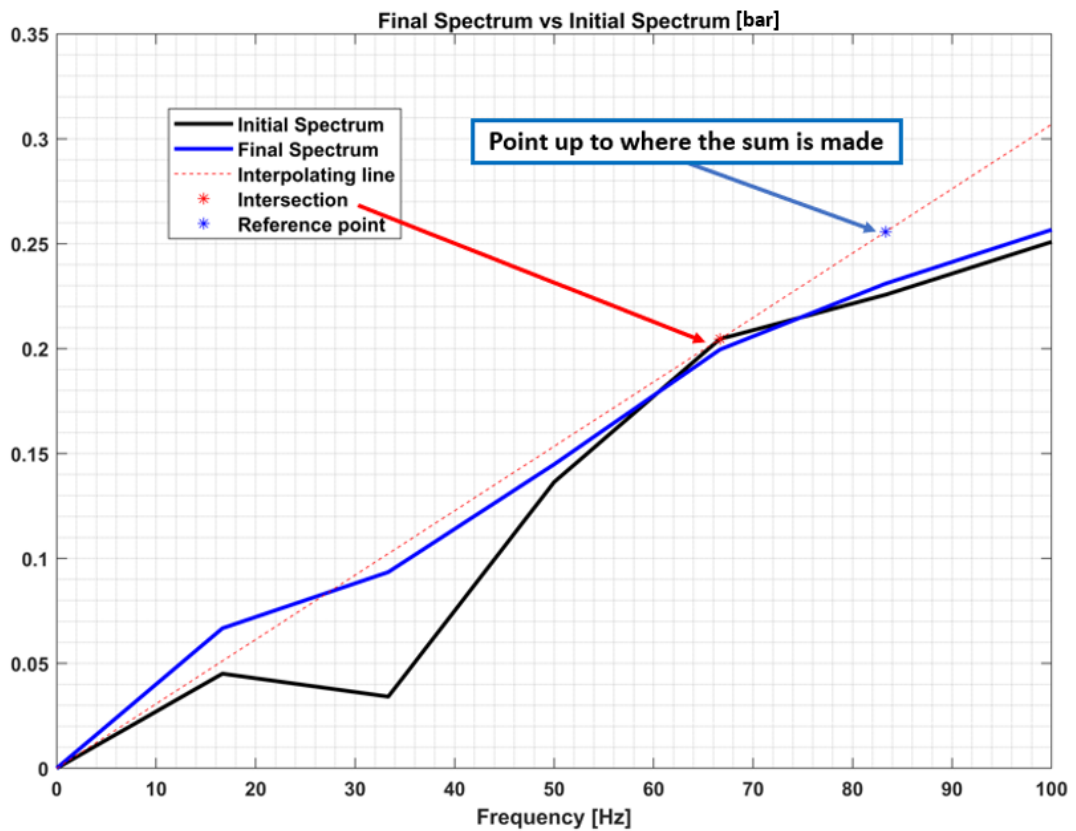


**Figure 5.5:** Example 1: Initial spectrum, final spectrum, intersection point and reference point for the initial algorithm

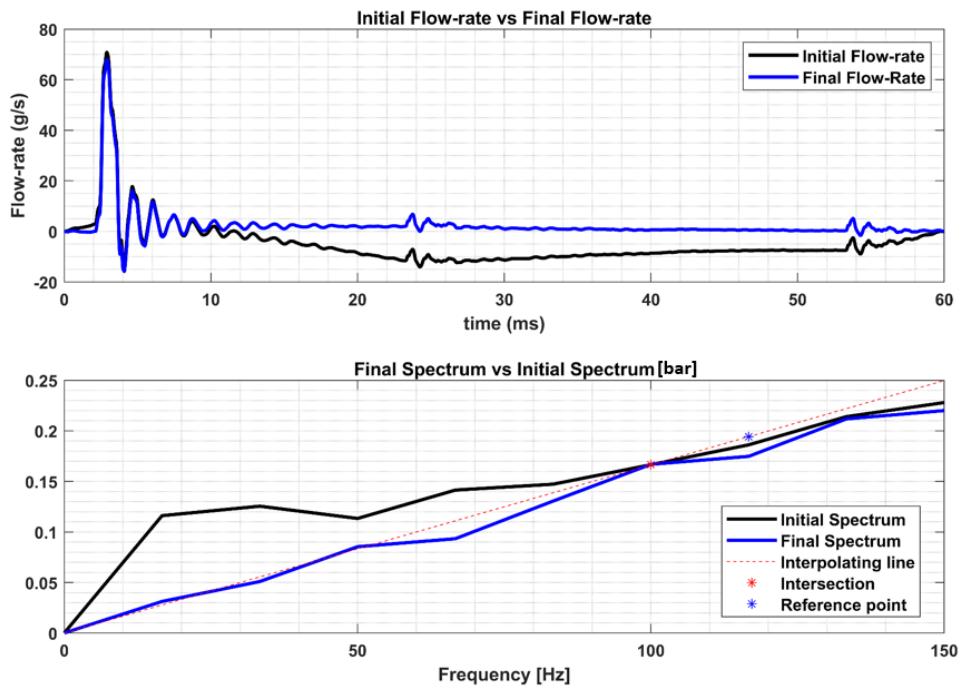


**Figure 5.6:** Example 2: Initial spectrum, final spectrum, intersection point and reference point for the initial algorithm

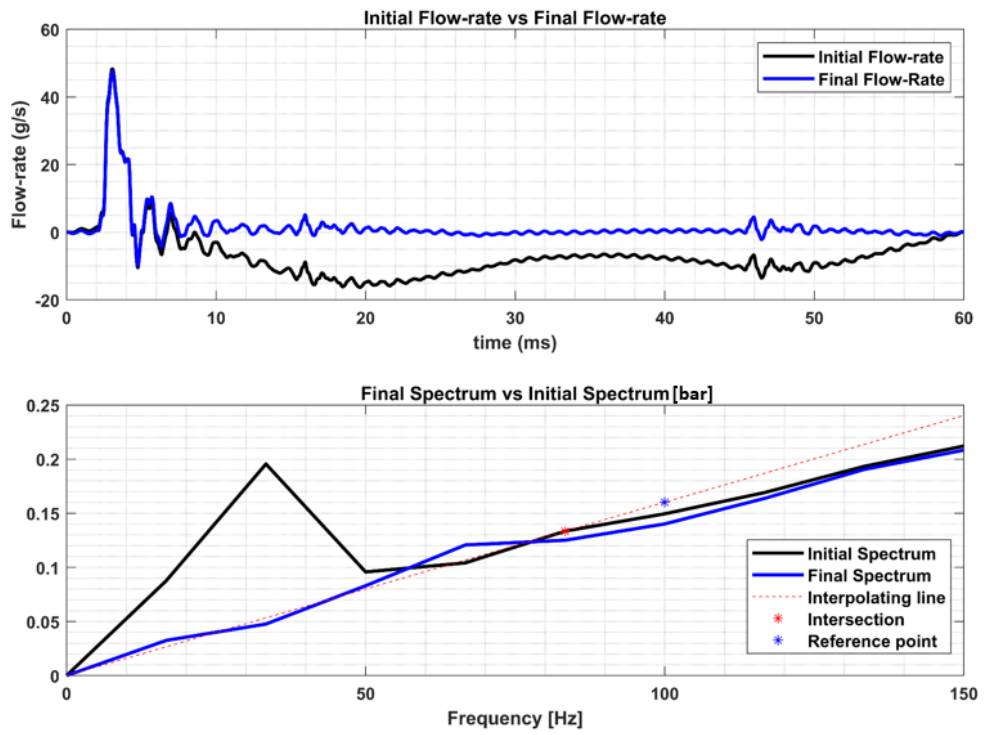


**Figure 5.7:** Example 3: Initial spectrum, final spectrum, intersection point and reference point for the initial algorithm

The end point problem is in the simplified algorithm because there is no correction effect of the first two controls.

The algorithm analyzes more wrong spectra and everyone has his own behaviour. See some examples if we consider the final point the one following the intersection point:

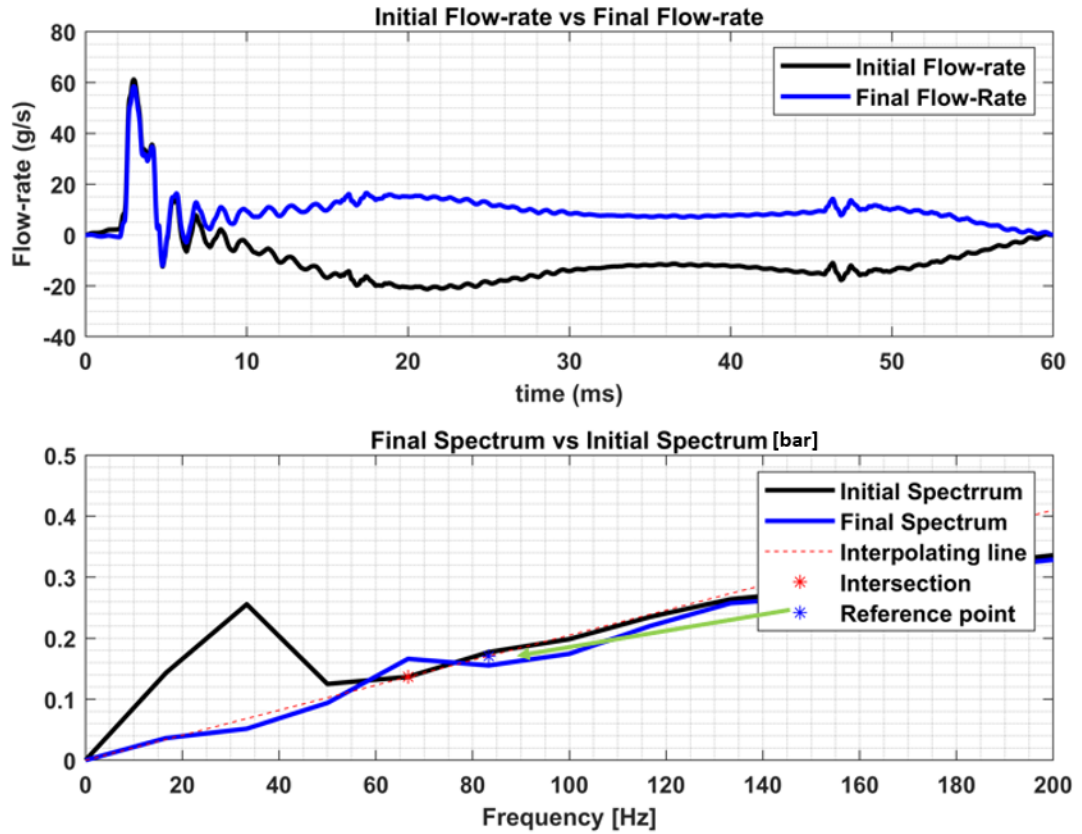


**Figure 5.8:** Simplified algorithm: Spectrum identified by reference point following the intersection point

It is therefore necessary to identify a point that is good for all experimental tests (150 Hz for example is good for all experimental test).

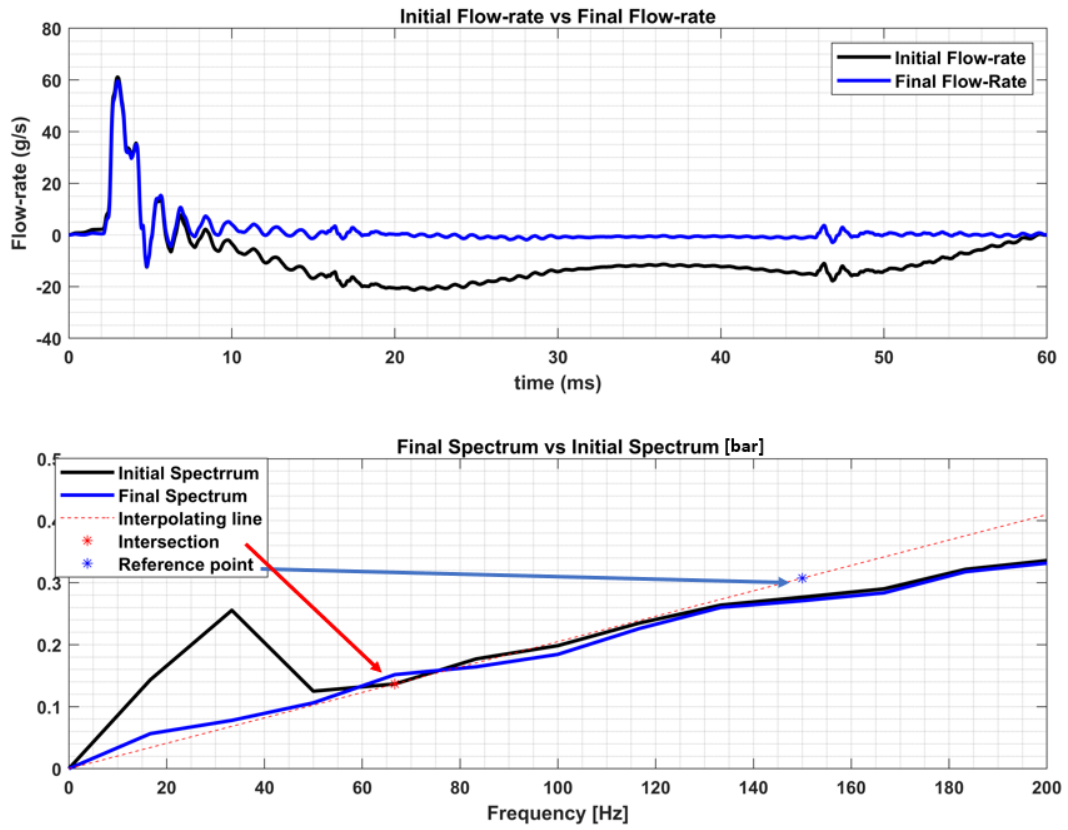


**Figure 5.9:** Simplified algorithm: Spectrum identified by reference point fixed to 150 Hz

## 5.5 Accuracy and efficiency

In this paragraph it wants to analyze the effect of the **discretization step** in the two algorithms.

Obviously the need for the discretization step to negatively affect the processing time, but it wants to see the effect it has on the algorithms.

Considering the first algorithm:

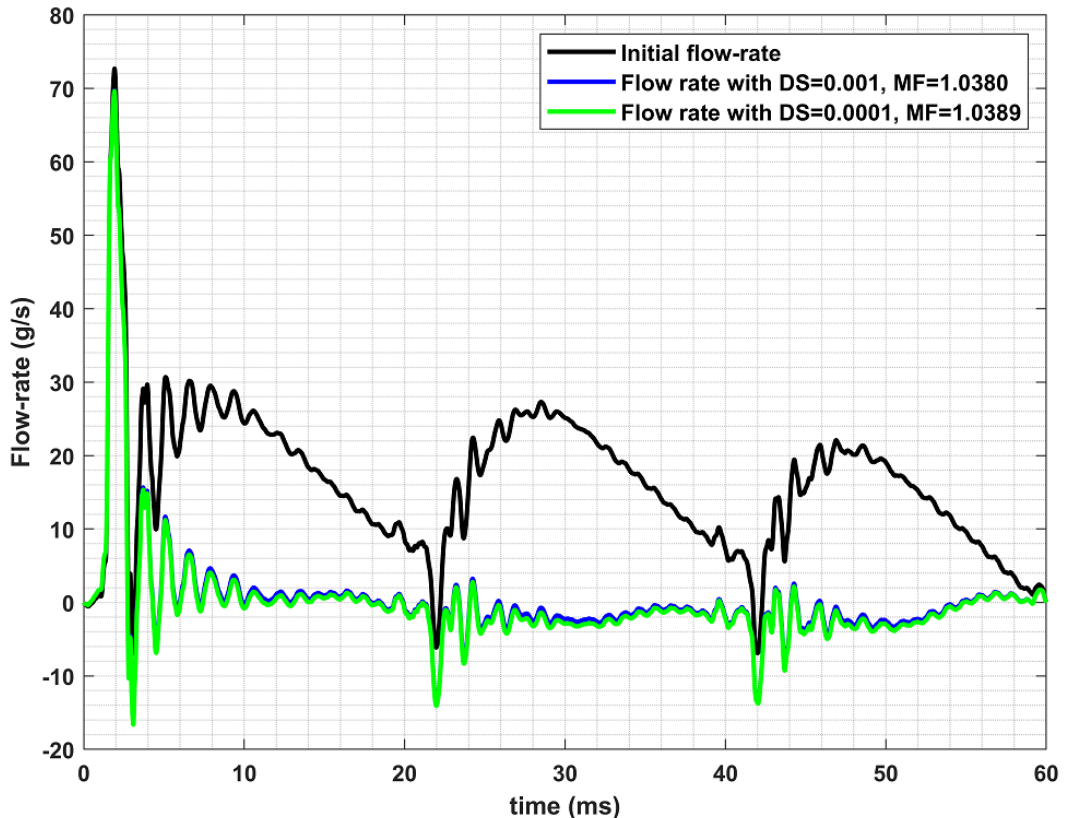


**Figure 5.10:** Effect of the variation of the discretization step: first algorithm

The decrease of the DS does not involve a substantial variation of the flow rate diagram (the variation is present), but the thing to note is that it passes from a processing time of 0.62 s ( $SD = 0.001$ ) to 2 s ( $DS = 0.0001$ ).

In these times it is necessary to consider the time to plot the graphs (the value is not important, but the effect of the discretization step).

In the simplified algorithm the multiplicative coefficients MF are different, but it should be noted that we go from 0.8 s ( $DS = 0.001$ ) to 8 s ( $DS = 0.0001$ ) which is

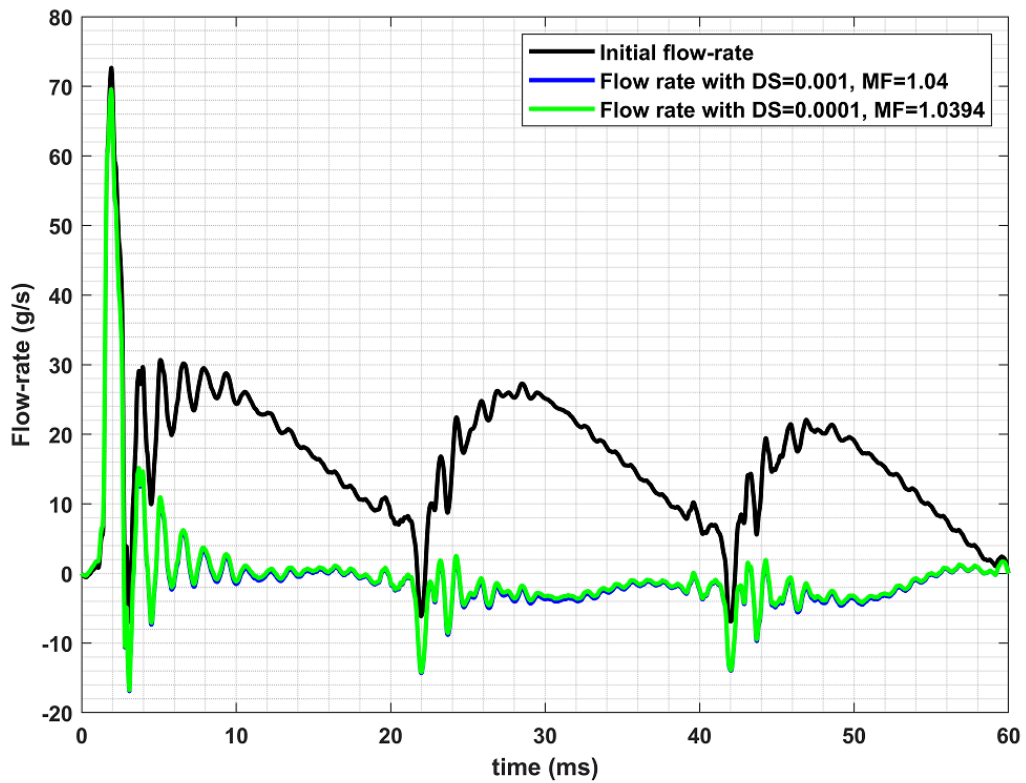


**Figure 5.11:** Effect of the variation of the discretization step: Simplified algorithm

absolutely an unacceptable situation.

**This is due to the fact that, by increasing DS, the number of spectra that the algorithm has to analyze increases (the simplified algorithm analyzed them all).**

The algorithm of the 3 controls does not have this problem because most of the spectra are eliminated by the two initial controls, so I will have increasingly larger matrices, but with lots of 0.

## 5.6 Absence of the solution

Due to how the algorithm of the three controls is set up, there is a possibility that the solution may not be found (due to the two initial controls that eliminate all the spectra).

This happens in a few experimental tests, so it is also necessary to manage this situation because the algorithm must have a totally general value.

If the experimental test with reference pressure 1000 bar,  $400\mu\text{s}$  ET, FMV regulation is considered it is possible to notice that, with 5 intersection frequencies analyzed, the algorithm does not find the solution.

This situation happens when the instant flow diagram is not totally wrong.

Initial flow-rate is:

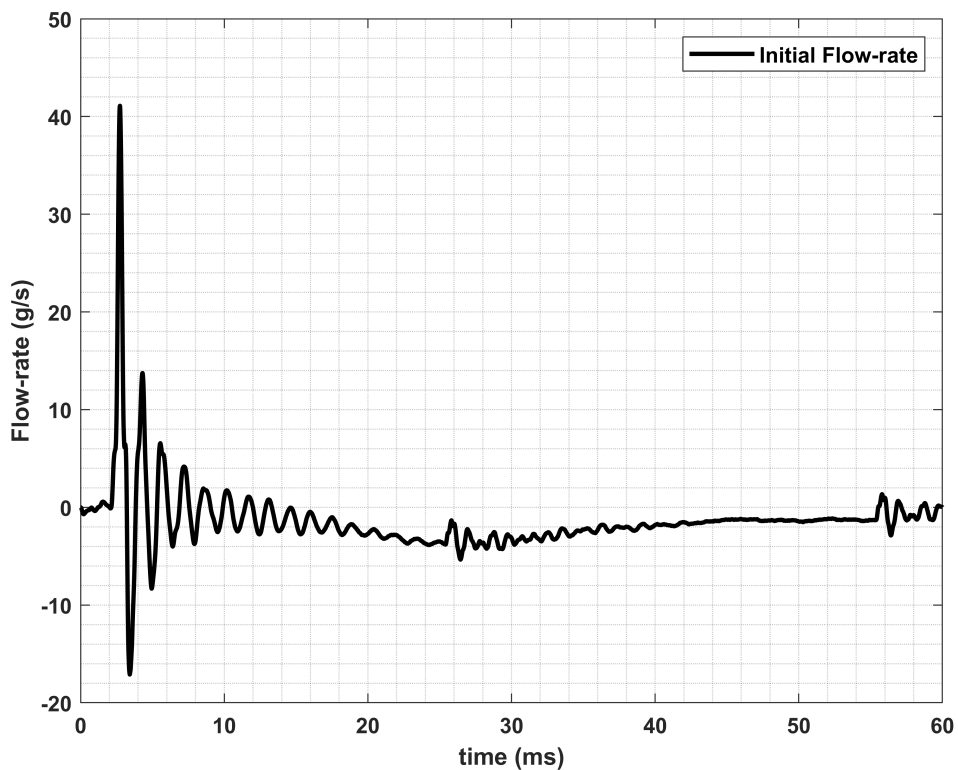


**Figure 5.12:** Initial Flow-rate, Reference pressure 1000 bar,  $400\mu\text{s}$  ET, FMV regulation,  $n=1000$  rpm

It's possible to see the same situation in other experimental tests.

Consider ,respectively, FMV regulation, reference pressure 800 bar,  $400\mu\text{s}$  ET and 1200 bar, 400 ET:

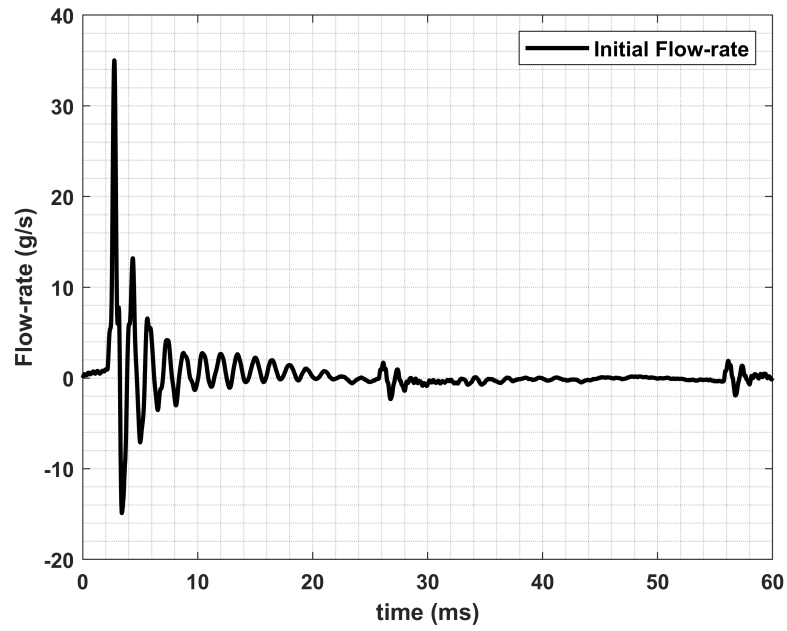


**Figure 5.13:** Initial Flow-rate, Reference pressure 800 bar,  $400\mu\text{s}$  ET, FMV regulation,  $n=1000$  rpm

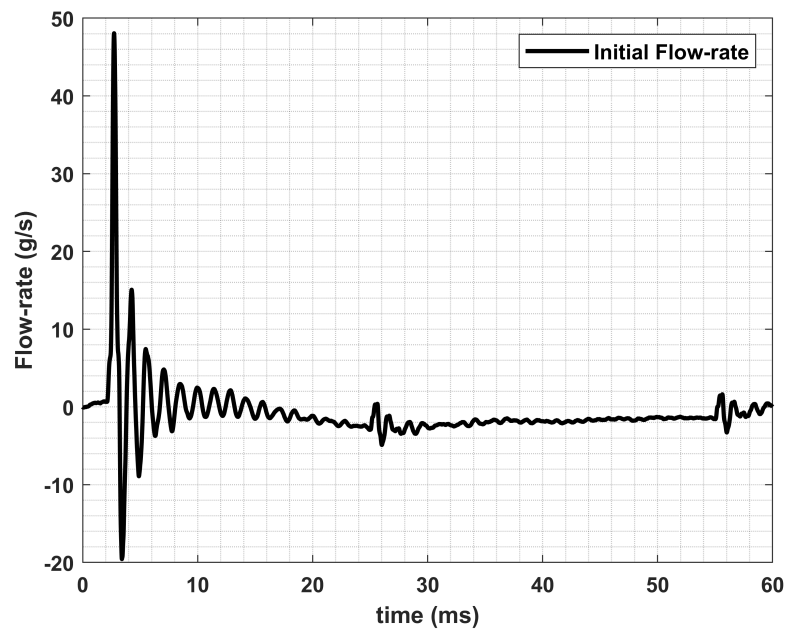


**Figure 5.14:** Initial Flow-rate, Reference pressure 1200 bar,  $400\mu\text{s}$  ET, FMV regulation,  $n=1000$  rpm

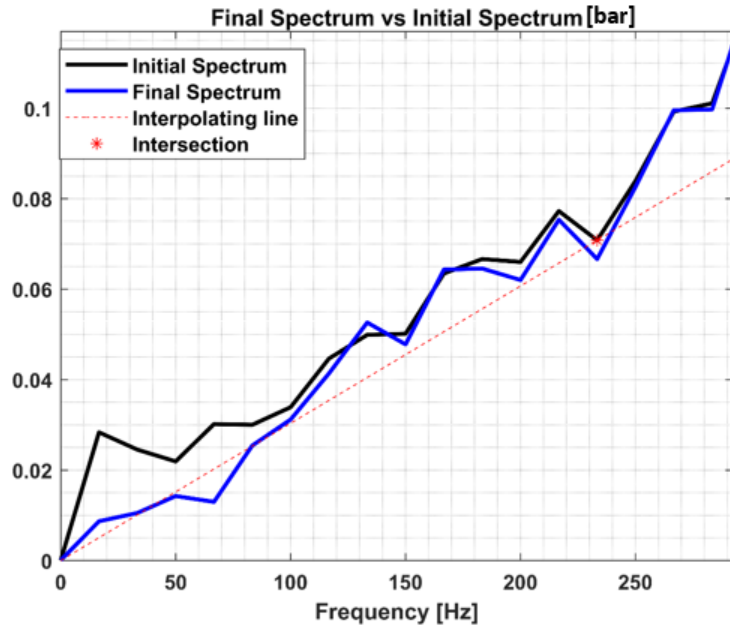


**Figure 5.15:** Initial Spectrum and Final spectrum, Reference pressure 1000 bar,  $400\mu\text{s}$  ET, FMV regulation,  $n=1000$  rpm

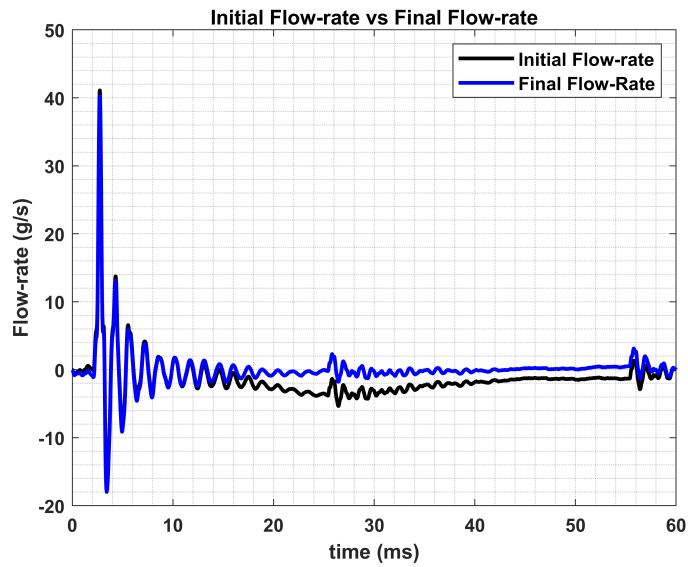


**Figure 5.16:** Initial flow-rate and Correct Flow-rate, Reference pressure 1000 bar,  $400\mu\text{s}$  ET, FMV regulation,  $n=1000$  rpm

The corrected and linearized spectrum is found at the 15-th frequency analyzed; this makes the algorithm computationally inefficient, so it is not possible to implement this solution.

The solution is to widen the acceptance range of the spectra of the first two controls (if it was previously set at  $\pm 15\%$ , it will now be  $\pm 20\%$ ).

in figure 5.17 the interval of the first two checks is increased to  $\pm 25\%$  and now the algorithm recognizes the correct frequency at 83.33 Hz.

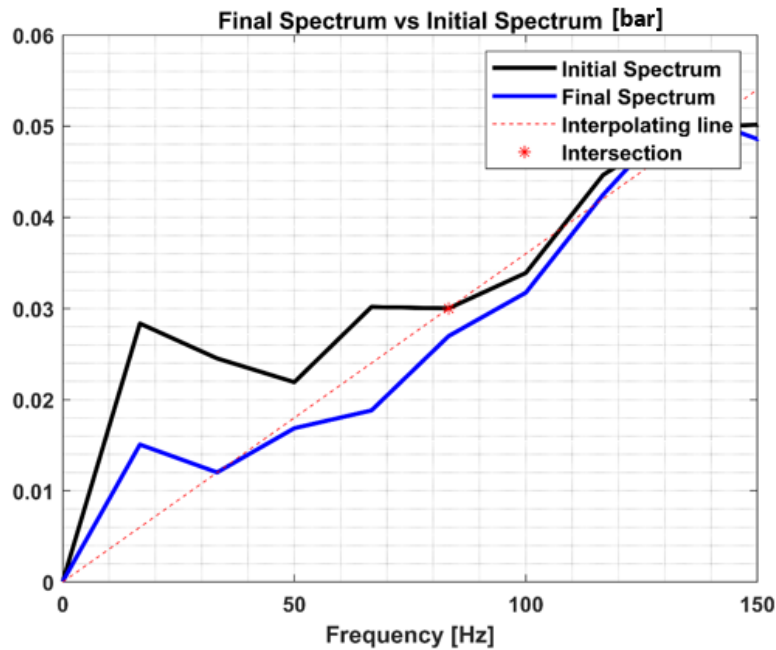


**Figure 5.17:** Initial spectrum and final spectrum with the interval of the two controls fixed at  $\pm 25\%$

**The algorithm must also take this problem into account.**

The situation is different, however, as regards the simplified algorithm.

**As it is implemented, the simplified algorithm will always be a solution (which corresponds to the minimum of the sum of the difference between the i-th spectrum and the j-th frequency).**

The simplified algorithm immediately recognizes the solution (figure 5.19).

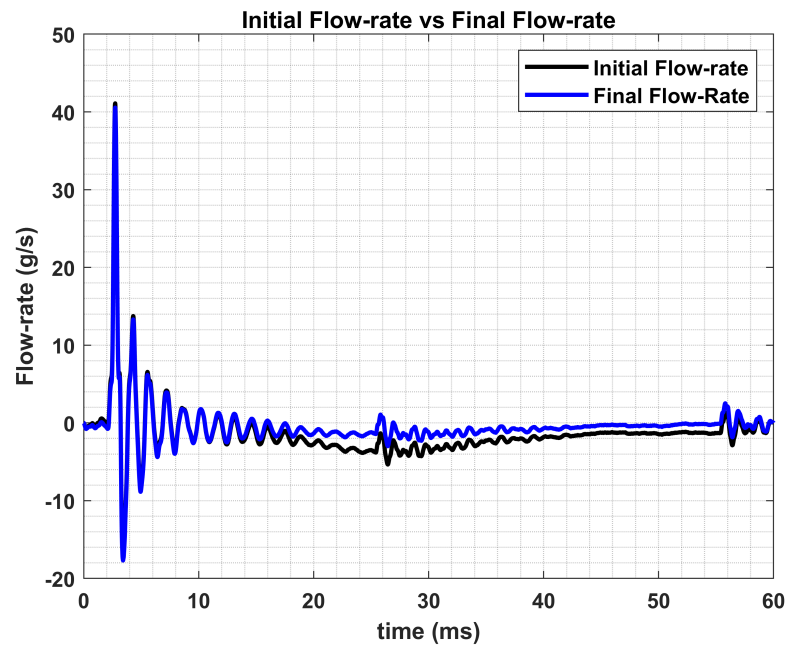


**Figure 5.18:** Initial Flow-rate and final flow-rate with the interval of the two controls fixed at  $\pm 25\%$

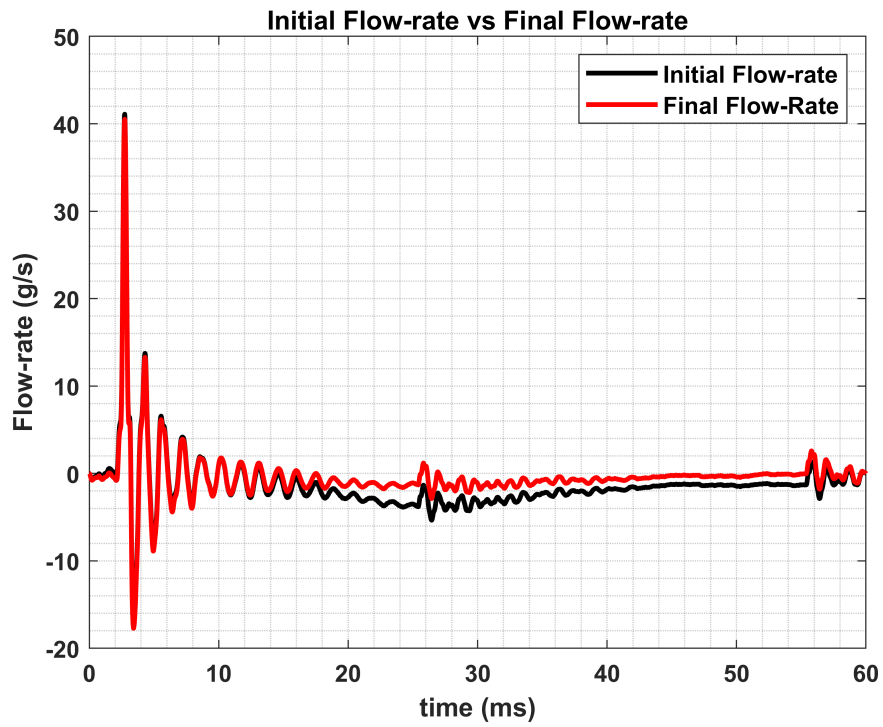


Figure 5.19: Initial Flow-rate and final flow-rate with the simplified algorithm

## Chapter 6

# Conclusions and Future Prospects

In the light of what has been said in the previous paragraphs, the algorithm of the three controls seems to be the most reliable and the most accurate.

**The simplified algorithm**, computationally, is much easier to understand, but has many problems (intersection of lines, end point, processing time and discretization step).

**The algorithm of the three controls**, on the other hand, does not present these problems.

The only drawback is the management of the absence of the solution, but as has been shown, it is possible to overcome this problem.

Another problem to be taken into account is that if the instantaneous initial flow rate is already correct the algorithm does not have to do anything (which happened in 1-2 experimental tests).

It must also be taken into account that all the graphs shown have been analyzed on Matlab, but there will be no sophisticated software in the flowmeter, so the perfectly correct graphs seen with the algorithm may not give the expected results. Everything becomes even more complicated if we consider the fact that the process is highly random, so **a simple systematic error** may not give the expected results.

Precisely to avoid this, as many experimental tests as possible have been analyzed (about 60-70), but such a small sample certainly cannot solve the statistics behind the problem.

**The goal is to introduce a correct and sensible methodology**, studied in every detail and correct from the point of view of electronic controls and obviously from the engineering point of view.

The implementation of the algorithm followed a careful analysis because, being

the phenomenon studied stochastic, it was necessary to identify a model that was suitable for all experimental tests.

Initially it seemed that the tests did not have a common point (some had Fourier spectrum peaks at 16.6 Hz, others at 33.33 Hz, others at 50Hz, some peaks were repeated for a certain remarkable frequency, for others the linearization seemed to have no effect), but with careful analysis an attempt was made to solve the problem by means of a common and general resolution.

**Fourier's analysis** made this possible and proved to be a powerful weapon for the general study of the phenomenon.

All this work goes into improving the flowmeter and ensuring **good repeatability** with each use.

In general, the flowmeter can be applied to hydraulic power systems equipped with pipelines, characterized by the presence of high pressure unsteady flows.

Other applications of the meter, beyond those in injection systems involving high-pressure flows (Diesel or Gasoline GDI) are the analysis of the flow-rate irregularity in the different typologies of high pressure positive displacement pumps and the investigation of the dynamic response of servo-valves to the electrical command.

# Appendix A

## Mechanical design of the flowmeter

The flow-meter includes two pressure sensors, installed at  $x_{up}$  and  $x_{down}$  of a pipeline in order to detect the pressure time distributions.

The ratio between the distance of the two sensors 'l' and the internal pipe diameter 'd' should be high enough to consider the flow as one-dimensional, since a nonuniform flow over the pipe cross section has a negative effect on the flow-meter measurements.

It was also designed the rack of the case (Figure A.5) that will contain the entire device where the input/output signals will be managed.

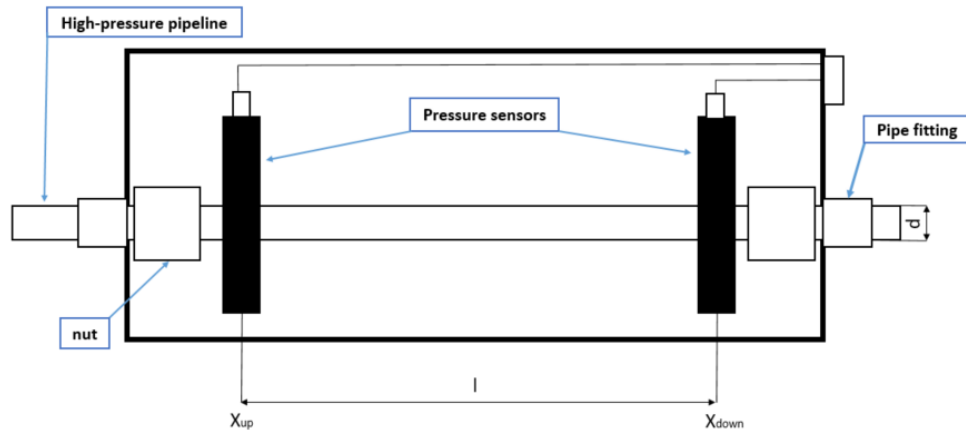


**Figure A.1:** Scheme of the flow-meter

The case that will be designed must take into consideration the overall dimensions

(minimum in order not to hinder the flow of high pressure liquid) and must contain the pressure transducers properly spaced.

Must be managed the appropriate mechanical connections to make easy the fluid path, then the mechanical devices that will be inserted (nuts, fittings etc..) should not be an obstacle to the flow path otherwise there will be concentrated induced pressure drop.

## A.1 Piezoresistive high pressure sensor

The pressure transducers used are those of Kistler, type 4065B...DS.

In Type 4065B...DS, the pressure acts through a robust diaphragm onto a piezoresistive measuring element. The compact dimensions and the shoulder sealing of the sensor provide ideal access to the measuring point. Only a minimal dead volume is created between the sensor front and the measured medium.

The sensor is therefore suitable for applications with a high requirement for frequency-accurate pressure measurements.

This sensors are used in applications where average to high pressures must be measured with a static and a dynamic component. [3]

Examples includes:

- General pressure measurements in gas and hydraulic systems;
- Frequency-accurate analysis of pressure curves in gasoline or diesel injection pressure systems.



**Figure A.2:** Pressure transducer

<b>Property [u.d.m.]</b>	<b>Value</b>
Measuring range [bar]	0 ... 200, 0 ... 500, 0 ... 1000
Overload [bar]	300, 750, 1000
Electrical connection	Fischer connector 5 pole (S103A054)
Amplifier compatibility [Type]	4665, 4665B, 4624A
Power supply	amplifier integrated
Reference temperature (Tref) [ $^{\circ}C$ ]	25
Sensor temperature, min ./max. [ $^{\circ}C$ ]	-40/140
Temperature compensation	digital
Temperature compensation range [ $^{\circ}C$ ]	25 ... 120
Max. deviation pressure [%FSO]	$\leq \pm 1,5$
Max. deviation temperature [ $^{\circ}C$ ]	$\leq \pm 3$
Linearity at Tref (LSQ) [%FSO]	$\leq \pm 0,3$
Natural frequency 200, 500 bar, 1000 bar [kHz]	>40, >100
Acceleration sensitivity [mbar/g]	$\leq 10$
Life cycle (typical) [load change]	$> 10^7$
Mounting torque sensor [Nm]	5
Weight (without connector and cable) [g]	9
Protective class	IP65

**Table A.1:** Technical Data of the transducer

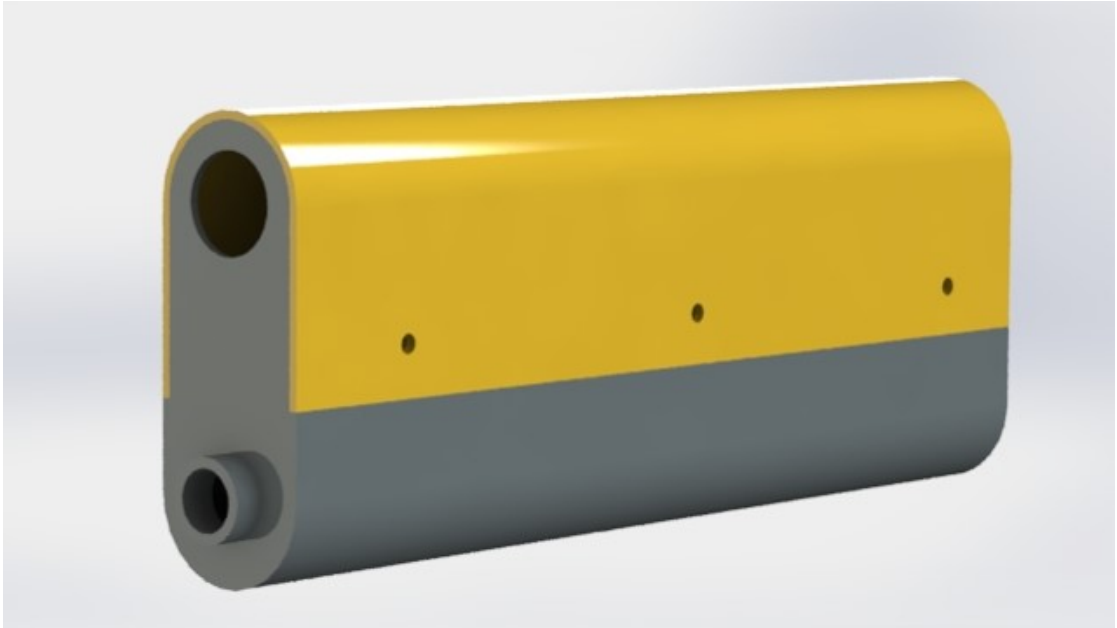


**Figure A.3:** 3D model of the flowmeter



**Figure A.4:** Flow-meter connected to the circuit for diesel injection



**Figure A.5:** Rack of the device

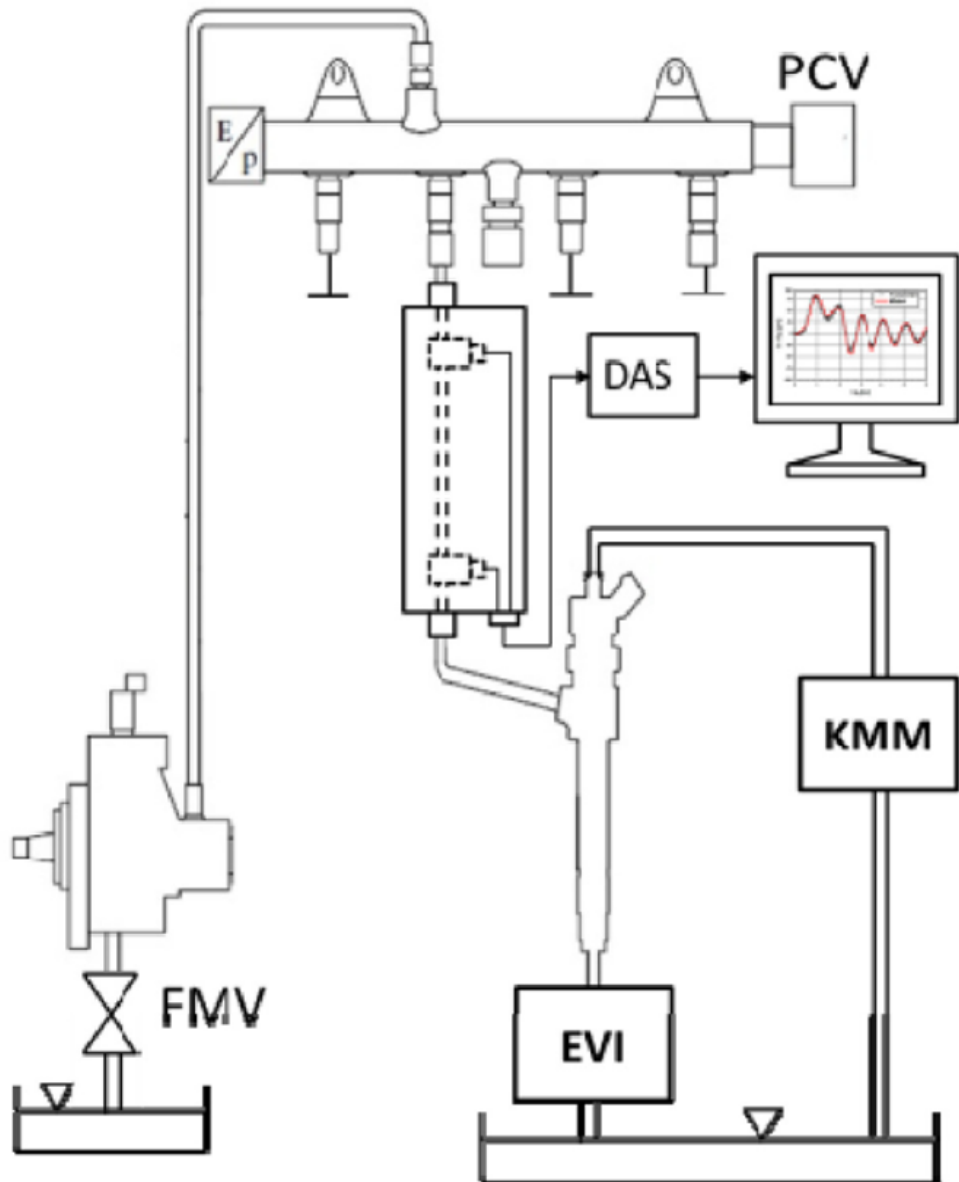


Figure A.6: Injection circuit diagram [4]

# Appendix B

## Fundamentals of Fluid Dynamics Model of the Flowmeter

All the theoretical concepts developed in the following appendix are derived from the book 'Fondamenti di termofluidodinamica delle macchine' by Prof. Ferrari and from his lectures of the course 'Advanced computational techniques for hydraulic and thermal machines'.

### B.1 Introduction to Navier-Stokes equations

The flow meter analyzed returns in output the flow value of the fluid that is passing through the mechanical system in question (in our case the injector).

The mass flow rate is calculated using the equations of thermofluid dynamics.

The equations of fluid dynamics for a viscous fluid are as follows:

$$\begin{cases} \frac{d\rho}{dt} + \rho \nabla \cdot v = 0 \\ \rho \frac{dv}{dt} = -\nabla p + \mu [\Delta v + \frac{1}{3} \nabla (\nabla \cdot v)] + \rho f_e \\ \frac{\partial(\rho e_t)}{\partial t} + \nabla \cdot [\rho v (e_t + \frac{p}{\rho})] = \nabla \cdot (k \nabla T) - \nabla \cdot ([\tau]v) + \rho \dot{l}_e + \dot{q}_H \end{cases}$$

These three equations represent the conservation of mass equation, momentum equation, and energy equation, respectively.

The set of equations defines **the equations of Navier Stokes**.

All the terms that appear in the system are analyzed in detail [5]:

- $\rho$  is the density of the fluid system under consideration;
- $f_e$  is the resultant of the external field forces per unit volume;

- $e_t$  is the total mass energy of the system;
- $k$  is the thermal conductivity of the fluid;
- $q_H$  and  $\dot{l}_e$  are the volumic sources of energy given by the sum of the work of the external field forces and the contributions of heat (radiation and chemical reactions);
- $[\tau]$  is the deviatoric component of the stress tensor  $[\sigma]$

## B.2 Stress tensor in dynamics

In the momentum balance equation it is necessary to consider the species of the fluid system being considered.

It is possible to decompose the tensor of the stress in a **static part** (characterized only from the pressure that acts along the correspondent normal  $\vec{n}$ ) and a component that takes into account the dynamics of the fluid system (**the deviatoric component**).

$$[\sigma] = p[I] + [\tau] \quad (\text{B.1})$$

It is possible to write the components of the deviatoric tensor by means of **Navier's constitutive equation for Newtonian fluids**:

$$\tau_{ij} = -2\mu\epsilon_{ij} - \lambda\delta_{ij}\nabla \cdot v \quad (\text{B.2})$$

It was possible to express a linear relationship between the deviatoric components of the tensor and the angular slip or elongation rates (components of the strain tensor  $[\epsilon]$ ) thanks to Newton's law.

From the equation (B.2) it is necessary to pay attention to the coefficients  $\delta_{ij}$  which are part of the tensor of Kronecker  $[\delta]$  which gives the value  $\delta = 0$  if  $i \neq j$  and 1 otherwise.

The coefficients  $\mu$  and  $\lambda$  are called Lamè coefficients.

Introducing the concept of dynamic pressure:

$$p_d = p - \eta\nabla \cdot v \quad (\text{B.3})$$

where  $\eta$  is the volumic viscosity and is equal to:

$$\eta = \frac{2}{3}\mu + \lambda \quad (\text{B.4})$$

Dynamic pressure and static pressure (the one that goes to be inserted in the equation of state of the fluid system considered) are equal if there is a specific condition between the Lamè coefficients:

$$\lambda = -\frac{2}{3}\mu \rightarrow \eta = 0 \quad (\text{B.5})$$

This is Stokes' relation.

If the relation of stokes is valid then (B.2)'ll is:

$$\tau_{ij} = -2\mu\epsilon_{ij} + \frac{2}{3}\mu\delta_{ij}\nabla \cdot v \quad (\text{B.6})$$

Substituting (B.6) into the starting equation (B.1):

$$\sigma_{11} = p - 2\mu\frac{\partial v_1}{\partial x_1} + \frac{2}{3}\mu\left(\frac{\partial v_1}{\partial x_1} + \frac{\partial v_2}{\partial x_2} + \frac{\partial v_3}{\partial x_3}\right) \quad (\text{B.7})$$

$$\sigma_{22} = p - 2\mu\frac{\partial v_2}{\partial x_2} + \frac{2}{3}\mu\left(\frac{\partial v_1}{\partial x_1} + \frac{\partial v_2}{\partial x_2} + \frac{\partial v_3}{\partial x_3}\right) \quad (\text{B.8})$$

$$\sigma_{33} = p - 2\mu\frac{\partial v_3}{\partial x_3} + \frac{2}{3}\mu\left(\frac{\partial v_1}{\partial x_1} + \frac{\partial v_2}{\partial x_2} + \frac{\partial v_3}{\partial x_3}\right) \quad (\text{B.9})$$

$$\tau_{12} = -\mu\left(\frac{\partial v_1}{\partial x_2} + \frac{\partial v_2}{\partial x_1}\right) \quad (\text{B.10})$$

$$\tau_{23} = -\mu\left(\frac{\partial v_2}{\partial x_3} + \frac{\partial v_3}{\partial x_2}\right) \quad (\text{B.11})$$

$$\tau_{13} = -\mu\left(\frac{\partial v_1}{\partial x_3} + \frac{\partial v_3}{\partial x_1}\right) \quad (\text{B.12})$$

In vector notation [5]:

$$[\sigma] = p[I] - \mu\left(\nabla v + (\nabla v)^T\right) + \frac{2}{3}\mu(\nabla \cdot v)[I] \quad (\text{B.13})$$

### B.3 Classic 1D Euler's equations

The Euler equations represent a simplified form of the Navier Stokes equations with the following assumptions:

- No friction;
- No form of heat transmission (no convection and radiation);
- entropy conserved in each trajectory (homoentropic field);

The system of equations transforms as follows:

$$\begin{cases} \frac{\partial \rho}{\partial t} + \frac{\rho v}{\partial x} = 0 \\ \frac{\partial \rho v}{\partial t} + \frac{\partial (p + \rho u^2)}{\partial x} = 0 \\ \frac{ds}{dt} = \frac{\partial s}{\partial t} + u \frac{\partial s}{\partial x} = 0. \end{cases}$$

Since the field is homoentropic it is possible to develop:

$$\frac{\partial p}{\partial x} = a_s^2 \frac{\partial \rho}{\partial x} \quad (\text{B.14})$$

where  $a_s$  is the isentropic speed of sound.

it is possible to write the system of equations in the following way:

$$\vec{U}_t + [A]\vec{U}_x = 0 \quad (\text{B.15})$$

Where:

$$\vec{U}_t = \frac{\partial \vec{u}}{\partial t} \quad (\text{B.16})$$

and

$$\vec{U}_x = \frac{\partial \vec{u}}{\partial x} \quad (\text{B.17})$$

and

$$\vec{u} = [\rho, \rho u, s]^T \quad (\text{B.18})$$

[A] is the Jacobi matrix and is defined in this way:

$$\begin{bmatrix} 0 & 1 & 0 \\ a_s^2 - u^2 & 2u & 0 \\ 0 & 0 & u \end{bmatrix}$$

Setting  $\det(A)=0$  and solving the characteristic equation I get the three eigenvalues of the matrix:

$$\lambda_1 = u - a_s; \quad (\text{B.19})$$

$$\lambda_2 = u; \quad (\text{B.20})$$

$$\lambda_3 = u + a_s \quad (\text{B.21})$$

Recognizing the eigenvalues of the system of equations is critical, as we can modify the equations to make them simpler and lead them back to forms that we can solve analytically (D'Alembert equation).

Euler equations are more critical than Navier-Stokes equations to be discretizing because in Euler we don't have any dissipation mechanism.

In Navier Stokes equations the diffusion mechanism is present and this tends to make the field homogeneous.

If numerical oscillations are present in the scheme, diffusion mechanism helps to cancel these oscillations.

This does not occur in Euler equations, the discretization should be very stable otherwise the oscillations will have an increasing amplitude in time [5].

## B.4 Generalized Euler equations

Although diffusive terms are absent from the Euler equations, it is possible to simulate viscous wall actions and heat exchanges with duct surfaces.

It is possible to modify them without changing the mathematics of the equations.

$$\begin{cases} \frac{\partial \rho}{\partial t} + \frac{\rho v}{\partial x} = 0 \\ \frac{\partial \rho v}{\partial t} + \frac{\partial (p + \rho u^2)}{\partial x} = -\frac{4\tau_w}{D} \\ T \frac{ds}{dt} = T \left( \frac{\partial s}{\partial t} + u \frac{\partial s}{\partial x} \right) = \rho (\dot{q} + \dot{l}_w). \end{cases}$$

where:

- $d$  is the diameter of the duct;
- $\tau_w$  are the wall stresses;
- $\dot{q}$  and  $\dot{l}_w$  are the thermal power exchanged by convection and the power dissipated by the viscous actions of the fluid.

The wall stress can be traced back to the equation:

$$\tau_w = \lambda \rho |u| \frac{u}{8} \tag{B.22}$$

where [5]

- $\lambda$  is the coefficient of pressure drop called Darcy-Weisbach coefficient and its value can be taken from the Moody diagram ;

## B.5 Numerical algorithm for the flow-rate evaluation

The numerical algorithm that identifies the mass flow rate in the mechanical system is based on the generalized Euler equations.

The mass conservation and momentum balance are written in 1D form for a slender pipe [4]:

$$\begin{cases} \frac{d\rho}{dt} + \rho \frac{\partial u}{\partial x} = 0 \\ \frac{\partial u}{\partial t} + u \frac{\partial u}{\partial x} + \frac{1}{\rho} \frac{\partial p}{\partial x} = -\frac{4\tau_w}{\rho d} \end{cases}$$

where:

- $u$  is the average cross-sectional fluid velocity;
- $x$  is the coordinate along the pipe;
- $\tau_w$  is the wall shear stress;
- $\rho$  and  $p$  are the density and pressure of the fluid.

A fundamental hypothesis that is carried out is that of incompressible fluid, this hypothesis is physically consistent, provided the Mach number is lower than 0.1.

The equations become the following:

$$\begin{cases} \frac{\partial u}{\partial x} = 0 \\ \frac{\partial u}{\partial t} + \frac{1}{\rho} \frac{\partial p}{\partial x} = -\frac{4\tau_w}{\rho d} \end{cases}$$

By integrating the moment balance equation and multiplying by appropriate coefficients I obtain:

$$\frac{d\bar{G}}{dt} = \frac{A}{l} \Delta p - \pi d \bar{\tau}_w \quad (\text{B.23})$$

The frictions are approximated in the following way:

$$\bar{\tau}_w = \tau_{sf} \approx \frac{\bar{f}}{8\rho A^2} |\bar{G}| \bar{G} \approx \frac{f}{8\rho A^2} |G| G \quad (\text{B.24})$$

where:

- $\tau_{sf}$  is the steady-state wall friction;
- $f$  is the space-averaged friction factor, which can be expressed as a function of Reynolds number;
- $A$  is the area of the pipe.

$$\bar{f} = 1.613 \left[ \ln \left( 0.234 \left( \frac{\epsilon}{d} \right)^{1.1007} - \frac{60525}{Re^{1.1105}} + \frac{56291}{Re^{1.0712}} \right) \right]^{-2} \quad (\text{B.25})$$

Equation (B.25) is a good approximation of the Moody diagram in the Reynolds number interval from  $Re = 3 \cdot 10^3$  to  $Re = 10^8$  and  $\frac{\epsilon}{d} \leq 5 \cdot 10^{-2}$  where  $\frac{\epsilon}{d}$  is the pipe relative roughness.

It is necessary to add an additional wall stress term due to the wall shear stress term friction and this changes the equation.

$$\bar{\tau}_w = \bar{\tau}_{sf} + \bar{\tau}_{fdf} \quad (\text{B.26})$$

$$\bar{\tau}_{fdf} = \frac{4\mu}{d} \int_{-\infty}^t \frac{\partial \bar{u}}{\partial t}(\lambda) W(t - \lambda) d\lambda \quad (\text{B.27})$$

where:

- $\bar{u}$  is the space averaged fluid velocity;
- $W$  is a weighting function, which is maximum when  $\lambda = t$  and decreases monotonically as  $(t-\lambda) > 0$  increases.

Substituting we obtain:

$$\frac{d\bar{G}}{dt} = \frac{A}{l} \Delta p - \pi d \frac{\langle \bar{f} \rangle}{8\rho A^2} \langle \bar{G} \rangle + \left| \langle \bar{G} \rangle \right| - \frac{4\pi\mu}{\rho A} \int_{-\infty}^t \frac{d\bar{G}}{dt}(\lambda) W(t - \lambda) d\lambda \quad (\text{B.28})$$

- $\langle \bar{f} \rangle$  is the space and time averaged friction factor;
- $\langle Re \rangle$  is the space and time averaged Reynolds number.

To simplify the numerical model the convolution integral can be neglected.

Integrating the equation B.27 we obtain:

$$\bar{G}(t) = \bar{G}_0 + \frac{A}{l} \int_0^t \Delta p dt - \pi d \frac{\langle \bar{f} \rangle}{8\rho A^2} \langle \bar{G} \rangle + \left| \langle \bar{G} \rangle \right| t \quad (\text{B.29})$$

By integrating B.29 over a complete working cycle  $T$  (exploiting that hydraulic machines are all periodic):

$$\frac{A}{l} \langle \Delta p \rangle = \pi d \frac{\langle \bar{f} \rangle}{8\rho A^2} \langle \bar{G} \rangle + \left| \langle \bar{G} \rangle \right| \quad (\text{B.30})$$

Using the fourier series (1.2):

$$\Delta p(t) = a_0 + \sum_{k=1}^{\infty} a_k \cos(\Omega_k t) + b_k \sin(\Omega_k t) \quad (\text{B.31})$$

$$\Delta p(t) \approx \langle \Delta p \rangle + \sum_{k=1}^N a_k \cos\left(\frac{k2\pi t}{T}\right) + b_k \sin\left(\frac{k2\pi t}{T}\right) \quad (\text{B.32})$$

The pressure transducers are affected by zero-offset errors, which can be larger in value than the physical time-averaged pressure difference and which result in spurious contributions to  $a_0$ .

In this way B.31 cannot be use to evaluate  $\langle G \rangle$ .

Substituting the previous equations the following expression can be obtained:

$$\bar{G}(t) = \bar{G}_0 + \frac{A}{l} \sum_{k=1}^N \left[ \frac{a_k}{w_k} \sin(w_k t) + \frac{b_k}{w_k} [1 - \cos(w_k t)] \right] \quad (\text{B.33})$$

With an appropriate integration and simplification we obtain:

$$\Delta \bar{G} = \frac{A}{l} \sum_{k=1}^N \left( \frac{a_k}{w_k} \sin(w_k t) - \frac{b_k}{w_k} \cos(w_k t) \right) \quad (\text{B.34})$$

(B.34) is a simple analytical expression and represents a robust algorithm.

If  $\langle G \rangle$  datum is available, the instantaneous flow-rate can be calculated with the relation [4]:

$$\bar{G} = \langle G \rangle + \Delta \bar{G} \quad (\text{B.35})$$

# Bibliography

- [1] S.Marchesiello A.Fasana. «Meccanica delle vibrazioni». In: (2006) (cit. on p. 7).
- [2] Autori Vari. «Manuali d'uso degli strumenti». In: () (cit. on p. 18).
- [3] www.kistler.com. «Piezoresistive high pressure sensor for measurements at gas and hydraulic systems». In: (2020) (cit. on p. 87).
- [4] P.Pizzo A.Ferrari. «Optimization of an algorithm for the measurement of unsteady flow-rates in high pressure pipelines and application of a newly designed flowmeter to volumetric pump analysis». In: *Journal of Engineering for Gas Turbines and Power* (2016) (cit. on pp. 91, 97, 99).
- [5] A.Ferrari. «Fondamenti di termofluidodinamica per le macchine». In: (2021) (cit. on pp. 92, 94, 96).